ENHANCEMENT OF MICROBIAL FUEL CELL ANODE THROUGH FUNCTIONALIZATION OF CONDUCTIVE POLYMER

KANG YEE LI

FACULTY OF ENGINEERING
UNIVERSITY OF MALAYA
KUALA LUMPUR

2016

ENHANCEMENT OF MICROBIAL FUEL CELL ANODE THROUGH FUNCTIONALIZATION OF CONDUCTIVE POLYMER

KANG YEE LI

THESIS SUBMITTED IN FULFILMENT OF THE REQUIREMENTS FOR THE DEGREE OF DOCTOR OF PHILOSOPHY

FACULTY OF ENGINEERING
UNIVERSITY OF MALAYA
KUALA LUMPUR

2016

UNIVERSITY OF MALAYA

ORIGINAL LITERARY WORK DECLARATION

Name of Candidate: Kang Yee Li

Matric No: KHA110067

Name of Degree: Doctor of Philosophy

Title of Project Paper/Research Report/Dissertation/Thesis ("this Work"):

Enhancement of Microbial Fuel Cell Anode through Functionalization of Conductive Polymer

Field of Study: Environmental Engineering (Civil Engineering)

I do solemnly and sincerely declare that:

(1) I am the sole author/writer of this Work;
(2) This Work is original;
(3) Any use of any work in which copyright exists was done by way of fair dealing and for permitted purposes and any excerpt or extract from, or reference to or reproduction of any copyright work has been disclosed expressly and sufficiently and the title of the Work and its authorship have been acknowledged in this Work;
(4) I do not have any actual knowledge nor do I ought reasonably to know that the making of this work constitutes an infringement of any copyright work;
(5) I hereby assign all and every rights in the copyright to this Work to the University of Malaya ("UM"), who henceforth shall be owner of the copyright in this Work and that any reproduction or use in any form or by any means whatsoever is prohibited without the written consent of UM having been first had and obtained;
(6) I am fully aware that if in the course of making this Work I have infringed any copyright whether intentionally or otherwise, I may be subject to legal action or any other action as may be determined by UM.

Candidate's Signature Date:

Subscribed and solemnly declared before,

Witness's Signature Date:

Name:

Designation:

ABSTRACT

The incompetency in handling energy and water leads to detrimental consequences to the environment. Hence, sustainable solutions to overcome this situation are crucial for the survival and conservation of ecosystem for the future generation. In recent years, Microbial Fuel Cell (MFC) emerged as the most promising technology that sustainably integrates energy generation and environmental clean-up. Though MFC research was prominent among the academics, it had numerous restrictions that need to be surpassed for real-time feasibility. Most of these are attributed to its components such as anode, biocatalyst and membrane. Hence, the present thesis focused on addressing one of its major limitation, the anode component. The objective of the present research is to develop an enhanced anode for MFC operation. Two different aspects were targeted namely the structural configurations and functionalization of anode with conductive polymer. Different configurations such as plate, cloth and felt were utilized to investigate the influence of geometry and morphology on anode performance. The second part perceive the applicability of a conductive polymer, poly(3,4-ethylenedioxythiophene) (PEDOT) as anode enhancer. The synthesized anodes were then applied onto dual chamber MFC reactor. The optimizations of PEDOT loading onto the three different configurations were evaluated through electrochemical characteristics, system performance and efficiency of these anodes. Subsequently, the biofilm, which governs the production and transfer of electrons in the system, were characterized to genetically identify the microbial genera that are responsible for electricity generation. The biodiversity between the different anodes were investigated and compared to evaluate the influence of PEDOT on biofilm selection and electron transfer mechanism that stimulate the MFC operation. The optimal anodes were then applied to real wastewater as substrate to assess the capability of the systems to utilize complex organic molecule. The felt configuration, which is three-dimensional (3D) and has an open structure, achieved promising results compared to the

plate and cloth anodes. The power density of GF anode is 0.52 W/m^2 while GP and CC recorded 0.16 W/m^2 and 0.35 W/m^2 respectively. GF also recorded better coulombic efficiency of 45.4% compared to both GP and CC which only achieved 39% and 31% correspondingly. The incorporation of PEDOT onto the anodes of varied configurations improved the electrochemical characteristics and their performance significantly. The present study also inferred that each anode configurations have different optimum PEDOT loading and peak performances. Among the PEDOT functionalized anodes, GF-P attained the highest power density of 1.62 W/m^2 while CC-2P is the most efficient with 58.2% of total electron converted into electricity. The molecular biology analyses were carried for stable biofilms and *Geobacter* was found to be the dominant genera responsible for the electron production. The study was similarly successful when adopting real wastewater as a substrate. The generated electricity and COD removal by the modified anodes proved its capability in utilizing complex organic waste effectively. Thus, the synergy between optimum structural configuration and PEDOT loading is essential to attain an ideal anode with improved electrochemical characteristics as well as peak voltage generation as discussed in this present study.

ABSTRAK

Ketidakcekapan dalam pengendalian tenaga dan air membawa kesan negatif kepada alam sekitar. Oleh itu, penyelesaian yang mampan untuk mengatasi situasi ini adalah penting untuk kesinambungan dan pemuliharaan ekosistem untuk generasi akan datang. Dalam kebelakangan ini, sel fuel mikrobial (MFC) muncul sebagai teknologi yang berpotensi untuk mengintegrasikan penjanaan tenaga dan rawatan air sisa. Walaupun MFC telah menarik minat ramai penyelidik, ia mempunyai beberapa batasan yang perlu diatasi sebelum dapat diaplikasikan pada tahap praktikal. Kebanyakan limitasinya adalah disebabkan oleh komponen-komponennya seperti anod, biomangkin dan membran. Oleh itu, tesis ini bertujuan untuk menangani salah satu batasan ini iaitu anod. Objektif utama kajian ini adalah menghasilkan anod yang telah ditambahbaikkan untuk operasi MFC. Dua aspek yang berbeza telah disasarkan iaitu konfigurasi dan penyalutan anod dengan polimer konduktif. Tiga konfigurasi yang berbeza, iaitu plat, kain dan felt telah diaplikasikan untuk menyiasat pengaruh geometri dan morfologi permukaan ke atas prestasi anod. Bahagian kedua penyelidikan ini menumpukan kepada polimer konduktif, poli(3,4-ethylenedioxythiophene) (PEDOT) sebagai bahan salutan anod. Anod yang telah disintesis kemudiannya diaplikasikan ke dalam reaktor MFC dua-ruangan. Pengoptimuman kadar salutan PEDOT kepada ketiga-tiga konfigurasi telah dinilai melalui ciri-ciri elektrokimia, prestasi sistem dan kecekapan anod-anod ini. Selain itu, biofilm yang mengawal pengeluaran dan pemindahan elektron dalam sistem itu dikenalpasti pada peringkat genetik untuk mengesahkan genera mikrob yang bertanggungjawab untuk penjanaan elektrik. Biodiversiti antara anod-anod berbeza telah disiasat dan dibandingkan untuk menilai pengaruh PEDOT pada pemilihan biofilm yang merangsang operasi MFC tersebut. Anod optimum kemudiannya mengaplikasikan air sisa sebagai substrat untuk menilai keupayaan sistem untuk mengoksidakan molekul organik yang kompleks. Anod berkonfigurasi felt yang mempunyai struktur tiga dimensi

(3D) dan ruangan terbuka mencapai keputusan yang lebih memberangsangkan berbanding konfigurasi plat dan kain anod. Anod GF mencapai ketumpatan kuasa sebanyak 0.52 W/m^2 manakala GP dan CC mencatatkan 0.16 W/m^2 dan 0.35 W/m^2 masing-masing. GF juga mencatatkan kecekapan coulombic yang lebih baik pada 45.4% berbanding dengan kedua-dua GP dan CC yang hanya mencapai 39% dan 31%. Penyalutan PEDOT ke atas anod pelbagai konfigurasi meningkatkan prestasi anod dengan ketara. Kajian ini juga menyimpulkan bahawa setiap konfigurasi anod mempunyai kadar salutan optimum PEDOT dan keputusan persembahan yang berbeza. Antara anod yang diselaputi PEDOT, GF-P mencapai ketumpatan kuasa tertinggi 1.62 W/m^2 manakala CC-2P adalah yang paling efektif dengan 58.2% daripada jumlah elektron ditukar menjadi tenaga elektrik. Analisis biologi molekul telah dijalankan selepas pembentukan lapisan biofilm yang stabil dan *Geobacter* didapati merupakan genera dominan yang bertanggungjawab untuk pengeluaran elektron melalui mekanisme pemindahan elektron langsung. Kajian ini juga berjaya menggunakan air sisa sebenar sebagai substrat. Tenaga elektrik yang dijana dan pengurangan COD oleh anod-anod yang telah diubahsuai membuktikan keupayaan mereka dalam menggunakan sisa organik yang kompleks dengan berkesan. Oleh itu, sinergi antara konfigurasi struktur optimum dan penyalutan PEDOT adalah penting untuk mencapai anod yang ideal dengan ciri-ciri elektrokimia serta generasi voltan yang lebih baik seperti yang dibincangkan dalam kajian ini.

ACKNOWLEDGEMENTS

I would like to sincerely express my gratitude to various people who have travelled with me on this research period. I would like to express my deepest appreciation to my supervisor, Dr. Saravanan Pichiah, who has guided and encouraged me throughout this research. His optimism and insightfulness in times of difficulty has given me the confidence and determination to complete this undertaking. Special thanks to my co-supervisor, Prof. Shaliza Ibrahim for her continuous support and administration in various areas. Both their supervisions have been a major source of motivation and inspiration.

To my beloved sister, Melanie Kang, who has been morally (and financially) supporting me through these challenging times, I could never thank you enough. Your care and affection has given me comfort and solace during these times. To my parents who have been patient and kind, none of this would have been possible without the love and nurturing given to me throughout the years.

To all my friends and colleagues in the lab, your presence have brought laughter and joy in an otherwise dull and isolated research life. Particular appreciations to Anis, Atiqah, Azimatul, Dr. Azrina, Izzuddin, Dr. Leong, Ranjini, Shan, and Dr. Sim for exchanging research ideas and teaching me laboratory analysis methods and equipment. Heartfelt thanks to the technical staff, Mdm. Rozita Yusop and Ms. Alya Farhana who have made the laboratory a pleasant and safe place to work in. To all my friends and family that have that has given your support and encouragement in various ways, thank you. Your constant encouragement and reassurance means a lot to me.

Lastly, I would like to thank University of Malaya for giving me the opportunity, resources and education throughout the years.

TABLE OF CONTENTS

LIST OF FIGURES

LIST OF TABLES

LIST OF SYMBOLS AND ABBREVIATIONS

Symbols / Abbreviation		Meaning
%	:	Percentage
~	:	Approximate
°	:	Degree
°C	:	Degree Celsius
3D	:	Three dimensional
A	:	Ampere
AC	:	Activated carbon
AD	:	Anaerobic digester
Ag/AgCl	:	Silver/ Silver chloride
APHA	:	American Public Health Association
Au	:	Gold
b	:	Number of electrons exchanged per mole of oxygen
BES	:	Bioelectrochemical systems
BOD	:	Biological Oxygen Demand
$C_6H_{12}O_6$	:	Glucose
CC	:	Carbon cloth anode
C_c	:	Cathode capacitance
CC-2P	:	Carbon cloth with 5.0 mg/cm^2 PEDOT loading anode
CC-3P	:	Carbon cloth with 7.5 mg/cm^2 PEDOT loading anode
CC-P	:	Carbon cloth with 2.5 mg/cm^2 PEDOT loading anode
CE	:	Coulombic efficiency
CH_3COO^-	:	Acetate
$CH_3COONa.3H_2O$	:	Sodium acetate trihydrate

Cl	:	Chlorine
CNT	:	Carbon nanotube
CO_2	:	Carbon dioxide
COD	:	Chemical Oxygen Demand
C_P	:	Electrons converted to electricity
CPD	:	Critical point drying
CPE	:	Constant phase element
C_T	:	Total available electrons
Cu Kα	:	Copper K-alpha emission
CV	:	Cyclic voltammetry
DET	:	Direct electron transfer
DNA	:	Deoxyribonucleic acid
e^-	:	Electron
e.g.	:	For example
EDOT	:	3,4-ethylenedioxythiophene
EDS	:	Energy dispersive X-ray spectroscopy
EIS	:	Electrochemical impedance spectroscopy
EPA	:	Environmental Protection Agency
ERGNO	:	Electrochemically reducing graphene oxide
F	:	Faraday constant
Fe	:	Iron
$Fe(CN)_6]^{3-}$	:	Ferricyanide
$Fe(CN)_6]^{4-}$	:	Ferrocyanide
Fe(III)	:	Ferric ion
Fe_3O_4	:	Iron oxide
$FeCl_3.6H_2O$	:	Ferric chloride hexahydrate

FRA	:	Frequency response analyser
FTIR	:	Fourier Transform Infrared spectroscopy
g	:	Gram
GF	:	Graphite felt anode
GF-2P	:	Graphite felt with 5.0 mg/cm^2 PEDOT loading anode
GF-3P	:	Graphite felt with 7.5 mg/cm^2 PEDOT loading anode
GF-P	:	Graphite felt with 2.5 mg/cm^2 PEDOT loading anode
GN	:	Graphene
GO	:	Graphene oxide
GP	:	Graphite plate anode
GP-2P	:	Graphite plate with 5.0 mg/cm^2 PEDOT loading anode
GP-3P	:	Graphite plate with 7.5 mg/cm^2 PEDOT loading anode
GP-P	:	Graphite plate with 2.5 mg/cm^2 PEDOT loading anode
G–S	:	Graphene–sponge
h	:	Hour
H^+	:	Proton
H_2	:	Hydrogen gas
H_2O	:	Water
H_2O_2	:	Hydrogen peroxide
H_2SO_4	:	Sulphuric acid
HCl	:	Hydrochloric acid
HSO_4^-	:	Hydrogen sulphate ion
Hz	:	Hertz
I	:	Current
i.e.	:	That is
IEA	:	International Energy Agency

I_{sc}	:	Short circuit current
KCl	:	Potassium chloride
KNO_3	:	Potassium nitrate
L	:	Litre
LSV	:	Linear scan voltammetry
m	:	Metre
M	:	Mol per litre (molar)
MDOT	:	3,4-methylenedioxythiophene
MET	:	Mediated electron transfer
MFC	:	Microbial fuel cell
min	:	Minutes
Mn (II)	:	Manganese ion
MnO_2	:	Manganese dioxide
M_w	:	Molecular weight of O_2
N_2	:	Nitrogen
Na_2HPO_4	:	Disodium phosphate
NaCl	:	Sodium chloride
NaH_2PO_4	:	Monosodium phosphate
NH_4Cl	:	Ammonium chloride
$NH_4MgPO_4 \cdot 6H_2O$	:	Struvite
NHE	:	Normal Hydrogen Electrode
Ni	:	Nickel
O_2	:	Oxygen
OCP	:	Open circuit potential
OLED	:	Organic light emitting diodes
OsO_4	:	Osmium tetroxide

OTU	:	Operational taxonomic unit
PAAP-NN	:	Poly(aniline-co-m-aminophenol) nanowire network
PADAP-NN	:	Poly(aniline-co-2,4-diaminophenol) nanowire network
PANI	:	Polyanilines
PAOA	:	Poly(aniline-co-o-aminophenol)
PBS	:	Phosphate buffer solution
PD	:	Power density
PEDOT	:	Poly(3,4-ethylenedioxythiophene)
PMS	:	Power management system
POME	:	Palm oil wastewater effluent
PPy	:	Polypyrrole
Pt	:	Platinum
R_a	:	Charge transfer resistance of anode
R_c	:	Charge transfer resistance of cathode
RCF-PP	:	Reticulated Carbon Foam-Pomelo peel
R_{ct}	:	Charge transfer resistance
R_d	:	Finite diffusion resistance
RDP	:	Ribosomal Database Project
R_{ext}	:	External resistance
rGO	:	Reduced graphene oxide
R_{int}	:	Internal resistance
R_s	:	Solution resistance
RuO_2	:	Ruthenium oxide
R_Ω	:	Ohmic resistance
s	:	Second
SD	:	Standard deviation

SEM	:	Scanning electron microscope
SHE	:	Standard Hydrogen Electrode
SS	:	Stainless steel
SSFF	:	Stainless steel fibre felts
SSS	:	Stainless steel sheet
t	:	Time
TGA	:	Thermogravimetric analysis
Ti	:	Titanium
TiO_2	:	Titanium dioxide
UN	:	United Nations
UV-Vis	:	Ultraviolet–visible
V	:	Volt
v_{An}	:	Volume of the substrate in anode chamber
VFA	:	Volatile fatty acid
W	:	Watt
W	:	Warburg diffusion
Wt.%	:	Weight percentage
XRD	:	X-ray diffraction
Z	:	Impedance
Δ *COD*	:	Change in chemical oxygen demand
η_{act}	:	Activation overpotential
η_{conc}	:	Concentration overpotential
η_{ohmic}	:	Ohmic overpotential
Θ	:	Theta
π	:	Pi
Ω	:	Ohm

CHAPTER 1

INTRODUCTION

1.1 Overview

Scarcities of water and energy are the most threatening challenges experienced by global citizens. The interdependence of energy and water is irrefutable, as traditional power generation requires huge quantities of water while handling of water and wastewater are energy consuming. Water plays a vital role in almost all types of electricity generation methods. According to the International Energy Agency (IEA), ~15% of total global water are utilized by the energy sector and of these, 11% is lost through evaporation and transportation (IEA, 2012a). Although most of the utilized water is recycled, they are susceptible to contamination and thermal pollution that drastically distress the aquatic ecosystem (IEA, 2012a).

On the other hand, the treatment, transportation and delivery of both fresh and wastewater require around 2-3% of world's energy usage (EPA, 2008). This percentage is estimated to increase significantly as demand for both quality and quantity of drinking water continue to rise. The escalation of water usage certainly increases the production and subsequently the treatment of wastewater, which is an energy intensive process. For example, treatment of sewage alone requires ~0.018 kWh of energy per inhabitant (Svardal & Kroiss, 2011). Complex industrial wastewater would require higher energy consumption in line with stringent effluent standards. However, inefficient and energy-intensive treatment technologies are preventing most nations from effectively managing their wastewater. United Nations (UN) estimated that around 80-90% of wastewater in developing countries is released into water bodies without or with minimal treatment

(Corcoran, 2010). The consequences of these issues are not only limited to the environmental but also the socio-economic aspects. The exposure and contact with contaminated water diminishes the living quality, increase in the health care cost and deterioration in labour productivity of mostly the vulnerable groups of society. Hence, effective water and wastewater management is crucial for poverty eradication and economic progress as well.

Consequently, climate is heavily influenced by the massive production of energy through the release of greenhouse gases such as carbon dioxide (CO_2). The excess emissions of these gases are the cause for increase in global average temperature and climate change. Climate change has resulted in erratic metrological conditions across the globe. The rising atmospheric temperature causes increase in evaporation, precipitation, surface water temperature, severe floods and droughts, delay in seasonal change etc. (IEA, 2012b). These calamities are now recurring at higher frequency and are threatening the whole ecosystem.

From these arguments, it is very clear that energy and water are strongly reliant on each other. The constraints to either one will cause vulnerability to the other and the ineffective management of these two elements will trigger catastrophic effect on the environment and socio-economic factor.

1.1.1 Microbial Fuel Cell

Wastewaters rich in organic content have promising potential to be converted as fuel. It was estimated that ~17GW of energy is stored in these types of wastewater, compared to ~15GW which is currently needed to treat them (B. E. Logan & Rabaey, 2012). It is very clear from the numbers that the stored energy is not extracted and instead, additional energy is used to treat them. Hence, new treatment technology has to be

implemented for simultaneous wastewater treatment and energy recovery. Microbial fuel cell (MFC) is one such technology that is capable of concurrently treating the wastewater and extracting the energy stored in the wastewater.

MFC is a category of fuel cell that is capable of converting the stored chemical energy of substrate into electrical energy through microbial catabolism process. These microorganisms are classified as "exoelectrogen" as they are able to transfer electrons outside their cells from oxidation reaction. The electrons are collected by the anode and transferred through an external circuit to the cathode where reduction reaction takes place. The movement of these electrons form the basis for generation of electrical energy in a MFC system (B.E. Logan, 2009). MFCs are capable of generating energy, treat pollutants and recover resources from various types of wastewater. This technology is ideal in reducing significant amount of energy consumption without compromising wastewater treatment efficiency. However, MFC is still in its infant stage of development as many of its limitations needs to be overcome before possible commercial implementation.

1.2 Problem Statement

This research focuses on the enhancement of anode as it holds the key to improve the power production of MFC. Anodes in MFC influence the biofilm formation as well as the collection and transfer of electrons released from the microorganism to the anode (C. Li, Zhang, Ding, Ren, & Cui, 2011). Hence, it is very clear that characteristics of anode must support microbial growth and attachment along with efficient electron collection and transfer. Properties like excellent biocompatibility, mechanical and chemical stability, large surface area, good conductivity and cost efficient are the common characteristics of an ideal anode. In general, materials like paper, cloths, foam,

felt, fibres and granules of carbon or graphite materials were generally employed as anode (Cai, Wang, Bu, & Zhong, 2013; B. E. Logan, 2008).

Electrodes can be differentiated by their structure into two categories; that is planar and three-dimensional (3D) (Wei, Liang, & Huang, 2011). Examples of planar materials such as paper and sheet are brittle and smooth while cloth materials are more flexible and has coarser surface. 3D electrodes such as foam and felt materials have higher surface area and pores that promotes bacterial growth and adhesion. However, due to their thick structure, the mass transfers of reactants and products on these materials are restricted. The accumulations of biomass could subsequently clog the inner surfaces of the material and thereby reduce the durability of these electrodes (Ghasemi et al., 2013). In short, every material has their own pros and cons that have to be considered based on their application and reactor design.

The utilization of unmodified or untreated carbon electrodes is still inadequate in terms of electrochemically active surface area and biocompatibility (C. Zhang, Liang, Jiang, & Huang, 2015). Specific modifications are necessary to enhance their overall performance as anode. Coatings on carbon-based materials are one of the possible methods to improve these electrodes. Attempts have been made using mediators, metal, polymers and composite of these materials (Godwin & Evitts, 2011; Wei et al., 2011). Simultaneously, conductive polymers as potential coating substance on carbon electrodes for MFC application has gain interest owing to their conductivity and environmental durability (C. Li et al., 2011). Conductive polymer such as polypyrrole (PPy), polyanilines (PANI) and their composites have been successfully applied on MFC electrodes (Cui, Du, Guo, Zhu, & Luong, 2015; C. Feng et al., 2010; Tang, Li, Du, Wang, & Ng, 2015). These reports substantiated the addition of conductive polymer for the improvement of MFC power production. However, these conductive polymers are not

stable over long-term operational condition and have low conductivity in neutral conditions.

Poly(3,4-ethylenedioxythiophene) or commonly known as PEDOT is considered to be an promising alternative that enhances the functionality of the anode. It is a highly conductive material which is stable and economical compared to the other conductive polymers (Abdiryim, Ubul, Jamal, Xu, & Rahman, 2012; Y. Wang, Zhao, Sun, Zhang, & Zhu, 2013). However, the efficacy of this material is not much investigated as an additive for anode. Y. Wang et al. (2013) and X. Liu, Wu, and Gu (2015) have successfully applied electropolymerized PEDOT on carbon-based anode for MFC application. Yet, there is still inadequate research on chemically or oxidative polymerized PEDOT, which is a more cost-effective and facile synthesis approach. Few research groups successfully implemented chemical polymerized PANI and PPy but to this point, there is a vacuum in employing PEDOT obtained through this method in MFC research (Gnana kumar et al., 2014; Hou, Liu, & Li, 2015).

Hence, this investigation reports on the synthesis of PEDOT using chemical polymerization as potential anode enhancer in MFC. Three base anode materials of different morphology were selected namely graphite plate, carbon cloth and graphite felt. The present study emphasized on the contribution of PEDOT as well as the impact of morphological and structural influence on the anode for improving the electrochemical and overall MFC performance.

1.3 Objectives of Research

The main aim of this research is to evaluate and develop improved anode for MFC application. Two different aspects are focused upon, that are (1) structural configuration of the anode specifically planar and 3D anodes as well as (2) functionalizing conductive

polymer for the enhancement of anode properties. This research discloses the relationship between physical structural configuration and conductive polymer coating towards the performance of MFC.

The specific objectives of this work are:

1. **Influence of Anode Structural Configuration:** To investigate the influence of anode configuration and its geometry for various electrochemical characteristics and electricity generation
2. **Functionality of PEDOT as Anode Enhancer:** To investigate the applicability of a conductive polymer, poly(3,4-ethylenedioxythiophene) (PEDOT) for stimulating the electron mobility and biofilm formation.
3. **Optimisation of Anode Enhancer:** To evaluate and optimize the electrochemical characteristics, system performance and efficiency of the modified anodes under varied PEDOT loading.
4. **Characterization of biodiversity:** To genetically classify the microbial genera present in the adopted inoculum and biofilm that contributed for the electricity generation.
5. **Interaction of Modified Anodes with Biofilm:** To evaluate the influence of PEDOT on exoelectrogen selection and the electron transfer mechanism of the classified biofilm that stimulate the MFC operation.

1.4 Thesis Outline

Chapter 1 of the thesis provides the general overview on the energy and water crisis followed by their effect on climate change. The urgent need for energy efficient wastewater treatment system is then discussed. This is followed by a brief note on MFC

and its limitations. The chapter ends with specific research hypothesis and objectives that aims to resolve the restrictions on MFC technology focusing on the anode component.

Chapter 2 starts with the elaboration on the basic principles and development of MFC. The chapter also expounds on studies by various researchers on the performances of different anode configuration and modification specific to MFC application. A general review on the different types of conductive polymers was also reported. It also presents the reviews on the electron transfer mechanisms and biofilm characteristics commonly found in MFC system. The chapter ends with feasibility of MFC for real time applications in niche areas as an indication of the future direction of this technology.

Chapter 3 discusses the synthesis method of the conductive polymer followed by coating techniques onto different base anodes. The chapter also narrates on the various analytical instruments applied for the characterization of synthesized materials as well as the specification of MFC reactor and experimental conditions employed throughout the study. The chapter is concluded by a brief explanation on the molecular biological methods adopted in characterizing the biofilm.

Chapter 4 imparts the results of the experiments performed to achieve the research objectives. The characterization, electrochemical analyses and substrate utilization performances of the synthesized conductive polymer and modified anodes were comprehensively analyzed and discussed. The chapter also demonstrates the outcome of the molecular biological analyses of the microbial consortium responsible for the MFC performances.

Chapter 5 recapitulates the significant outcome of the thesis and recommendations for future studies to overcome the drawbacks of the present study.

CHAPTER 2

LITERATURE REVIEW

2.1 Bioelectrochemical System

Bioelectrochemical systems (BES) are systems that are capable of using biological interactions to catalyse electrochemical reaction (Pant et al., 2012). In recent years, BES has emerged as one of the promising technology for energy recovery and environmental remediation. The characteristic that distinguish BES is the application of biocatalyst to instigate oxidation and reduction reactions. BES can be further categorised by their biocatalysts that are either enzymatic or microbial (Osman, Shah, & Walsh, 2011). Unlike traditional fuel cell, BES operates at mild conditions with diverse biological components and variety of fuels, thus expanding its range of application (Pant et al., 2012; Schroder, 2007). Recent advancement in BES has increased its potential to a wide range of applications and it has been investigated for various usage like electricity generation, biodegradation product, recovery and synthesis. This specific study focused on one of the two subset of BES i.e., MFC.

2.2 Basic Working Principle of MFC

Fuel cell converts chemical energy to electrical energy through redox reaction. The oxidation of fuel, such as hydrogen at the anode was supported by a catalyst e.g. platinum, Pt while reduction of oxygen takes place at the cathode resulting in water molecule (B.E. Logan, 2009). There are different classifications of fuel cell but their fundamental working principles are generally the same and usually consists of three

principal components i.e. the anode, cathode and electrolyte. Direct methanol fuel cell, proton exchange membrane fuel cell and solid oxide fuel cell are types of fuel cells that are available commercially while others are still under research and development (Badwal, Giddey, Munnings, Bhatt, & Hollenkamp, 2014).

MFC is one of the fuel cell that is still in its development stage. The most defining characteristic of the MFC is the anode catalyst, where microorganism is used as biocatalyst for the redox reaction. These species are capable of generating and transferring electrons outside their cell membrane and are denoted as "exoelectrogenic" bacteria (Franks & Nevin, 2010). Once the electrons are transferred to the anode, they are mobilised to the cathode through an external circuit. These electrons reduce the catholyte and protons at the cathode chamber, completing the redox reaction. A schematic of the MFC operation is illustrated in Figure 2.1.

The reactions that take place at the anode are shown in Equation (2-1) and (2-2) respectively for glucose and acetate as substrate. The reaction on the cathode chamber with oxygen and ferricyanide are represented in Equation (2-3) and (2-4) correspondingly. If the cathode chamber adopts anaerobic condition, hydrogen gas (H_2) is produced as shown in Equation (2-5). However, this reaction is not spontaneous and additional potential is needed for its occurrence.

$$C_6H_{12}O_6 + 6H_2O \rightarrow 6CO_2 + 24H^+ + 24e^- \quad (2\text{-}1)$$

$$CH_3COO^- + 2H_2O \rightarrow 2CO_2 + 7H^+ + 8e^- \quad (2\text{-}2)$$

$$O_2 + 4H^+ + 4e^- \rightarrow 2H_2O \quad (2\text{-}3)$$

$$Fe(CN)^{3-} + e^- \rightarrow Fe(CN)^{4-} \quad (2\text{-}4)$$

$$2H^+ + 2e^- \rightarrow H_2 \quad (2\text{-}5)$$

Lovley (2008) reviewed that electricity production through biological methods has great viability as bioenergy source as they can harvest electrons from a large pool of organic wastes and renewable biomass. However, the present prospect of MFC is still far from realistic application.

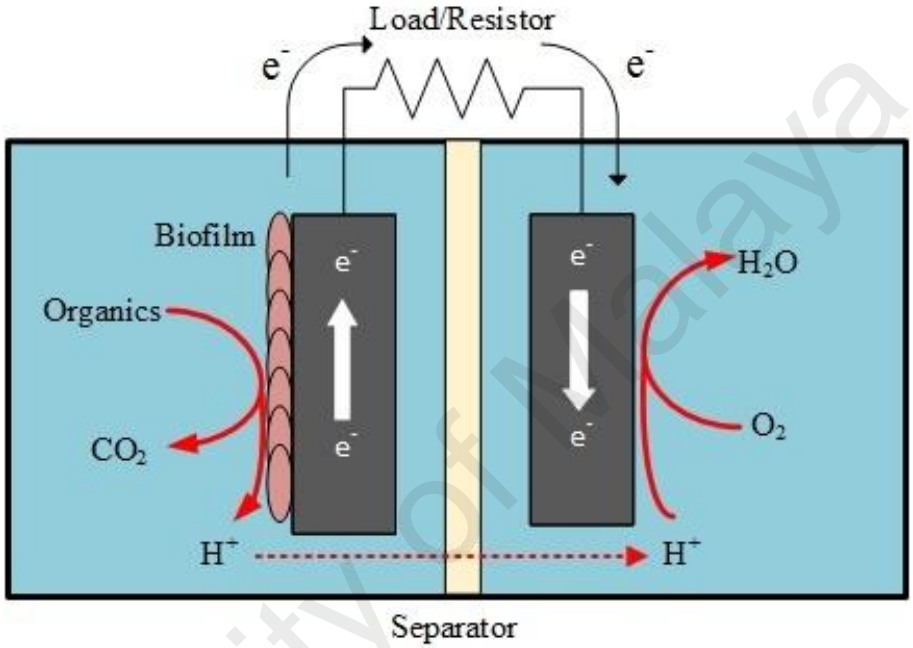

Figure 2.1: Schematic of Microbial Fuel Cell Reactions

2.3 Development of MFC

The electricity generation through microorganism was first ever reported by M.C. Potter in 1911 in the Proceedings of Royal Society of London (M. Zhou, Chi, Luo, He, & Jin, 2011). A general hypothesis during that period was "any physiological process accompanied by chemical changes involves an associated electrical change" (Potter, 1911). Early studies implicated that metabolism process of macro-organism produces electrical changes. Hence, Potter hypothesised that fermentation or the decomposition of organic compound would result in similar effect. In 1931, Barnett Cohen successfully observed the substrate reduction during bacteria growth potentiometrically in the form of

a half-cell. Although Potter has instigated the first step into MFC, it was not taken into serious consideration until 1970s (Min, Cheng, & Logan, 2005). The earlier development mostly focused on the use of pure bacteria strains and simple molecules like glucose and acetate as fuel. Habermann and Pommer (1991) was the first to demonstrate the implication of complex organics in the form of domestic wastewater as fuel. The application of wastewater as a fuel signified the feasibility of MFC for wastewater treatment process. However, their operation was delimited owing to the unsustainable use of mediators, high component cost and low efficiency. In the last two decades, the MFC has seen various improvements in reactor configuration and materials. Efforts on scaling-up of MFC also have encountered various complications. MFCs with large operating capacity was found to be inefficient and suffered from multiple setbacks. Their current and power density performances were not comparable with the results obtained from lab-scale model. Alternatively, stacked MFC (multiple MFCs connected either in series or in parallel) were found to be a better design assembly for large-scale applications. However, the congestion of matrix resulted in voltage reversal and system failure (An, Kim, Chang, & Lee, 2015; B. E. Logan, 2010; Oh & Logan, 2007).

In recent years, the MFC application has seen pragmatic shift in research direction. Power generation is no longer the main emphasis of MFC performance and application. Instead, many researchers attempt to increase the viability of MFC in niche areas such as biosensors and biorecovery (Fraiwan, Mukherjee, Sundermier, Lee, & Choi, 2013; B. Liu, Lei, & Li, 2014; L. J. Zhang et al., 2012). Advancement has been made for MFC-based biosensors to detect volatile fatty acid (VFA) and biological oxygen demand (BOD) (Chang et al., 2004; Kaur et al., 2014). Biorecovery is also one of the promising applications for MFC technology where metals such as copper, silver and gold (Au) are successfully recovered through reduction of metal ions at the cathode (Choi & Cui, 2012; Choi & Hu, 2013; Lu et al., 2015; Motos et al., 2015). This is specifically appropriate for

treating wastewater generated from mining, metallurgical, electronics as well as jewellery industries. The recovery of these metals propagates the advancement of this technology into the commercial sector as the monetary benefits of biorecovery outweighs the electricity generation. Non-metals were also recovered using the same principle. The retrieval of struvite ($NH_4MgPO_4 \cdot 6H_2O$), a phosphate mineral from nitrogen and phosphorus rich wastewater has been gaining attention as there has been diminishing supply of phosphorus. The recovery of struvite using swine wastewater and urine were demonstrated by Ichihashi and Hirooka (2012) and Zang et al. (2012) respectively. These biorecovery processes enhanced the functionality of MFC and increased its market value as both a power production and mineral recovery technology.

The above discussion substantiates that MFC has high potential not just in electricity generation but also in various niche areas. It is evident that MFC is a robust, flexible and versatile system that finds application in numerous fields. One review states "…the commercial viability of MFC will rely on side benefits and not purely on the generation of electrical power" (F. Zhao, Slade, & Varcoe, 2009).

2.4 Overpotentials in MFC system

The theoretical thermodynamic potential attainable by MFC when using O2 as catholyte is 1.1 V (B. E. Logan et al., 2006). However, due to energy losses in various components, the actual measured voltage in MFC is much lower than the hypothetical value. These losses are described as overpotentials or overvoltages and can be categorized into activation, concentration and ohmic resistance. Hence, the experimental voltage obtained can be represented by Equation (2-6) where E_t denotes the theoretical potential and the η_{act}, η_{conc} and η_{ohmic} are due to activation, mass transfer and ohmic overpotentials respectively (He & Mansfeld, 2009; B. E. Logan et al., 2006).

$$V = E_t - \eta_{act} - \eta_{conc} - \eta_{ohmic} \quad (2\text{-}6)$$

Additionally, due to the presence of bacteria in the MFC system, the losses incurred by bacterial metabolic activity were also taken into consideration. The losses are well described in literatures and a brief summary are stated below (B. E. Logan et al., 2006; P. Y. Zhang & Liu, 2010):

Activation or charge transfer losses: Activation energy is demanded to initiate electron transfer during the redox process and is affected by the reaction kinetics at the electrodes. This activation energy is solely used by the redox process and hence is categorized as a loss. It is significant at low currents and decreases as current increases. Electrode plays a vital role in decreasing this overpotential. A high surface area and better catalytic ability of the electrode can reduce activation loss.

Concentration losses: Concentration loss generally involves the exhaustion of redox species near the electrode surface. This loss occurs for fast electrochemical reactions, causing substrate concentration near the electrode surface to be lower than the bulk solution. This overpotential happens mainly during high current density where insufficient amount of reduced ions are supplied to the anode. The concentration losses increased gradually with current and spiked up when approaching a certain current that is referred as limiting current (P. Y. Zhang & Liu, 2010).

Ohmic resistance: It is the resistance towards the flow of electrons in the MFC system and is usually proportional to current. These include the flow of electrons through the electrolytes, electrodes, interconnections and membrane. The materials and reactor configuration used in the MFC will greatly affect this resistance. B. E. Logan et al. (2006) suggest minimizing the electrode spacing; increasing electrolyte conductivity and using a low resistance membrane could reduce this ohmic resistance.

Bacterial Metabolic Losses: The respiration of anaerobic bacteria uses compound other than oxygen as their terminal electron acceptor. These electrons are transported from low to high potential substance or material. In MFC, anode acts as the terminal electron acceptor and substrate as the donor. Hence, the bacterial is capable to gain more energy owing to the wide potential difference between these acceptors and donors. However, bacteria use this energy for its survival rather than for power generation. Stabilising the anode potential to more negative could decrease this loss.

By understanding the factors affecting the internal resistance present in the MFC system, approaches that are more systematic can be carried out in order to overcome these limitations.

2.5 Electrodes in MFC

Electrodes play an essential role in determining the viability of MFC systems. They can influence the performance and overall capital cost of the system (Wei et al., 2011). Hence, electrodes are the major component in determining the efficiency of the system. The basic characteristics of good electrodes include high conductivity, corrosion resistance, and high surface area and scalable (B. E. Logan, 2008). Electrodes that promote biofilm immobilization must be biological compatible and possess rough surface area whereas abiotic electrodes require the application of catalyst. A few categories of electrode improvements include coating, chemical and heat treatment (Cheng & Logan, 2007; Chou, Lee, Lee, Tai, & Chang, 2014; Y. Feng, Yang, Wang, & Logan, 2010; Lv, Xie, Yue, Feng, & Wei, 2012; Zhou, Chi, Wang, & Jin, 2012).

Carbonaceous materials are the most widely used electrode materials. This is due to their robust resistance against chemicals and corrosion. Carbonaceous materials are also highly conductive, cost effective and biocompatible. Multiple forms of carbon have

been successfully applied as electrodes such as carbon, graphite, reticulated vitrified carbon, graphene, carbon nanotube, carbon nanofiber and activated carbon (D. Jiang & Li, 2009; Xiao et al., 2012). Although metal and its oxide are more conductive, they are highly corrosive and have smooth surface area. (Ozkaya et al., 2012). Some of the metal and its alloys that have been successfully applied as MFC anode include Au, titanium (Ti) and stainless steel (SS) (Pocaznoi, Calmet, Etcheverry, Erable, & Bergel, 2012; Richter et al., 2008; ter Heijne, Hamelers, Saakes, & Buisman, 2008). However, there is no concluding result indicating which electrode material is superior to the other. Aside from material properties, surface and structural modification in addition to coatings on electrodes have also been widely researched. Certain modifications have found to increase the performance of the system tremendously and notable findings are discussed below.

2.5.1 Electrode structure

Electrodes can be distinguished by their structure into two categories; planar and 3D assemblies (Wei et al., 2011). Most conventional laboratory electrodes are of planar structure e.g. paper, cloth, mesh, plates or sheets. It is evident that structures with rough surfaces accomplish better power generation e.g. cloth and mesh materials. These characteristics promote better biofilm growth and adhesion. 3D structures are materials with considerable thickness such as packed beds, brush, felt, foam and sponges. These electrodes have higher surface area compared to planar electrodes that facilitates in better biofilms growth. However, their dense structure might pose a problem to the mass transfer of reactants and products into the inner surfaces of these materials (Chou et al., 2014; Wei et al., 2011). The presence of dead zones, decrease in porosity, clogging and other complications also prevails in 3D electrodes after long-term operation (B. E. Logan, 2008). For instance, brush structures have efficient current collection and high porosity

but the formation of conductive network between the individual fibres in order to create a fully conductive electrode structure is still a challenge (B. E. Logan, Cheng, Watson, & Estadt, 2007). Although these materials showed good power generation, the durability of electrodes should be further investigated.

Currently, materials that have high surface area along with macro-porous structure such as sponge, felt or foam are gaining popularity as MFC anodes. The macro-pores enable bacteria to grow and attach on the material without blocking the entire pore (Xie, Yu, et al., 2012). Furthermore, the mass transfer restrictions are also reduced owing to their open structure. Other aspects such as flexibility, cost and stability of the electrode materials have to be taken into consideration equally.

A summary of some of these findings are tabulated in Table 2.1. Generally, electrode with high surface area and 3D configuration performed better compared to flat or planar electrodes. The maximum power density or short-circuit current density, I_{sc} reported was per area of said electrode unless stated otherwise

Table 2.1: Various Anode Configurations for MFC Application

Electrode Configuration	Operating Conditions	Maximum Power Density/ I_{sc}	References
Graphite block Graphite sheet Carbon cloth Carbon fibre reinforced plate	Glucose, *Pseudomonas aeruginosa* , Two chamber	▪ Graphite block: 392.04 mW/m^2 ▪ Graphite sheet: 274.7±11.6 mW/m^2 ▪ Carbon cloth: 132.9±179.1 mW/m^2 ▪ Carbon fibre reinforced plate: 42.1±7.9 mW/m^2	Jayapriya and Ramamurthy (2014)
Graphite fibre brush Woven carbon mesh	Domestic wastewater, Mixed culture, Single chamber	▪ Graphite fibre brush : 230 ± 9.3 mW/m^{2*} ▪ Woven carbon mesh : 45 ±12 mW/m^{2*}	Hays, Zhang, and Logan (2011)
CNT–sponge	Glucose, Mixed culture, Two chamber	▪ CNT sponge: 1990 mW/m^2	Xie, Ye, et al. (2012)
Reduced graphene oxide–nickel foam (rGO–Ni)	Trypticase soy broth (TSB), *Shewanella oneidensis* MR-1, Two chamber	▪ rGO-Ni: 661 W/m^{3†} ▪ Carbon cloth: 42 W/m^{3†} ▪ Plain Ni foam: 35 W/m^{3†} ▪ Carbon felt: 23 W/m^{3†} ▪ Carbon paper: 12 W/m^{3†}	H. Wang et al. (2013)
rGO–CNT on melamine sponges or stainless steel sheet (SSS)	Glucose with methylene blue, *Escherichia coli*, Two chamber	▪ rGO–CNT sponge:~ 500 mA/m^2 ▪ SSS coated with rGO–CNT ink: 400 mA/m^2 ▪ SSS: 200 mA/m^2	Chou et al. (2014)

* Per cathode area
† Per anode chamber volume

Table 2.1, continued

Electrode Configuration	Operating Conditions	Maximum Power Density/ I_{sc}	References
Graphene–sponge (G–S) composite on stainless-steel (SS)	Glucose, Mixed culture, Two chamber	▪ G-S-SS: 1570 mW/m^2 ▪ G-S: 111 mW/m^2 ▪ SS: negligible	Xie, Yu, et al. (2012)
Ni-coated polyurethane sponge	Glucose, Mixed culture, Two chamber	▪ Ni coated sponge : 996 mW/m^2 ▪ Carbon paper: 910 mW/m^2	X. Liu et al. (2013)
Carbon nanoparticles; Graphene: GN Carbon nanotube: CNT Activated carbon: AC Carbon cloth: CC on stainless steel fibre felts (SSFF)	Acetate, Mixed culture, Two chamber	▪ GN-SSFF: 2142 mW/m^2 ▪ CNT-SSFF: 1280 mW/m^2 ▪ AC-SSFF: 560 mW/m^2 ▪ GN/CC: 1014 mW/m^2 ▪ SSFF: 0.8 mW/m^2 ▪ CC: 476 mW/m^2	J. Hou, Liu, Yang, and Zhou (2014)
SS with different configuration (smooth, macro-structured or micro-structured)	Acetate, Mixed culture, Three electrode half cell	▪ SS : 20600 mA/m^2 (no significant difference between different configuration of SS) ▪ Flat graphite: 9500 mA/m^2 ▪ CC: 3700 mA/m^2	Pocaznoi et al. (2012)
Reticulated Carbon Foam prepared by Pomelo peel (RCF-PP)	Acetate, Mixed culture, Three electrode half cell	▪ RCF-PP: 1.81 ± 0.15 mA/cm^2 ▪ Reticulated Vitreous Carbon : 2.39 ± 0.19 mA/cm^2 ▪ Graphite felt: 1.79 ± 0.09 mA/cm^2	Chen et al. (2012)

2.5.2 Coatings

Coating to the base materials of electrodes is one of the electrode enhancements techniques. These coatings are added to enhance the conductivity and catalytic activity of electrodes especially carbon electrodes which lacks in electrocatalytic properties (C. Zhang et al., 2015). Some of the coatings that are being experimented are CNTs, graphene, mediators, metals and composites of these materials (Godwin & Evitts, 2011; C. Li et al., 2011).

Conductive polymer coatings have shown to improve the performance of electrode. Among the conductive polymer coatings that have been attempted in MFC, electrodes are PPy and PANI (C. Feng et al., 2011; C. Li et al., 2011). These conductive polymers were coated onto electrode base material as itself or as a composite material. Carbonaceous materials such as graphene, carbon black and CNT have been successfully coated with conductive polymer to form composite electrode (B. Hou, Hu, & Sun, 2012; J. Hou, Liu, & Li, 2015; Yuan, Ahmed, & Kim, 2011). Mediator such as poly(methylene blue) is also added to PANI to form immobilised mediator composite electrode (Godwin & Evitts, 2011). The advantages of conductive polymer coatings are the increased surface area and electrochemical capacitance on the electrodes (J. Hou et al., 2015; C. Li et al., 2011). The different surface functional groups of the conductive polymer were found to change the community of biofilm attached to the anode (C. Li et al., 2011).

However, there are certain limitations to these conductive polymers in terms of operational conditions and durability. For example, PANI has low conductivity and electrochemical reactivity at pH > 4. Hence, it is suitable only for substrate with low pH. (Lai et al., 2011; J. Zhang, Shan, & Mu, 2007). On the other hand, the biggest drawbacks of PPy are the toxicity and high vapour pressure. The intense colour and poor transparency also hinders the usage of PPy in various industries.

One of the possible alternative conductive polymer is the PEDOT. PEDOT and its composites are ideal research material because of their stability and robustness. PEDOT possess electrocatalytic property that enhances various electrochemical reactions. In recent years, it is used to improve the lifespan of electrodes in batteries and fuel cells as a replacement for platinum electrode. Detailed information on the development and commercial application of this material will be discussed in the next section.

In general, the durability, stability and cost effectiveness of PEDOT makes it a viable candidate as an electrode additive. However, the studies pertaining to the coating of PEDOT is scant. Hence, one of the objectives of this research is to investigate the performance of PEDOT coated anode in MFC system. Some of the past researches on various types of coating are tabulated in Table 2.2 and conductive polymers specifically are tabulated in Table 2.3. It is evident from the tables that the coatings on MFC electrodes improved the performances drastically.

Table 2.2: Various Coatings Used For MFC Anodes

Coating on Electrode	Operating Conditions	Maximum Power Density/ I_{sc}	References
Electrodeposited manganese dioxide (MnO_2) on carbon felt anode	Acetate, Mixed culture, Two chamber	▪ Modified: 3580 ± 130 mW/m^2, ▪ Control: 2870 mW/m^2	C. Zhang et al. (2015)
Nano-molybdenum carbide/CNT on carbon felt	Glucose, *Escherichia coli*, Single chamber	▪ Modified: 1050 ± 26.4 mW/m^2 ▪ Control : 80 ± 24.1 mW/m^2	Y. Wang, Li, Cui, Xiang, and Li (2014)
Iron oxide (Fe_3O_4)/CNT on carbon paper	Glucose, *Escherichia coli*, two chamber	▪ Modified: 830mW/m^2	I. H. Park, Christy, Kim, and Nahm (2014)
Titanium dioxide (TiO_2) nanoparticles-decorated CNT on carbon cloth	Acetate, Mixed culture, Two chamber	▪ TiO_2@CNTs: 1120 mW/m^2, ▪ TiO_2-MFC : 670 mW/m^2 ▪ CNTs-MFC: 730 mW/m^2	Wen et al. (2013)
Ruthenium oxide-coated (RuO_2) carbon felt	Lactate, Mixed culture, Two chamber	▪ Modified: 3080 mW/m^2 ▪ Control: 180 mW/m^2	Lv et al. (2012)
Ti-TiO_2	Glucose, Mixed culture, Two chamber	▪ Modified: ~ 2300 mW/m^2 ▪ Control: ~9.2 mW/m^2	Ozkaya et al. (2012)
Biocompatible chitosan and vacuum-stripped graphene	Glucose, *P. aeruginosa*, Two chamber	▪ Modified : 1530 mW/m^2 ▪ Control (carbon cloth): 19.5 mW/ m^2	He, Liu, Qiao, Li, and Tan (2012)

Table 2.3: Various Conductive Polymers Used for MFC Anodes

Conductive Polymer Coating on Electrode	Operating Conditions	Maximum Power Density/ I_{sc}	References
Electrodeposited PANI Modified SSFF	Acetate, Mixed culture, Two chamber	▪ Modified: 360 mW/m^2 ▪ Control : 0.8 mW/m^2	J. Hou et al. (2015)
Electropolymerized PANI on macroporous graphite felt followed by the electrophoretic deposition of CNTs	Acetate, *Shewanella putrefaciens*, Two chamber	▪ Modified: 257 mW/m^2 ▪ Control: 49 mW/m^2	Cui, Du, Guo, Zhu, and Luong (2015)
PANI modified by ethylenediamine on carbon paper	Glucose, Mixed culture, Two chamber	▪ Modified: 136.2 mW/m^2	Ghasemi et al. (2013)
Electrochemically reducing graphene oxide (ERGNO)/PANI nanocomplex on carbon cloth	Acetate, Mixed culture, Two chamber	▪ PANI/ERGNO/CC: 1390 mW/m^2 ▪ ERGNO/CC: 1003 mW/m^2 ▪ Control: 468 mW/m^2	J. Hou, Liu, and Zhang (2013)
PANI and poly(aniline-co-o-aminophenol) (PAOA) on carbon felt	Acetate, Mixed culture, two chamber	▪ PANI: 27.3 mW/m^2 ▪ PAOA: 23.8 mW/m^2 ▪ Control: 20.2 mW/m^2	C. Li et al. (2011)
HSO_4^- doped PANI modified carbon cloth anode	Acetate, Mixed culture, Two chamber	▪ Modified: 5.16 W/m^{3†} ▪ Control: 1.94 W/m^{3†}	Lai et al. (2011)

† Per anode chamber volume

Table 2.3, continued

Coating on Electrode	Operating Conditions	Maximum Power Density/ I_{sc}	References
Nanostructured PANI/TiO_2 Composite Anode on Ni foam	Glucose, *Escherichia coli*, Two chamber	▪ Modified: 1495 mW/m^2	Qiao et al. (2007)
Electropolymerized poly(aniline-co-2,4-diaminophenol) nanowire network (PADAP-NN) and poly(aniline-co-m-aminophenol) nanowire network (PAAP-NN) on carbon plate	Starch, Mixed culture, Two chamber	▪ PAAP-NN : 0.28 mW/cm^2 ▪ PADAP-NN : 0.27 mW /cm^2 ▪ PANI-NN : 0.18 mW/cm^2 ▪ Control : 0.028 mW /cm^2	Y. Zhao, Nakanishi, Watanabe, and Hashimoto (2011)
PPy/ GO composites on the graphite felt	Lactate, *Shewanella oneidensis* MR-1, Two chamber	▪ PPy/GO-GF: 1326 mW/m^2 ▪ PPy-GF : 1100 mW/m^2 ▪ Control : 166 mW/m^2	Lv et al. (2013)
In-situ chemical polymerization PPy coated CNTs composite on carbon paper	Glucose, *Escherichia coli*, Two chamber	▪ Modified: 228 mW/m^2	Zou et al. (2008)
Electro-polymerized PEDOT on carbon cloth	Marine broth, *Shewanella loihica* strain PV-4, Two chamber	▪ Modified: 140 mW/m^2 ▪ Control: 98 mW/m^2	X. Liu, Wu, and Gu (2015)
GN/PEDOT on carbon paper	Glucose, *Escherichia coli*, Two chamber	▪ Modified: 873 mW/m^2 ▪ Control: 55 mW/m^2	Y. Wang, Zhao, Sun, Zhang, and Zhu (2013)

2.6 Intrinsically Conductive Polymer

The significance of the discovery of conductive polymer in 1977 was substantiated by awarding Nobel Prize in Chemistry to Professor Heeger, MacDiarmid and Shirakawa "for the discovery and development of conductive polymers" in 2000. Conductive polymers are organic compounds that possess inherent electrical conductivity characteristic i.e. without the addition of other metallic materials. They consist of polymer backbone with delocalised p_z orbitals due to their overlapping sp^2 hybridized orbital. Hence, they are also known as π-conjugated polymers. The electrons on these orbitals are highly mobile when these orbitals are partially filled. This is achieved by removing or adding some electrons to the orbital through doping. However, most of the doping for these conductive polymers is done by removing electron or oxidative doping to form p-type materials.

Conductive polymer can be classified into few categories depending on their molecular structure. Their main structure may consists of aromatic ring, double bond or a combination of both. Additionally, these polymers are also categorized by the presence of heteroatoms. Some of the more established conductive polymers are poly(acetylene), poly(p-phenylene vinylene), PPy, PANI and PEDOT. As this research focuses on the incorporation of PEDOT onto MFC anodes, more information on this conductive polymer is discussed in the following section.

2.6.1 PEDOT

By the late 1980s, several conductive polymers have emerged such as PANI, PPy, polythiophene, polyacetelyne and their derivatives. Conductivity has reached remarkable high levels of 100,000 S/cm, achieved by stretched iodine-doped polyacetylene (Elschner, Kirchmeyer, Lovenich, Merker, & Reuter, 2010; Naarmann & Theophilou,

1987). However, due to the instability of the carbenium ions in presence of oxygen and humidity caused the conductivity of these polymers to deteriorate and rendering them inapplicable anywhere (Billingham & Calvert, 1989; Münstedt, 1988). The breakthrough came when doped PEDOT was discovered. The molecular structure of PEDOT is illustrated in Figure 2.2.

The stability of PEDOT lies in the bicyclic ring system of its monomer, EDOT. Initial investigations revealed that alkoxy groups stabilize doped polythiophenes due to further electron delocalization (Elschner et al., 2010). From this observation, researchers at Bayer AG, Germany decided to expand the structure of thiophene by adding dialkoxy ring. The purpose of this is to both extend the resonance stabilization effect and reduce the steric effect. In order to achieve these conditions, one of the earlier attempt was to synthesize MDOT (3,4-methylenedioxythiophene) compound. However, the polymerization of this monomer was unsuccessful. Further research then led to the development of EDOT and consequently PEDOT in 1988. PEDOT recorded high conductivity and more importantly was stable in the presence of oxygen and water. This discovery catalysed massive scientific investigation and various industrial applications for PEDOT. Some of the notable examples are capacitors, anti-static coatings and organic light emitting diodes (OLEDs). Over the years, limitations of PEDOT were amended through the incorporation of different types of PEDOT derivatives and counterions.

PEDOT can be produced through its monomer by two methods; that are in-situ polymerization or chemical polymerization and electrochemical polymerization. The former uses a chemical oxidant, usually metal ions like Fe (III) and Mn (II) to polymerize and dope the polymer. At the same time, their anion also serves as the counterions. Until date, this method produces PEDOT with the highest achievable conductivity compared to latter (Elschner et al., 2010). In-situ polymerized PEDOT also requires less capital investment compared to electrochemical method as it only involves simple equipment.

However, certain limitations of this method are the long processing time and the wastage of material.

For the electrochemical polymerization method, EDOT is polymerized electrochemically while the ionic dopant in the electrolyte dopes the polymer and provides the counterions. The counterions from this method are more varied as its salt can be easily added into the electrolytes. The main advantage of this method is the uniform layer achieved on the outer surface of electrode. However, this method is not suitable for porous materials as the polymer will not be able to grow inside the pores of the electrode due to the low current density. Hence, the polymer layer will be dense on the surface but not on the walls of the inner pores.

Based on these deliberations, in-situ polymerization was adopted owing to the different structural configurations and thickness of the anode materials employed in this study. Electrochemical polymerization method would not be suitable for the functionalization of felt anodes as PEDOT would not be able to penetrate into the inner sections of the felts. Furthermore, the practicability and simplicity of this method makes it a preferred option.

During the course of present study, only electropolymerized PEDOT anodes were adopted for MFC operation (Y. Wang et al., 2013). Recently, vapour-phase polymerized PEDOT was used to study the interaction between the *P. aeruginosa* with graphene-PEDOT composite in terms of electron transfer (Webb, Notley, & Evans, 2015). Both of these researches polymerized their graphene-PEDOT composite on planar anodes. Hence, it is interesting to investigate the feasibility of in-situ polymerized PEDOT coated onto different configurations in MFC systems.

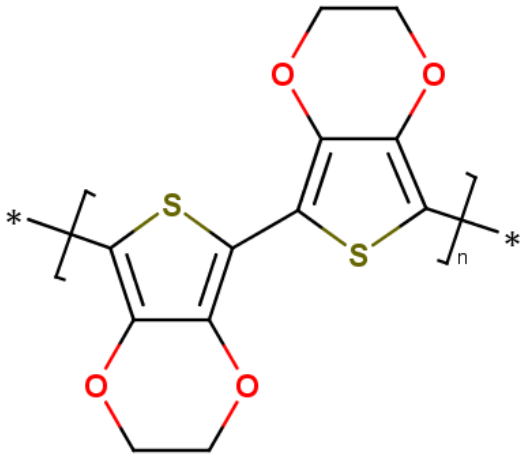

Figure 2.2: Molecular Structure of PEDOT

2.7 Biofilm Studies of MFC

Microorganism holds the key that governs the performance of MFC. The ability of exoelectrogens to transfer electrons produced from their metabolism process of organic substrate to anode serves as the basis of electricity generation in MFC (X. Jiang et al., 2010). Hence, in order to understand and overcome the limitations imposed by these microorganisms on the efficiency of the system, microorganisms involved in the oxidation of organic substance and its electron transfer mechanism must be examined. A better insight of microbial activities in the system will certainly lead to more relevant engineering solution and strategies (Lovley, 2008).

Earlier reports were focused on optimizing the current production by physical modification of materials and reactor configurations. The activities of microbes involved were treated as a black box (Debabov, 2008). The main idea behind microbial catalytic oxidation is that the electrons have to be transported from "central cellular metabolism extracellularly to the electrode" (Franks & Nevin, 2010). Although the oxidation of substrate is part of the metabolic activity of microbes, the need for them to transfer these electrons out of their cell was explained by B.E. Logan (2009). He suggested three

possible reasons why bacteria have a need for this unique characteristic. The first reason is to respire using solid metal oxide. These metal oxides are the electron acceptor in the respiratory electron transport chain, replacing the role of oxygen in aerobic respiration. The next possible explanation is that bacteria can transfer electron among themselves directly, without the help of mediators as observed between fermentative bacterium and methanogen. The last inference is the least studied reason for electron transfer is the communication between cells. Logan proposed that electron transfer exocellularly between cells, a form of communication between them.

As electron transfer mechanism from the microbes to the anode relates both the microbiology and electrochemistry factor, they are the fundamental factor that establishes the theoretical limitation of energy conversion in MFC system (Schroder, 2007). The electrons are transferred via two main types of mechanisms, which is the direct electron transfer (DET) and the mediated electron transfer (MET).

The main difference between DET and MET is the absence of diffusional redox component involved in the electron transfer pathway. DET can further be divided into two segments, i.e. through physical contact of the microbes and the electron acceptor (anode) or through nanowires. The electron is carried outside of the cell through outer membrane cytochromes. Due to the essential direct physical contact of these membranes on the anodes, only a single layer of these biofilms is electrochemically active (Lovley, 2006). Hence, the capabilities of MFC performance based on this mechanism are restricted by the cell density on this particular layer. However, another pathway that allows longer range of electron transfer under the DET mechanism is through conductive pili or nanowires. As these pili are attached to the membrane-bound cytochromes, it is considered as DET. The evolvement of these nanowires drastically increases the performance of MFC, as more layers of biofilms are able to contribute electrons (Reguera et al., 2006).

MET mechanism are said to produce higher current and power densities compared to DET mechanism (Schroder, 2007). MET can occur through artificial or endogenous redox mediators. Some of the commonly used synthetic mediators are neutral red, methylene blue and phenazines. However, this type of research is aborted due to toxic nature and expensive replenishment of the mediators (Gil et al., 2003). Certain bacteria are able to produce endogenous redox-active metabolites to self-mediated electron transfer. These mediators can consists of primary or secondary metabolites (Hernandez & Newman, 2001). However, the production of these compounds will cause additional biological energy losses. These mediators are being swept away in continuous system and only efficient in batch systems.

Microorganisms usually exhibit one or the other mechanism but there are some cases that the microorganism can adopt both methods concurrently. Research had found that *Shewanella oneidensis* MR-1 could simultaneously use overlapping mode for transferring the electron depending on environmental factors (Lies et al., 2005; Lovley, 2008). Conversely, for real wastewater MFC application the use of pure culture is not practical and hence mixed culture is preferred. The most feasible solution is to use microbes from the existing biological treatment of that particular wastewater itself as these microbes are already acclimatised to those conditions. Therefore, these mixed culture systems should comprise of both DET and MET mechanism.

2.8 Future Commercial Feasibility of MFC Technology

At the peak of MFC development, this technology was foreseen as the solution to overhaul existing wastewater treatment technology that is inefficient in terms of both economics and resources. MFC was emphasised as a technology that can sustainably recover the energy and other resources from the wastewater and simultaneously treat

these effluents for safe disposal. However, in recent years, due to lack of promising results from pilot studies and large-scale application, there have been many doubts on commercial feasibility and application of MFC (W. W. Li, Yu, & He, 2014). Hence, there has been a shift in attention for MFC application in recent years.

It is evident that MFC can never be a stand-alone technology, especially for wastewater treatment application. One of the most popular approaches is the process integration of anaerobic digester (AD) with MFC. The overall treatment process can be more energy efficient and sustainable as both technology were able to harvest resources and energy from the wastewater, (Pham et al., 2006). ADs are efficient in treating high organic loading but operate at high temperature range of 40°C-60°C. MFCs, in contrast, are more suitable for mid to low range of organic concentration and are able to operate in ambient temperature. Thus, the incorporation of MFC at the downstream of AD will further increase effluent quality, resource and energy recovery, replacing the conventional energy intense processes. Additionally, the breakdown of complex molecules by fermentation and pre-hydrolysis during AD also provides the MFC with simpler substrate, increasing its operating efficiency (Goud & Mohan, 2011). To improve the discharge quality, algae and membrane treatment have been proposed as MFC post-treatment (W. W. Li et al., 2014). Algae treatment has the added advantage of CO_2 sequestering and its biomass can then be extracted into biofuels (He, Kan, Mansfeld, Angenent, & Nealson, 2009; Jonker & Faaij, 2013). However, these "hybrid" processes come with their own additional set of challenges as each treatment process has different optimization condition and maintenance. As wastewater processes are linked with one another, a failure in the upstream process may affect other operations and disrupts the efficiency of the entire system. Hence, all these complications must be deliberated and overcome before any actual implementation of hybrid systems can be carried out.

Although MFC researchers remained optimistic on its potential in large-scale wastewater treatment technologies application, the challenges of scaling-up MFC must be resolved. Multiple factors involving reactor design and configuration, materials, biological component and economics should be developed further before any realistic application is viable. Hence, a more practical and realistic approach is by applying MFC in remote sensing devices and wireless sensor networks. MFC has been successfully used to power sensors in isolated areas or operate as biosensors. Benthic MFC has been effectively deployed to power various marine-related sensors. The advantages of using these technologies are the constant power supply as it is fuelled by its surrounding environment and required low-maintenance. This will reduce the cost of replacing batteries, especially in remote areas (Tender et al., 2008). The development of low-power electronic devices such as wireless sensor networks is also on the rise to reduce the energy consumption of these appliances. Hence, MFC with the help of power management system (PMS) is an ideal renewable energy source for these situations (Zheng et al., 2015). Additionally, MFC itself can act as biosensors. The voltage generation or coulomb generated gives a good correlation with certain environmental indicators such as BOD levels, chemical oxygen demand (COD) and copper (II) toxicity levels (Y. Jiang et al., 2015; Kim, Chang, Gil, Park, & Kim, 2003; Z. Liu, Liu, Li, Zhang, & Xing, 2014). Hence, the change in current or voltage recorded by these MFC biosensors gave good indication of the concentration of these pollutants in a specific range.

Other application that can be deemed economical for the implementation of MFC is through resource recovery. Both metals and nutrient recovery have been reported from MFC operation. Metals such as copper, vanadium, zinc, chromium and silver have been reduced at the cathodic compartment of MFC simultaneously with energy recovery (Fradler, Michie, Dinsdale, Guwy, & Premier, 2014; Lim, Lu, Choi, & Liu, 2014; Motos et al., 2015; B. Zhang, Feng, Ni, Zhang, & Huang, 2012). Organic components such as

ammonium, struvite, ethanol and other gases products such as hydrogen and methane have also been remedied or synthesized from MFC systems (Ichihashi & Hirooka, 2012; Kuntke et al., 2012; Pant et al., 2012). The recovery and synthesis of these value-added products may tip the balance in favour of MFC. The efficiency and value of these materials garnered should be taken into account to disclose the feasibility and viability of MFC in these systems.

In conclusion, there is a wide range of applications for MFC technology in both large and miniature scale. The flexibility and robustness of this technology makes it easily adaptable to various conditions and environments. Hence, the development and improvement of MFC should persist in order to realise the full potential of this sustainable technology.

CHAPTER 3

MATERIALS AND METHOD

3.1 Synthesis of PEDOT

PEDOT was polymerized using chemical oxidative method. The monomer, EDOT (97%, Sigma-Aldrich) and oxidant, ferric chloride hexahydrate, $FeCl_3.6H_2O$ (R&M Chemical) were dissolved in anhydrous acetonitrile (99.8%, Sigma-Aldrich) separately. The obtained solutions were mixed together in a mole ratio of 2:1. The polymerization initiated immediately and the solution turned to dark blue. The reaction was resumed for 4 h with stirring to ensure complete polymerization. The synthesized PEDOT particles were separated from the solution through filtration (Whatman® qualitative filter paper, Grade 1) and washed with acetonitrile: methanol mixture (1:1) to remove excess oxidant from the sample. The schematic diagram of the process is shown in Figure 3.1. The rinsed samples were then dried at 80°C for 24 h and kept in desiccator before further use.

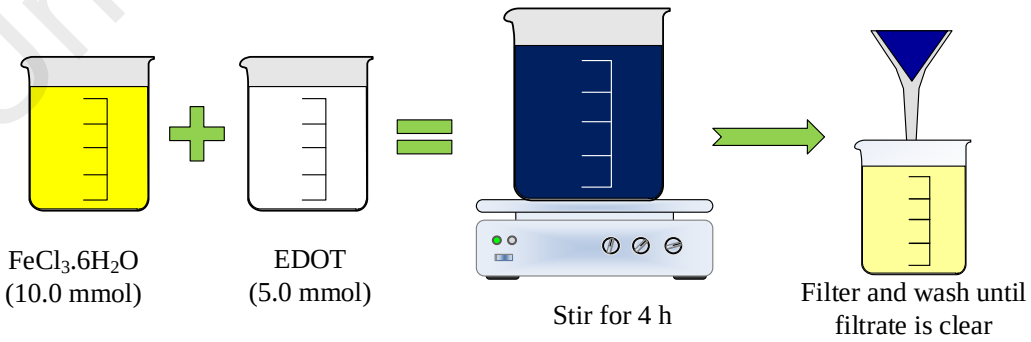

Figure 3.1: Schematic of the Synthesis of PEDOT Particles

3.2 Characterization of Synthesized PEDOT

Characterization analyses were carried out to confirm the nature of the synthesized PEDOT particles. Among the analysis performed were Fourier Transform Infrared spectroscopy (FTIR), UV-Vis spectroscopy, X-ray diffraction (XRD) and thermogravimetric analysis (TGA). The microscopic images of the particles was captured using field emission scanning electron microscope (SEM) while the elemental composition of the particles were analysed with energy dispersive X-ray spectroscopy (EDS) attached with the SEM.

The FTIR spectrum (Perkin Elmer Spectrum 400) for PEDOT was obtained in the range of 4500-500cm^{-1}. UV-Vis absorption spectrum was measured using UV-Vis spectrometer (UV-2600, Shimadzu) equipped with integrating sphere attachment. XRD was performed using PANalytical Empyrean with copper as the x-ray source (Cu Kα = 0.154 nm). The TGA analysis (TG 449 F3 Jupiter, Netzsch) was carried out for temperature ranged between 28°C and 1500°C with a heating rate of 20°C/min. The SEM images and elemental analysis were capture using Quanta 450 FEG, FEI equipped with an EDS detector.

3.3 Electrode modification

Three different configuration of carbon-based anodes were used in this research; that are graphite plate (HSCF Co. Ltd, China), carbon cloth (Fuel Cell Earth, USA) and graphite felt (HSCF Co. Ltd, China). These materials were functionalized with the synthesized PEDOT and varied coating procedures were adopted due to their different configurations and morphologies. Three PEDOT loading were attempted on each configuration to examine the effect of PEDOT concentration on anode performances. The

loading were fixed as 2.5 mg/cm^2, 5.0 mg/cm^2 and 7.5 mg/cm^2 for all three types of anodes.

3.3.1 PEDOT coating on Graphite Plate Anodes

Graphite plates were polished and smoothed using sand paper. The polished plates were then soaked in diluted hydrochloric acid (0.1 M HCl, Sigma-Aldrich) overnight to remove residues and deposits. PEDOT were functionalized onto the plate anodes with the help of binders. This was achieved by mixing known amount of PEDOT with Nafion (5%, Sigma-Aldrich) and iso-propanol solutions (R&M Chemicals, UK). For every 1 mg of PEDOT, 4.67 µL of Nafion and 2.33 µL of iso-propanol solution were added. The mixtures were vortexed rapidly (20 s) at high speed with the help of glass beads to form a paste-like substance. The prepared pastes were then gently spread onto the plates using nylon brush. The coated plate anodes were left to dry at room temperature for 24 h. Air-dry method was used because rapid drying lead to the cracking of PEDOT layer. The above steps were repeated on the other side of the plate to ensure complete coating. The electrodes were connected through Ti wires (1 mm diameter, Sigma-Aldrich) using silver conductive epoxy (Penchem Technologies Sdn Bhd, Malaysia). Plate anode without PEDOT was used as control electrode and was denoted as GP. The PEDOT coated plate anodes were referred to as GP-P, GP-2P and GP-3P corresponding to their loading of 2.5, 5.0 and 7.5 mg/cm^2 respectively.

3.3.2 PEDOT coating on Carbon Cloth Anodes

The coating of PEDOT onto carbon cloth anodes is similar with the method adopted for graphite plates. The carbon cloths were first soaked in dilute HCl (0.1M) for 24 h in order to remove impurities and other residue. The preparation of binder-PEDOT

paste was synthesized in a similar procedure adopted for GP. However, due to the absorptive nature of cloth anodes, the volume of the binder composition was increased to 10 µL for each 1 mg of PEDOT (6.67 µL Nafion and 3.33 µL iso-propanol). The coated cloth anodes were then placed in an oven at 60°C overnight to facilitate drying process. The above steps were repeated on the other side of the anodes and Ti wires were attached for electrical connection. Cloth anode without PEDOT coating was prepared as a control sample and was denoted as CC. The PEDOT coated cloth anodes were referred to as CC-P, CC-2P and CC-3P corresponding to their loading of 2.5, 5.0 and 7.5 mg/cm^2 respectively.

3.3.3 PEDOT coating on Graphite Felt Anodes

Graphite felts were cleaned as done for previous anode materials by soaking in 0.1 M HCl to remove loose fibres and surface impurities. The coating process for felt anodes varied from previous methods due to their different structural morphology. A dip-dry approach was adopted for these anodes as they consist of loose network of fibres and have a significant thickness of 3 mm compared to plate (0.55 mm) and cloth (0.35 mm) anodes. The PEDOT loadings were similar to those used in plate and cloth anodes. The appropriate amount of PEDOT powder were weighed and dispersed in 20 mL of deionized water. Sodium dodecylbenzenesulfonate (SDBS, 1%, Sigma-Aldrich) was added as a surfactant to assist the dispersion of PEDOT particles in aqueous condition as well as the adsorption of PEDOT onto the felts. The mixture was sonicated for 2 h and a homogenous dispersed PEDOT solution was formed. Felt anodes with required dimension were then dipped into the dispersed PEDOT and dried at 60°C in an oven. The dip-dry process was repeated until the PEDOT solution was completely consumed. Felt anode without PEDOT attachment was used as a control sample for subsequent characterization and experiments and was denoted as GF. The PEDOT coated felt anodes

were referred to as GF-P, GF-2P and GF-3P corresponding to their loading of 2.5, 5.0 and 7.5 mg/cm^2 respectively.

3.4 Characterization of Synthesized Anodes

The surface morphology and conditions of coating onto the three different anode configurations were probed using SEM. Electrochemical analysis involving cyclic voltammetry (CV) and electrochemical impedance spectroscopy (EIS) were carried out using a potentiostat equipped with frequency response analyser (FRA) (PGSTAT 128N/FRA32M, AUTOLAB, Netherlands). These ex-situ electrochemical analyses were operated under three-electrode mode setting in an electrochemical cell. The synthesized electrodes were positioned as the working electrodes while Pt wire and Ag/AgCl electrode in 3 M NaCl (0.209V vs. SHE) (RE-5B, BASi, USA) were used as counter and reference electrodes respectively. A schematic diagram of the three-electrode mode is shown in Figure 3.2 below. The CV analysis was performed by employing 1 mM ferricyanide ($[Fe(CN)_6]^{3-}$) as electrolyte and 0.5 M potassium nitrate (KNO_3) was added as supporting electrolyte. The scan rate was set at 10 mV/s and the potential was shifted from –0.8 V to 0.8 V. EIS measurements were carried out with 2.5 mM ferric/ferrocyanide, $[Fe(CN)_6]^{3-/4-}$ in 0.5 M KNO_3 as electrolyte. The frequency ranged from 100 kHz to 1 mHz with 10 mV amplitude. The EIS plots were then fitted into a modified Randle's equivalent circuit as shown in Figure 3.3 where R_s and R_{ct} are the solution resistance and charge transfer resistance respectively while the *CPE* and *W* components represent the constant phase element and the Warburg diffusion element. The electrolytes for both analyses were purged with nitrogen (N_2) gas before every analysis to ensure the anaerobic condition.

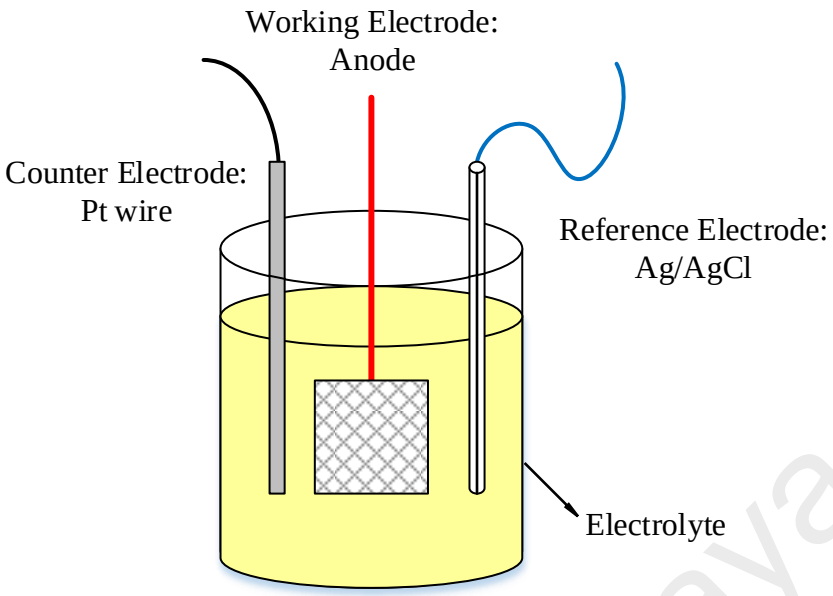

Figure 3.2: Schematic of Three-Electrode Mode Setup

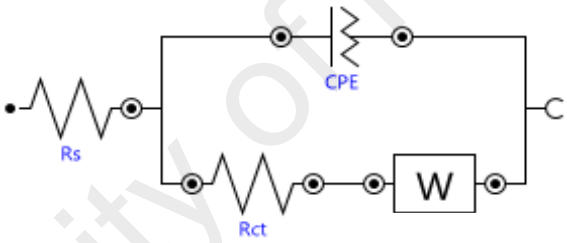

Figure 3.3: Modified Randle's Equivalent Circuit

The anodes were characterized optically and electrochemically to ascertain their physical and chemical nature before being operated in MFC systems. These preliminary analyses are useful to distinguish the influence of their structural configuration without the interference of biofilm and other external factors arising after the anodes were operated in MFC reactors. Hence, it should be noted that the characterization techniques discussed in the above section were employed for anodes without any biofilm formation.

3.5 Applications of Synthesized Anodes in MFC system

A dual-chamber MFC with working volume of 150 mL each was fabricated with acrylic material. The synthesized electrodes with dimension of 40 mm x 40 mm each were used as anodes while carbon cloth of the same dimension without any modification was used as cathode throughout the study. The chambers were separated by a proton exchange membrane, Nafion 117 (Sigma-Aldrich). The obtained membrane was pre-treated by soaking in 3% hydrogen peroxide (H_2O_2, R&M Chemicals), distilled water and 0.5 M sulphuric acid (H_2SO_4, R&M Chemicals) successively under boiling condition for an hour each. The treated membrane was then soaked in distilled water of room temperature before further use. An external resistor of 1 kΩ was connected across the anode and cathode to complete the circuit. Phosphate buffer solution (PBS, 100 mM, pH 7) consisting of monosodium phosphate (NaH_2PO_4) and disodium phosphate (Na_2HPO_4) were used as buffering solution for both electrolytes. Ammonium chloride (NH_4Cl, 0.6 g/L) and potassium chloride (KCl, 0.3 g/L) were also added to increase the conductivity of the electrolyte. Sodium acetate trihydrate ($CH_3COONa.3H_2O$, 1 g/L) and trace elements (12.5 mL/L) were added to the PBS as carbon and micronutrient source for the anolyte. The solution was purged with N_2 before use to ensure anaerobic condition in the anode chamber. Catholyte solution was prepared by adding 100 mM $[Fe(CN)_6]^{3-}$ into the PBS.

The anodes were inoculated with sludge obtained from an anaerobic pond of palm oil mill effluent treatment (POME) plant (Seri Ulu Langat Palm Oil Mill,Dengkil, Malaysia). The initial inoculation was carried out with 1:1 ratio of sludge to acetate (1 g/L). This step was repeated until the voltage across 1 kΩ resistor reached above 100 mV. The anolyte was then replaced with acetate solution without the addition of sludge. The reactor was operated under step fed-batch mode in room temperature. A schematic diagram of the reactor is illustrated in Figure 3.4.

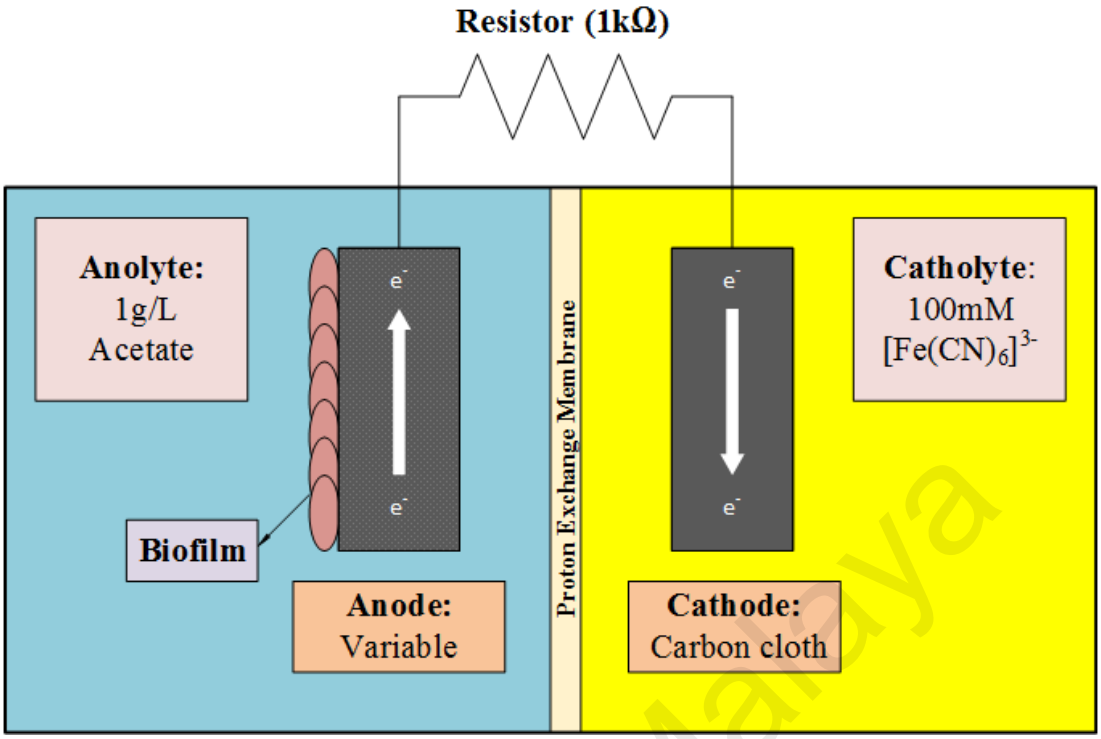

Figure 3.4: Schematic of the MFC Reactor Employed

3.6 Performance Analysis of Synthesized Anodes in MFC system

The voltage across the resistor was recorded every 5 min using a digital multimetre (UT61D, Uni-Trend) with a data acquisition module. The anolyte was replaced once the operating voltage dropped below 50 mV. Three repeatable cycles of voltage generation were recorded for every anode to ensure stable biofilm formation. The electricity generation performance of MFC systems were evaluated using coulombic efficiency (CE). CE is defined by the ratio of electrons converted to electricity (C_P) to the total available electrons (C_T) in the solution as shown in Equation (3-1). For fed-batch mode, C_P is calculated by integrating current over time (I-t) while C_T is a function of change in COD ($\Delta\ COD$) as shown in Equation (3-2) where F is the Faraday constant (96500 C/mole), b is the number of electrons exchanged per mole of oxygen, M_w is the molecular weight of O_2 and v_{An} is the volume of the substrate in anode chamber. The

COD concentrations were determined using the Standard Methods for the Examination of Water and Wastewater (APHA., 2005).

$$CE(\%) = \frac{C_P}{C_T} \times 100\% \quad (3\text{-}1)$$

$$CE(\%) = \frac{M_W \int Idt}{Fbv_{An}\Delta COD} \quad (3\text{-}2)$$

After three repeatable cycles of voltage generation were achieved, polarization curve analysis was carried out at stable voltage. Linear scan voltammetry (LSV) was performed at a scan rate of 1 mV/s using anode as the working electrode and cathode as the counter and reference electrode. The potential was scanned from open circuit potential (OCP) to 0 V and the corresponding current was recorded. From the voltage-current data, current density and power density curve were calculated. Current densities were computed by dividing the obtained current with the projected surface area of the anodes while power densities were the multiplication of voltage and current over the projected surface area of the anodes.

The components of internal resistance in these systems were obtained through EIS analyses under the two-electrode mode. These analyses were carried out under a fixed external resistance of 1 kΩ to ensure the stability of the systems and to obtain the internal resistance components under working conditions (Hutchinson, Tokash, & Logan, 2011; C. Zhang et al., 2015). Bode plots were used to depict the EIS analyses and logarithmic scales were used for the frequency and impedance modulus axes. The data at the high frequency estimates the ohmic resistance, R_Ω while the low frequency gives an indication of the total resistance of the system. The acquired plots were then fitted into appropriate equivalent circuits using the NOVA 2.0 software (Metrohm, Autolab). Two models of

equivalent circuit were applied based on the two or three time-constant circuit as shown in Figure 3.5(a) and (b) respectively (He & Mansfeld, 2009; C. Zhang et al., 2015). The equivalent circuit that gave better correlation were used to quantify the components of internal resistance. The two time-constant circuit represents the anode and cathode compartments respectively while the third time-constant denoted the resistance from finite diffusion (He, Wagner, Minteer, & Angenent, 2006; J. Hou et al., 2014). R_Ω denotes the ohmic resistance that includes the resistance of both anolyte and catholyte as well as the membrane. *W* symbolises the Warburg impedance and is related to the semi-finite diffusion of the anode component. The *CPE* represents the constant phase element arise from the double layer capacitance due to the charged species accumulating near the anodes (Borole, Aaron, Hamilton, & Tsouris, 2010). *CPE* was inserted instead of a capacitor element due to the inhomogeneity of the anode surfaces (He & Mansfeld, 2009). The charge transfer resistance of the anode and cathode were expressed as R_a and R_c respectively. Meanwhile, C_c conveys the capacitance of the cathode. R_d represented finite diffusion resistance. The total internal resistance, R_{int} were computed by summation of all the resistance components. A R_{ext} of 1 kΩ is inserted in the equivalent circuit corresponds to the fixed external resistance connected to the MFC during analysis.

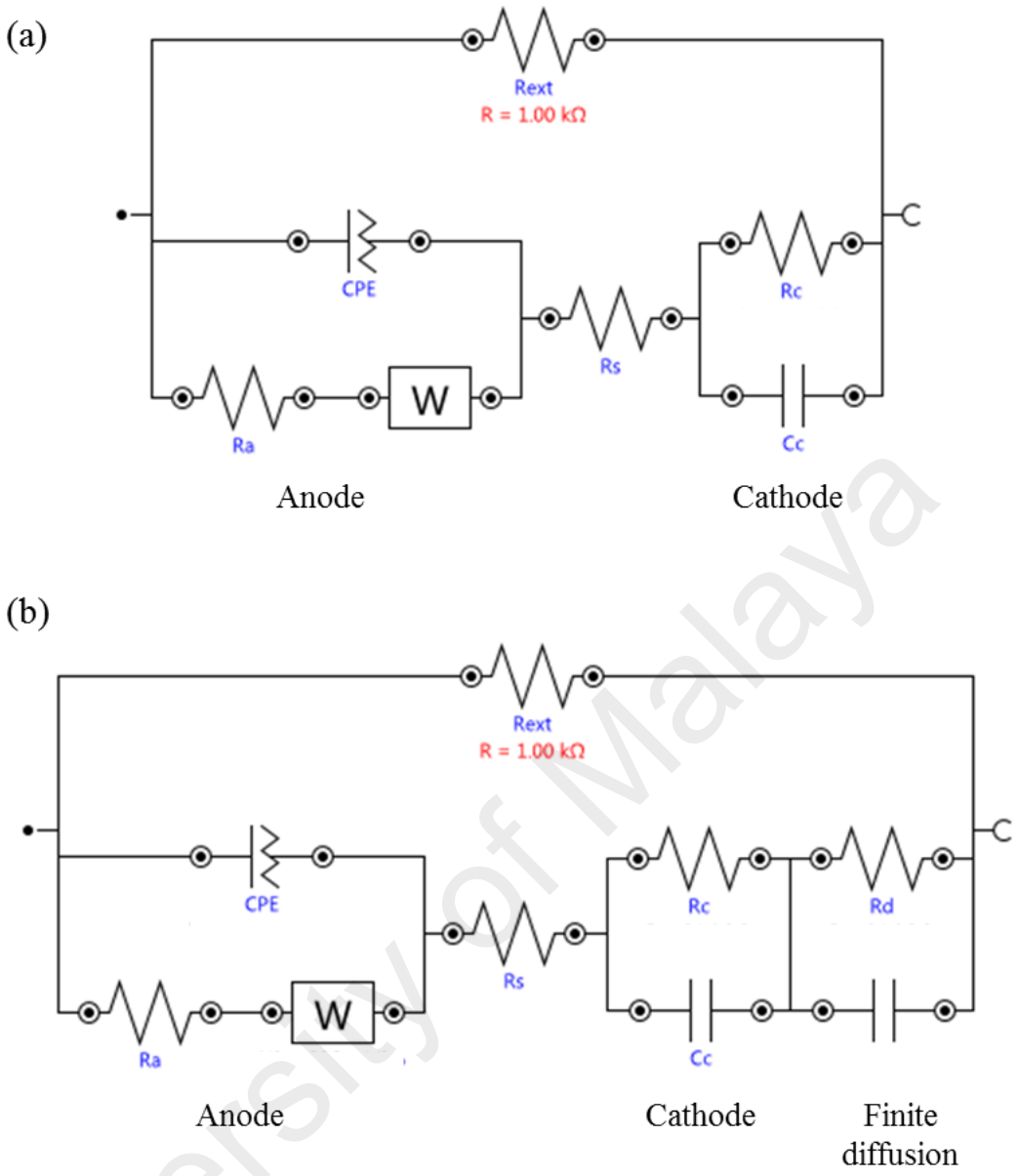

Figure 3.5: Equivalent Circuit of the MFC Reactor; (a) Two Time-Constants and (b) Three Time-Constant

The individual electrode potentials with respect to current density were monitored through the external resistance method. External resistors in the range of 100 kΩ to 100 Ω were connected across the electrodes for 10 min each to achieve a pseudo-steady state. The potential of anode and cathode were then recorded against Ag/AgCl reference electrode for each resistor.

3.7 Determination of Exoelectrogens Distribution

A simple experiment was carried out to examine the contribution of anodic biofilm and planktonic cells in electron transfer for both the control and modified anodes (X. Jiang et al., 2010; Yamamuro, Kouzuma, Abe, & Watanabe, 2014). The electron transfer from the anodic biofilm was explored by inserting an anode with established biofilm into a reactor containing fresh anolyte. Conversely, a new anode without biofilm was inserted into the reactor with the used electrolyte to determine the contribution from planktonic cell. The obtained voltage by these reactor systems were monitored for 48 h. Finally, 1% glutaraldehyde (Sigma-Aldrich), a biocide was added into the reactor to distinguish the role of microbes and abiotic factor on the voltage generated by the system.

3.8 Biofilm Characterization

The attachments of microorganism on the anodes were captured using SEM. Samples of utilized anodes were cut out and preserved before they were viewed under the electron microscope. Sample anodes were first soaked in 4% glutaraldehyde (Sigma-Aldrich) in 0.1 M sodium cacolyate buffer (pH 7.4, Sigma-Aldrich) for more than 4 h. The samples were then rinsed with the buffer for 15 min twice before immersing them in 1 mL of osmium tetroxide (OsO_4, Sigma-Aldrich) overnight. The OsO_4 was washed out using distilled water and the samples were ready for ethanol dehydration. The samples were dehydrated through a series of ethanol concentration (10, 20, 30, 40, 50, 60, 70, 80, 90, 95, and 100%). Finally, the ethanol in the samples was substituted with acetone through gradual dilution. The samples were then dried using critical point drying (CPD) and sputtered with Au before viewing.

The biodiversity analysis was performed by extracting deoxyribonucleic acid (DNA) from pieces of anodes as well as from the sludge used for inoculum with the PowerBiofilm ® DNA Extraction Kit (MO BIO Laboratories, Inc., Carlsbad, CA, USA). DNAs' integrity and quality were evaluated by agarose-gel electrophoresis and quantified using fluorometer (Qubit® 2.0, Thermo Fisher Scientific). The samples were sequenced on Illumina MiSeq sequencer (Illumina Inc., San Diego, USA). Operational taxonomic unit (OTU) clustering was performed using UCLUST algorithm and the percentage of similarity within the OTU was set to be ~97%. Taxonomy was then classified using Ribosomal Database Project (RDP) classifiers with the Greengenes Database released on May 2013.

3.9 Study on Wastewater as Carbon Source for MFC

The feasibility of the modified anodes towards wastewater containing complex organics was examined by introducing palm oil mill effluent. As MFC is suitable for post AD treatment, diluted POME with an initial COD of ~350 mg/L as substrate was introduced. The anodes were first inoculated with acetate and were acclimatized with the wastewater by gradually increasing the POME to acetate ratio (50%, 75% and 100%). The performances and efficiencies were then compared between the pure acetate and POME substrates.

CHAPTER 4

RESULTS AND DISCUSSION

This chapter consolidates the obtained results and their relevant discussions. The preliminary section of the chapter discusses the characterization and performance of anodes with varying structural configuration. The discussion is then directed to the characterization of synthesized PEDOT, a conductive polymer employed to enhance the properties of MFC anodes. The later sections thoroughly investigate the functionalization of the synthesized PEDOT onto anodes with assorted configurations and its effect on MFC performances. The chapter further focuses on the microbiological aspects like the distribution and identification of biofilm. The last section presents the feasibility of the current system in using industrial wastewater as substrate.

4.1 Characterization and Application of Anodes with Different Configurations

Carbon-based materials were adopted as anodes throughout this study. These materials exist in many variations in terms of construction and arrangement. Each configuration has their specific advantages and disadvantages depending on reactor design and the means of application. Hence, three base anodes of different morphology were employed in this study, namely graphite plate, carbon cloth and graphite felt to assess the impact of morphological and structural configurations on the electrochemical characteristics and MFC performance. GP and CC materials represent the planar electrodes while GF with a considerable thickness of 3 mm is categorized as 3D electrode. The anodes did not undergo any pre-treatment other than minor cleaning and hence they are referred as control anodes.

4.1.1 Characterization

4.1.1.1 Surface Morphology

The surface morphology of the anode configurations were observed through SEM under both low and high magnifications. The obtained images are depicted in Figure 4.1(a-f). The image for GP illustrated in Figure 4.1(a) revealed the smooth surface of the anode with minor abrasive impressions formed during the polishing process. A higher magnification (Figure 4.1 (b)), fracture lines can be observed, indicating the fragile and brittle nature of the GP. The figures 4.1(c-f) depict the surface characteristics of CC and GF. The CC anode is made up of carbon fibres that are arranged in a weaving pattern with diameter ranging from 8-10 µm while the graphite fibres of GF are entangled in a disorganised fashion. The loose arrangement of the felt fibres formed wide gaps of more than 50 nm, making the GF a macro-porous structure.

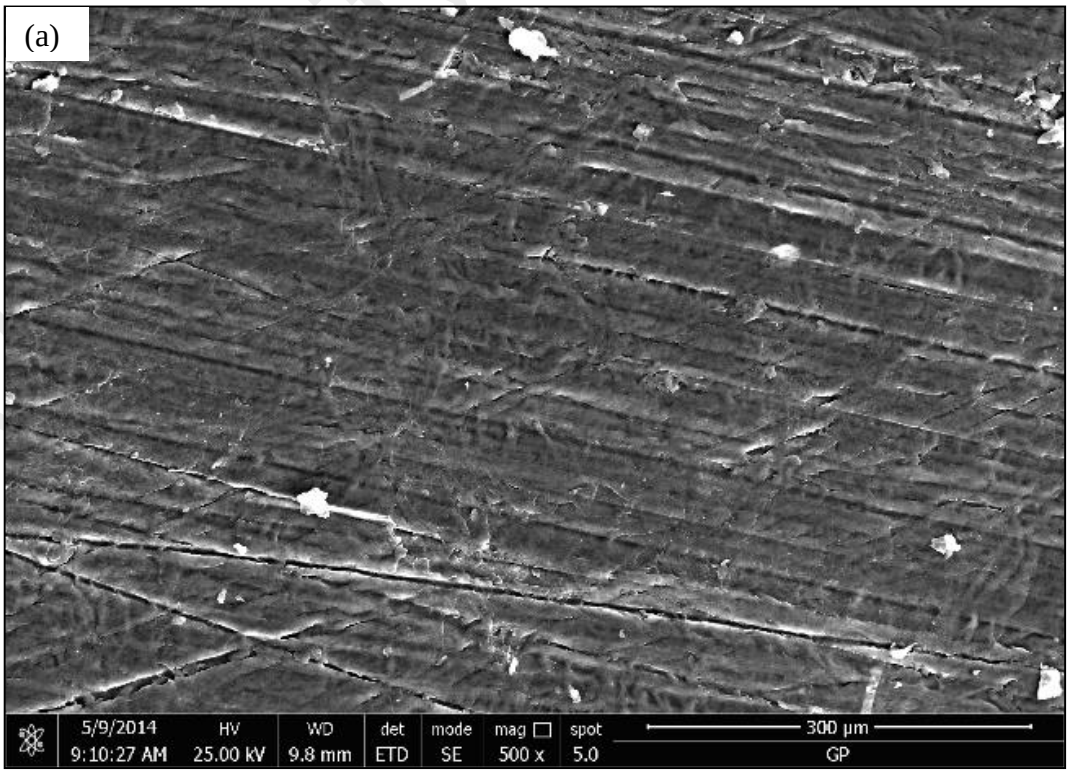

(b)

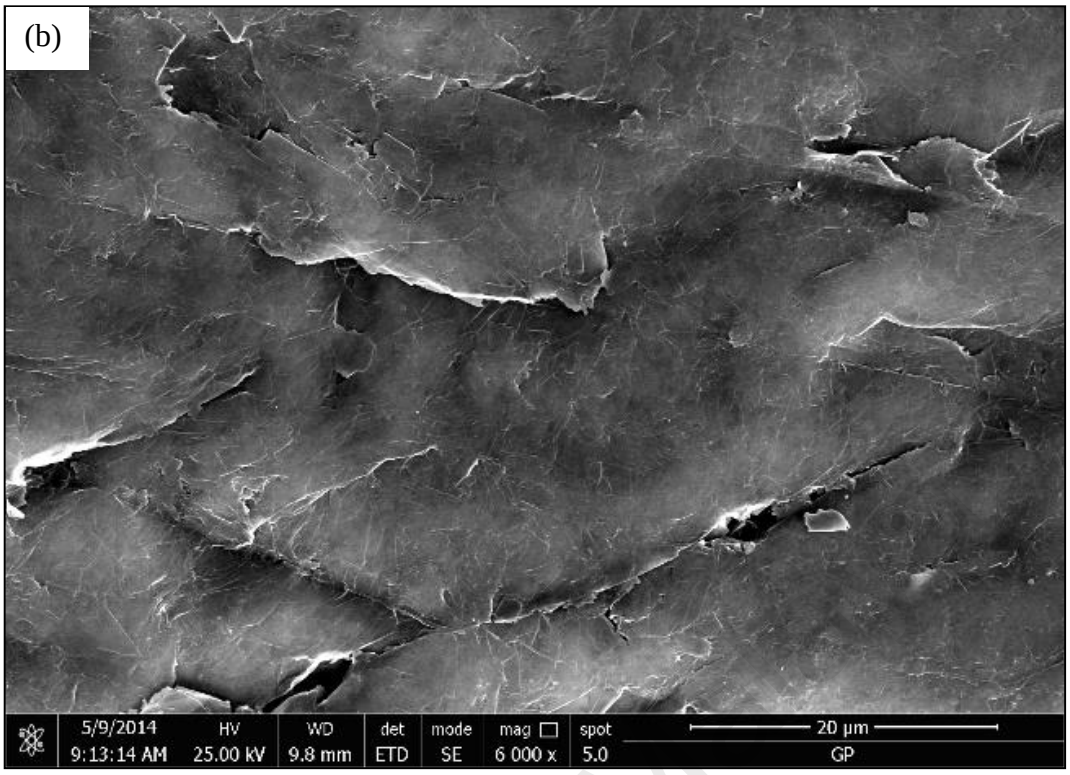
5/9/2014
9:13:14 AM
HV
25.00 kV
WD
9.8 mm
det
ETD
mode
SE
mag
6 000 x
spot
5.0
20 µm
GP

(c)

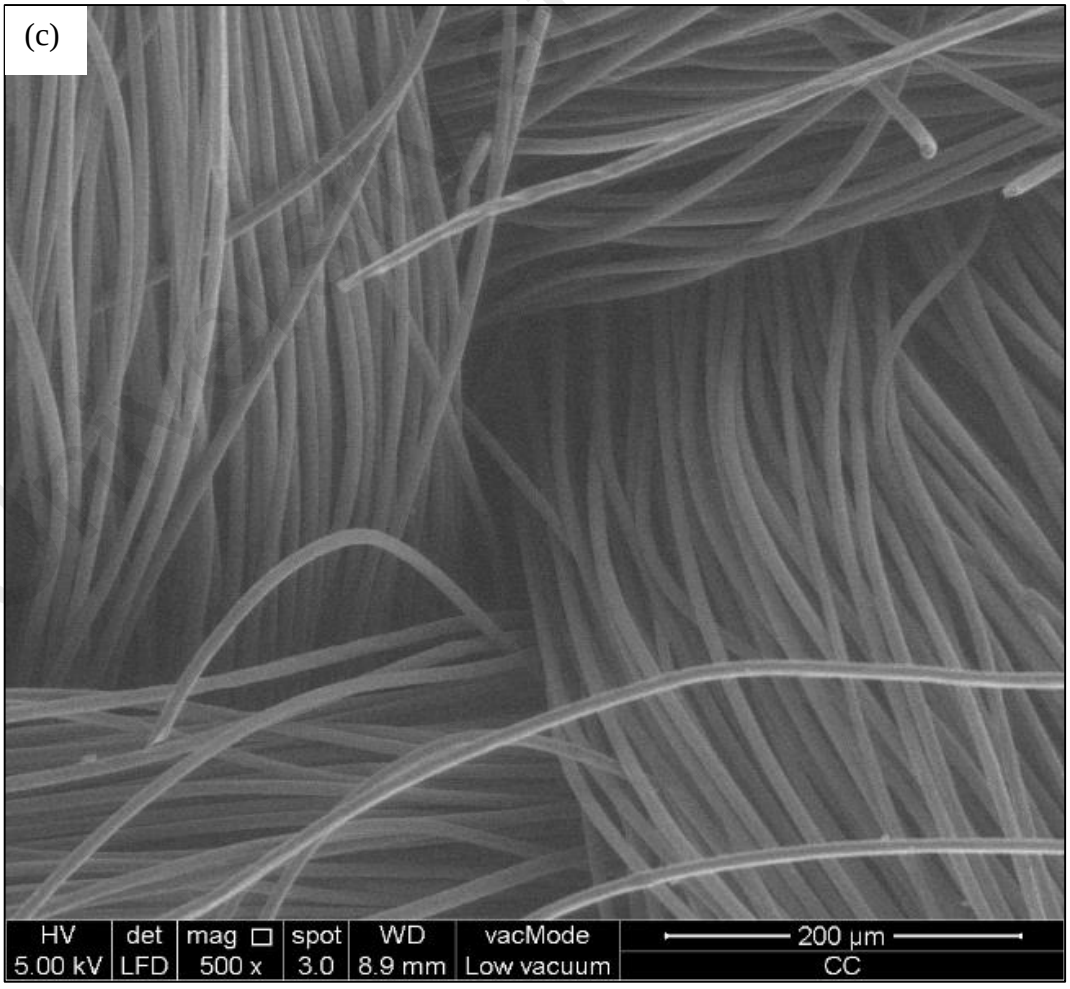
HV
5.00 kV
det
LFD
mag
500 x
spot
3.0
WD
8.9 mm
vacMode
Low vacuum
200 µm
CC

(d)

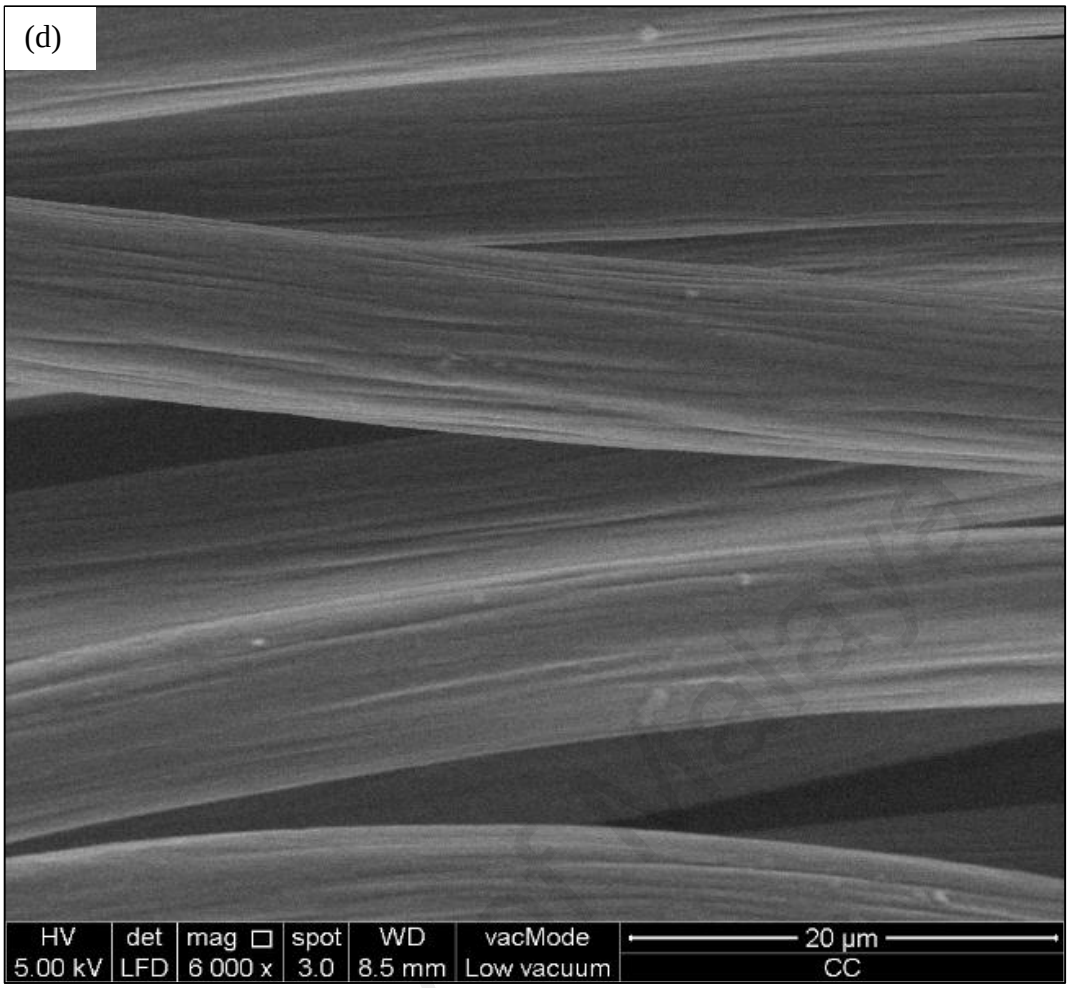
HV
5.00 kV
det
LFD
mag
6 000 x
spot
3.0
WD
8.5 mm
vacMode
Low vacuum
20 µm
CC

(e)

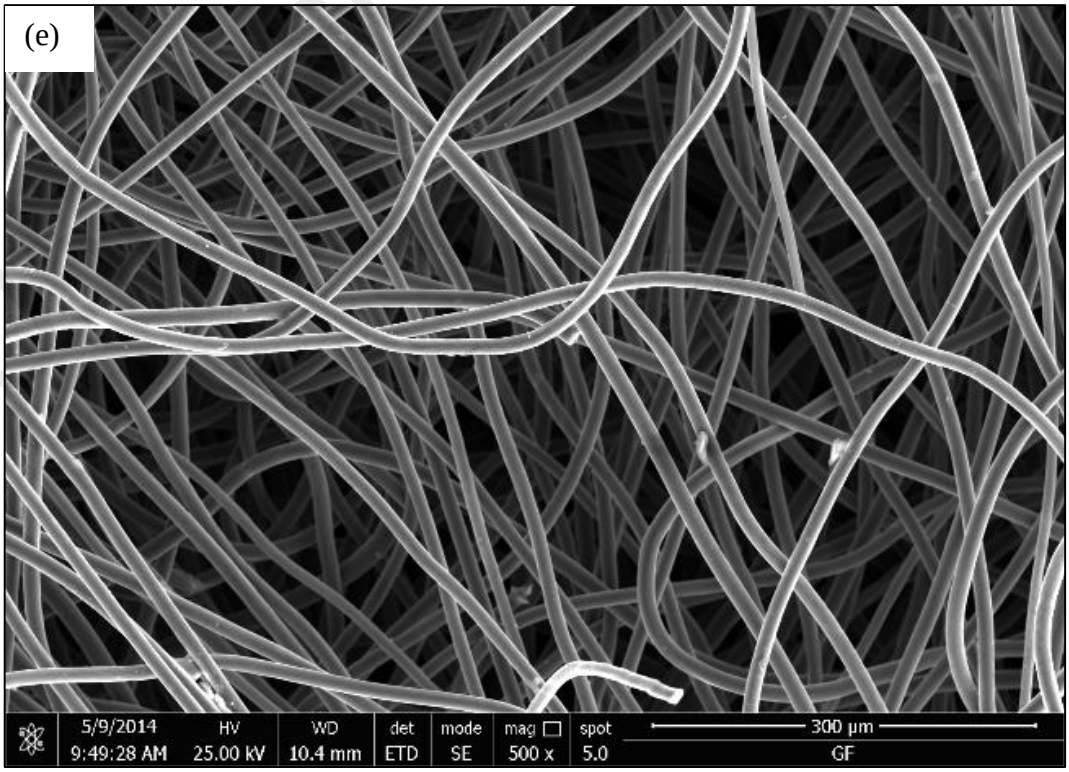
5/9/2014
9:49:28 AM
HV
25.00 kV
WD
10.4 mm
det
ETD
mode
SE
mag
500 x
spot
5.0
300 µm
GF

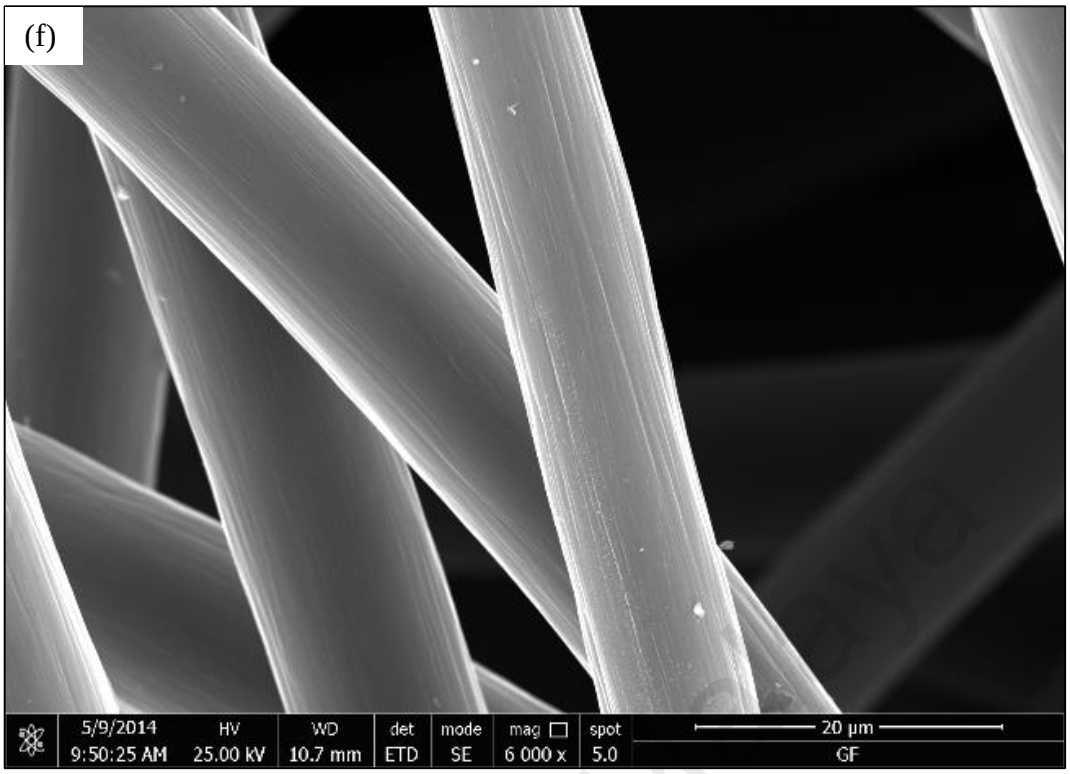

Figure 4.1: SEM Images of Control Anodes with 500 × and 6,000 × magnification; (a-b) GP, (c-d) CC and (e-f) GF

4.1.1.2 Electrochemical Analysis

The CV analyses of the control anodes were carried out to analyse the qualitative electrochemical reactiveness of the materials and is presented in Figure 4.2. The three anodes recorded almost similar voltammogram and peak currents. Redox peaks observed for the GF anode are due to the electrochemical activity of the graphite itself and was consistent with the CV obtained from literatures for graphite felt in ferricynide electrolyte (J. Hou et al., 2014; Tang et al., 2015).

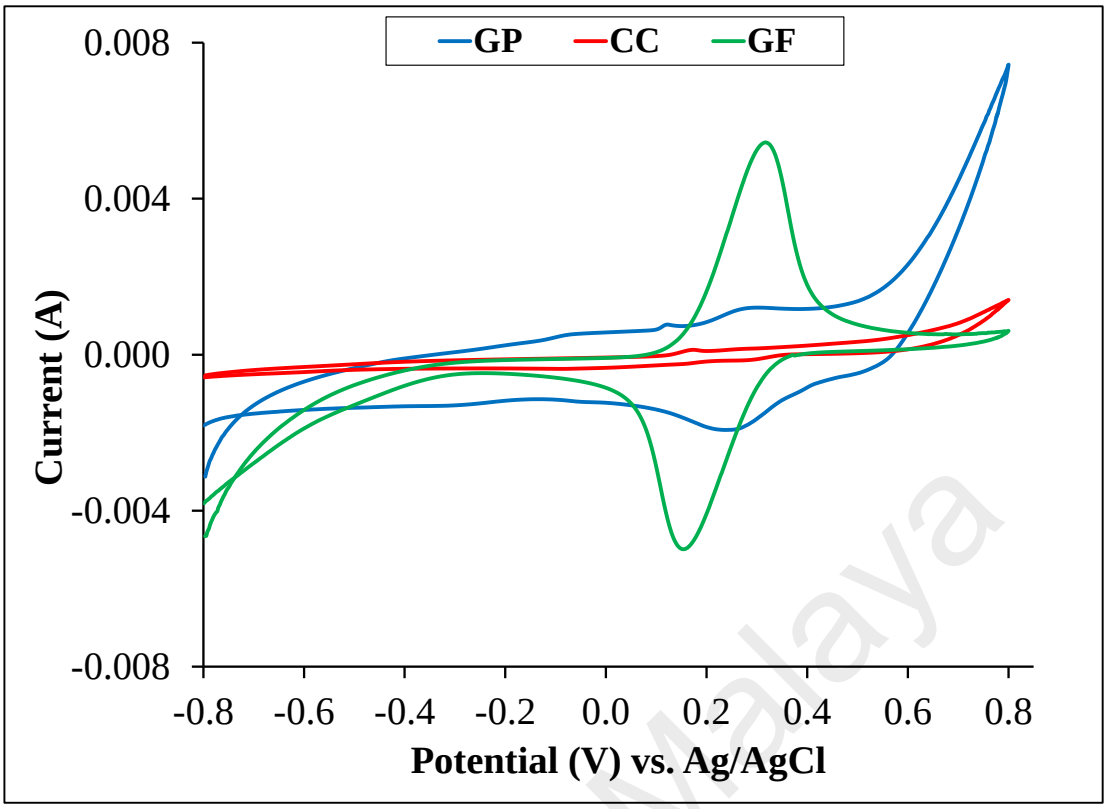

Figure 4.2: CV of Control Anodes in 1 mM $K_3[Fe(CN)_6]$ and 0.5 M KNO_3 electrolyte at a scan rate of 10 mV/s.

EIS analyses of the control anodes were performed and the corresponding Bode plots are presented in Figure 4.3. The analyses were then fitted into the modified Randle's equivalent circuit (Figure 3.3). Both GP and GF anodes recorded very low R_{ct} of ~19 Ω and 17 Ω respectively. However, CC attained very high R_{ct} of ~150 Ω, which is almost 10 x higher than the other anodes. The low R_{ct} of GP was due to its solid state that enables complete conductive network across its surface area. GF has a high surface area that translates to increased reactive area compared to the planar anodes. The presence of Warburg impedance in the equivalent circuit for all the tested anodes established that the reactions were also governed by mass transfer resistance.

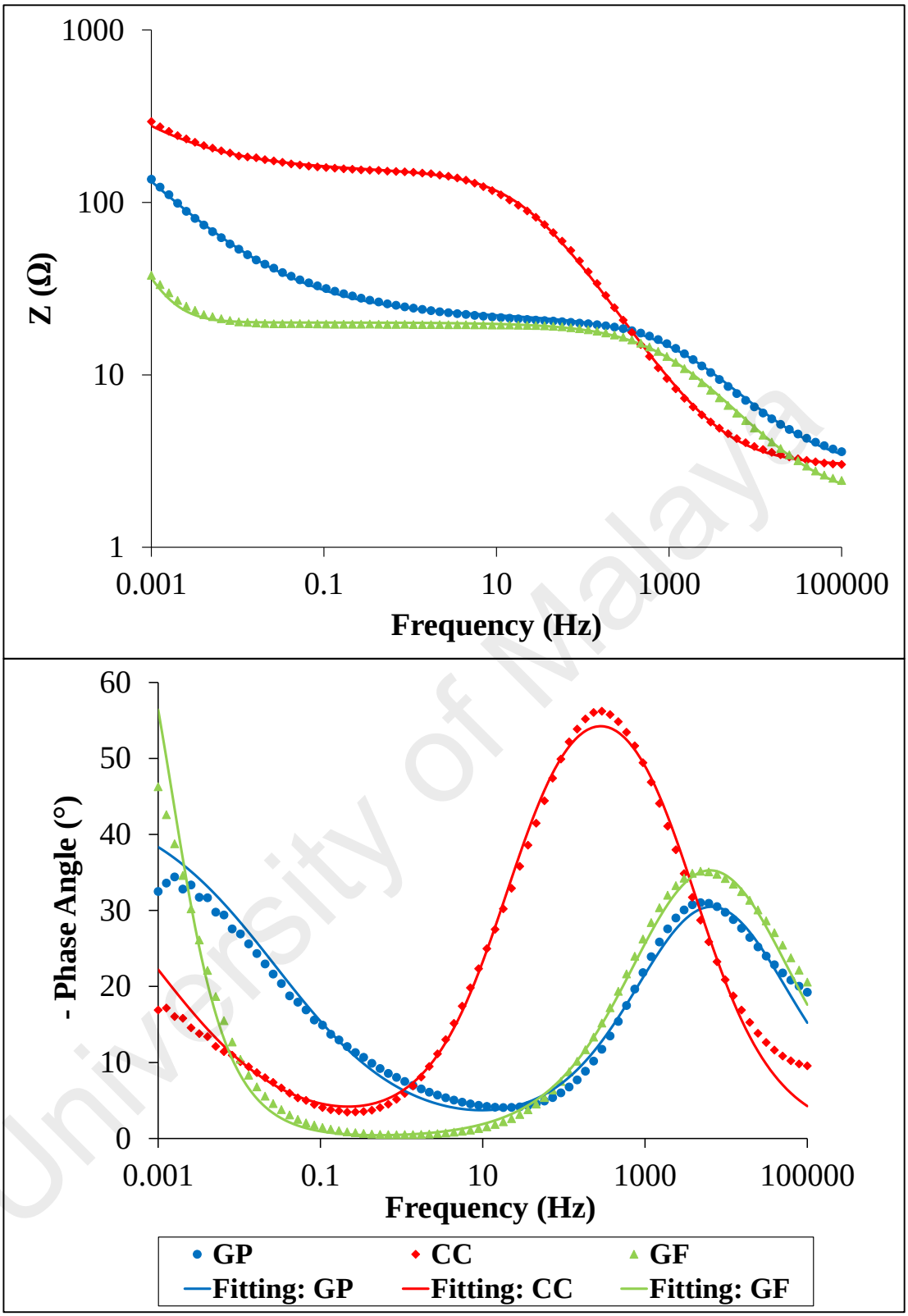

Figure 4.3: Bode Impedance Modulus Plot and Its Corresponding Phase Angle of Control Anodes in 2.5 mM $[Fe(CN)_6]^{3-/4-}$ and 0.5 M KNO_3 as electrolyte.

4.1.2 MFC Performance

4.1.2.1 Voltage Generation

The anodes and cathode were connected with a 1 kΩ resistor and the obtained voltage outputs for three stable cycles are shown in Figure 4.4. The peak voltage generation for GF, CC and GP are 637.0 ± 25.8 mV, 553.3 ± 0.5 mV and 444.5 ± 12.3 mV respectively. The minor standard deviation (SD) of the peak voltages and repeatability between the three cycles of voltage generation indicates the stability of the biofilm formed on the anodes. The difference in voltage generation between these three anodes is attributed to the distinctive configuration of each anode. The structural arrangement of GF supports better biofilm immobilisation and diffusion of substrates, which is reflected in the high voltage generation.

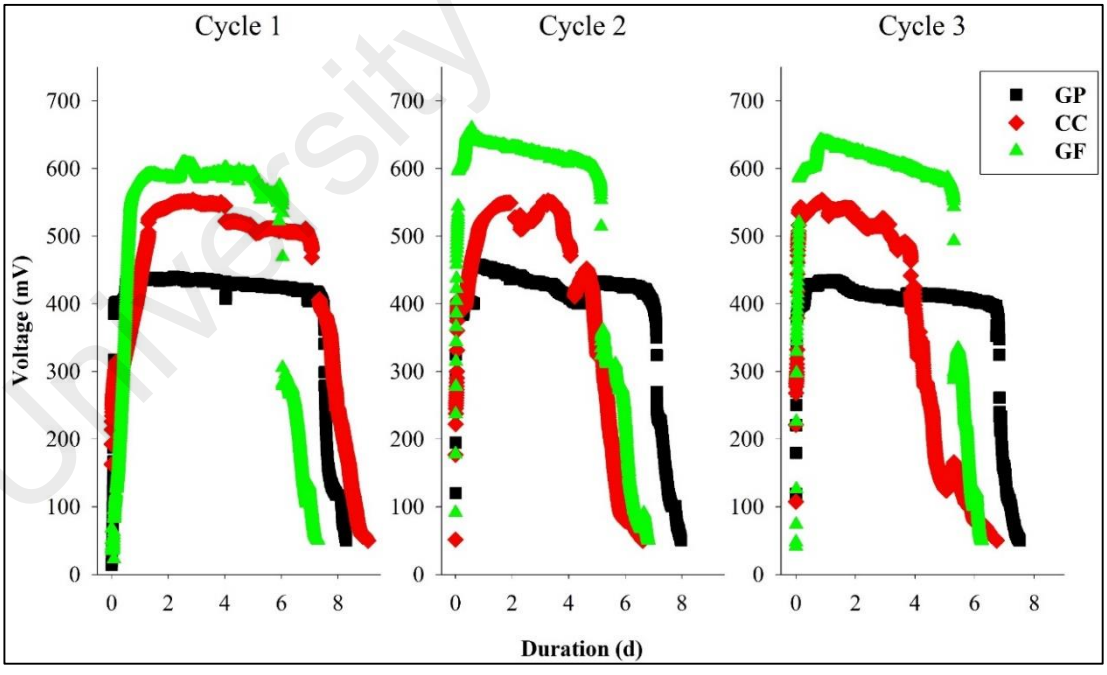

Figure 4.4: Voltage Generation for Three Consecutive Cycles of Control Anodes

4.1.2.2 Current and Power Density

Polarization and power density curves were computed to obtain a more comprehensive analysis of the anodes' performance and are presented in Figure 4.5. The I_{sc} of all the three control anodes falls in the range of 0.43-0.55 A/m^2. Voltage overshoots were clearly observed for CC and GF anodes but was not evident in GP system. Such voltage or power overshoot has been reported in literatures and several inferences on the cause of this phenomenon have been discussed. Few researches attributed this occurrence to mass transfer limitation (Oh & Logan, 2007; Thorne et al., 2011). However, a research by Min, Román, and Angelidaki (2008) demonstrated that this was not the case for their system. They attempted to reduce the mass transfer limitation by increasing the stirring speed during the analysis but found no improvement in their performance. Hence, they concluded that the power overshoot was not due to mass transfer limitation. This prompted another hypothesis that the overshoot is due to the restriction from the microbes (Ieropoulos, Winfield, & Greenman, 2010; B. E. Logan & Regan, 2006a). At low external resistance or applied potential, the conductivity of the external circuit is high and enables more electrons to pass through (Ieropoulos et al., 2010). However, the rate of substrate oxidation of the microbes and electron transfer to the anode was unable to sustain the high electron demand, hence limiting the current and power production (F. Zhao et al., 2009). The drastic oxidation of substrate by the microbes at during this condition also contributes for the depletion of electrons near the anodes and inhibits the achievement of high current density. Ieropoulos et al. (2010) also observed that the overshoot appeared to be temporary and the voltage or power recovered after a certain time. This was due to the replenishment of substrate as the MFC was operated under continuous flow condition. No recovery of current densities was observed in Figure 4.5 because the reactor was operated under batch mode and substrate was not replaced during analysis period.

In conclusion, both hypotheses can be applied to elucidate the overshoot experienced by CC and GF systems. Although Min et al. (2008) refuted the bulk mass transfer limitation but the impact of internal or micro-scale diffusion limitation could not be ignored for porous electrodes and within the biofilm matrix (Beyenal & Babauta, 2012; Picioreanu, van Loosdrecht, Curtis, & Scott, 2010). Both CC and GF have uneven surfaces and GF has a significant thickness of 3 mm. Hence, the internal diffusion of reactants and products in and out of the core section of these electrodes and their biofilm matrix could be the rate-limiting step that hindered the high rate of electron transfer. This was further validated by the absence of power overshoot in the GP system, as it possess flat geometry. The presence of smooth surface does not encourage the formation of thick biofilms therefore preventing this phenomenon. Additionally, microbial limitations also play a role for the voltage overshoot as explained earlier.

The polarization curve for GP anode can be clearly divided into two parts. The first part of the curve demonstrated gradual voltage decline that were fairly proportional with the current density. This is indicative of ohmic losses experienced by the system. The second part of the curve exhibited a plunge when approaching high current density. It is attributed to the concentration losses arise from bulk mass transfer constraint posed by both oxidized and reduced species (B. E. Logan et al., 2006).

Maximum power density of GP was 0.16 W/m^2 while CC and GF both had greater maximum power density of 0.35 W/m^2 and 0.52 W/m^2 respectively. The high power density obtained by GF is in good agreement with earlier research by Chaudhuri and Lovley (2003) stating that better surface area of graphite felt increases its current generation compared to graphite rod. The disorganised network of graphite fibres provides ample space for bacterial growth and biofilm formation whereas the smooth surface of GP electrodes discourages the biofilm formation. Cloth anodes have fairly rough surface that encourage the biofilm formation but has less surface area compared to

felt materials. The complete analyses on the biofilm formation are discussed in later sections.

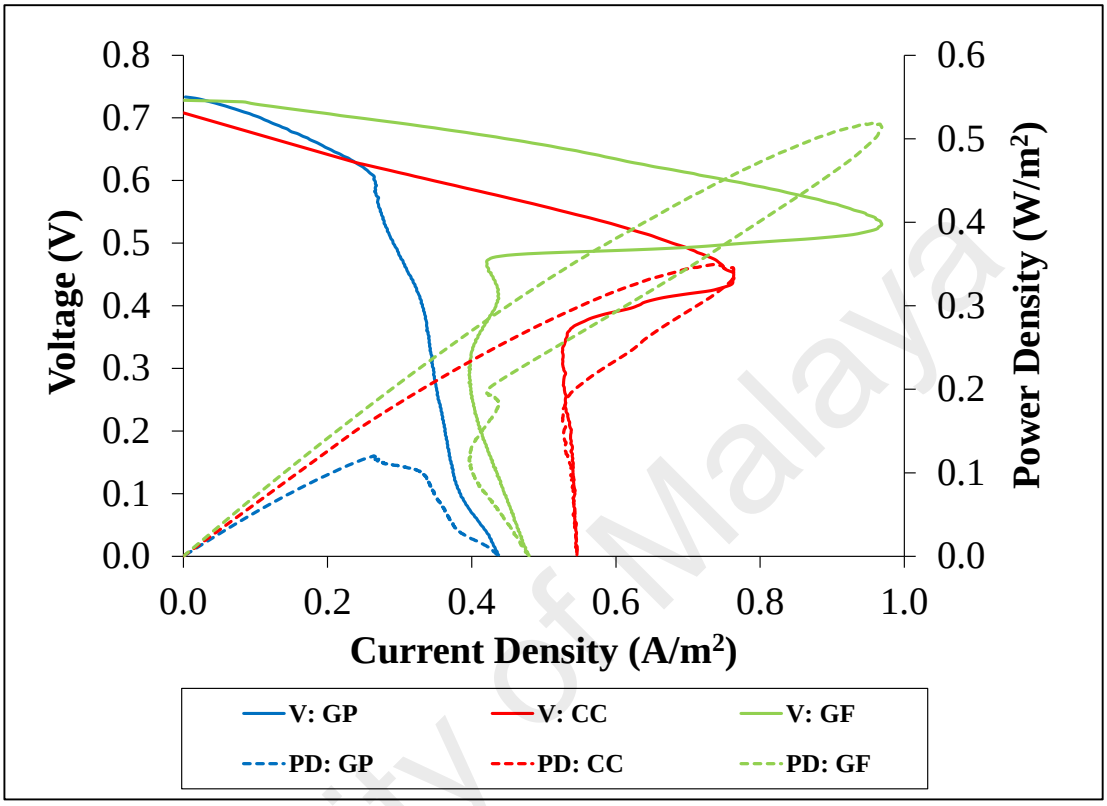

Figure 4.5: Polarization (V) and Power Density (PD) Curves of Control Anodes

4.1.2.3 Internal Resistance and Overpotential

Figure 4.6 illustrates both the experimental and generated Bode plots. Both the planar anodes were fitted using the two time-constant model while three time-constant equivalent circuit was applied to the GF anode to include the finite diffusion element for better correlation.

The components of internal resistance, R_{int} are tabulated in Table 4.1. From the fitted plot, it was observed that the GP system recorded the highest R_{Ω} of 39.7 Ω while GF and CC recorded 13.2 Ω and 9.3 Ω respectively. The difference in R_{Ω} was due to the membrane resistance as the analyses were recorded after three stable cycles. The

membrane inside the reactors experienced slight fouling after long-term operation therefore increasing the R_Ω. Minor discrepancies in electrolyte conductivity during preparation of buffer solution contributed to the variation of R_Ω values as well.

The R_a values obtained for the control anodes were consistent with the voltage generation and polarization analysis. GP demonstrated significantly high R_a of 440.9 Ω, justifying the low voltage and power generation. The CC anode recorded R_a of 98.7 Ω, which is ~ 4 times lower than that of GP. The GF displayed the lowest R_a among the three configurations with 27.7 Ω. This trend reveals that higher anodic resistance results in lower power output which is consistent with previous findings (He et al., 2006; Manohar, Bretschger, Nealson, & Mansfeld, 2008).

The resistance of the anodes before and after biofilm growth showed considerable transformation especially for planar anodes. Prior to the biofilm formation, the CC anode recorded very high R_{ct} compared to GP and GF anodes. However, after stable operation in MFC system, the R_a of CC was lower than GP. This decline was due enriched bacterial growth on CC anodes that increased electron transfer capabilities. Meanwhile the cathodic resistance, R_c for GP, CC and GF were 18.1 Ω, 53.7 Ω and 58.6 Ω respectively.

When comparing all the internal resistance components, it is clear that anodic resistance is the limiting factor for all the anode configurations. Hence, the anode component controls the performance of MFC and its improvement should be emphasized.

Table 4.1: Components of Internal Resistance for Control Anodes

Anode	R_Ω	R_a	R_c	R_d	R_{int}	χ^2
GP	39.7	440.9	18.1	-	498.7	0.5806
CC	9.3	98.7	53.7	-	161.7	0.0125
GF	13.2	27.7	58.6	27.1	126.6	0.0075

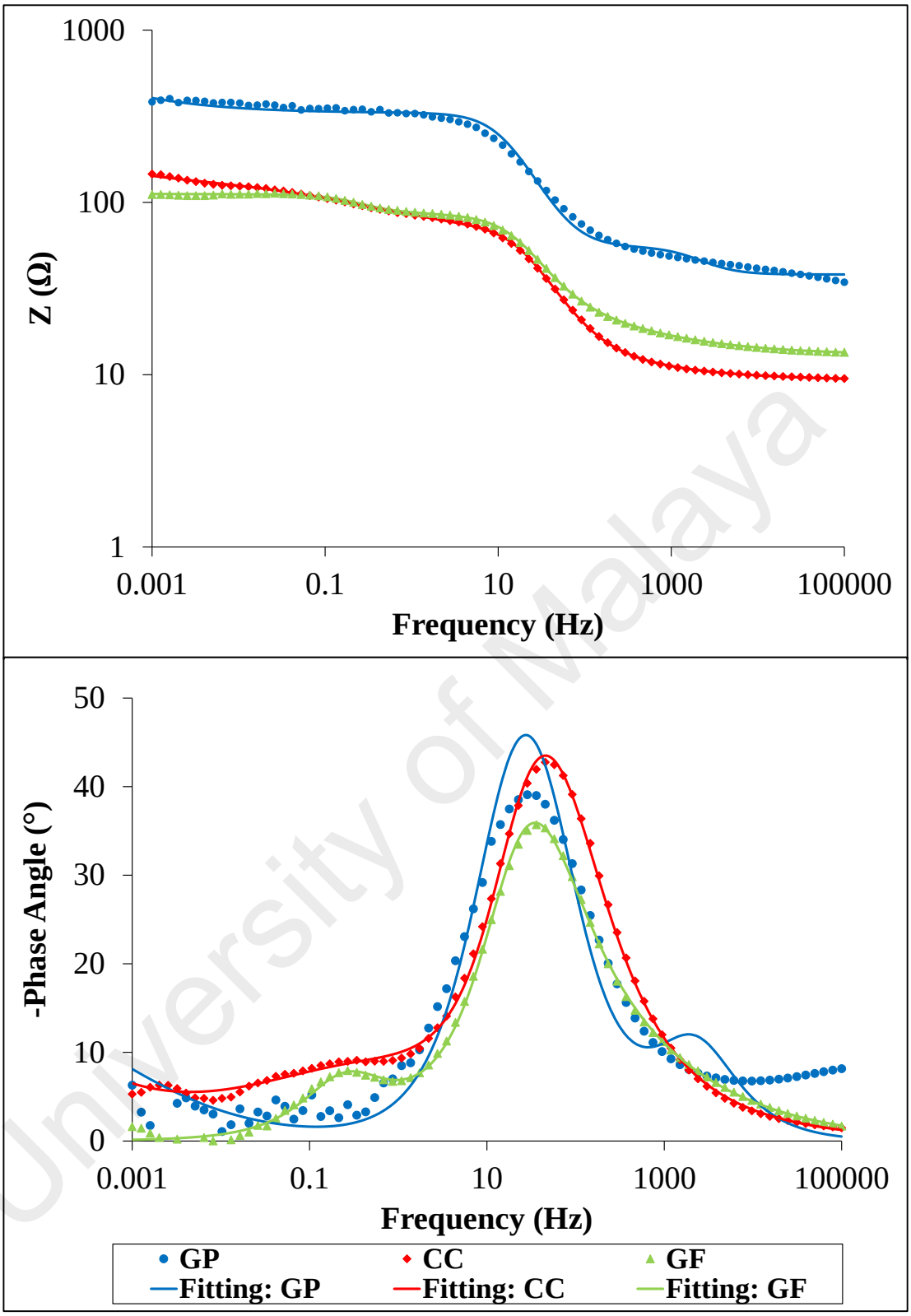

Figure 4.6: Bode Impedance Modulus Plot and Its Corresponding Phase Angle under 1k Ω condition of Control Anodes

4.1.2.4 Individual Electrode Potential

The potential of individual electrodes with respect to current density is disclosed in Figure 4.7. The OCP of the anodes were in the range of -420 to -460 mV vs. Ag/AgCl (3 M NaCl) reference electrode (+0.209 V vs. NHE). These values are in agreement with the theoretical thermodynamics calculation for acetate oxidation as reported by B. E. Logan (2008) i.e., ~ -0.28 to -0.30 V vs. NHE.

The analysis further substantiate that anode is the limiting electrode in these systems. The cathode potential for all systems remained constant even at high current density. However, the potential of anodes plunged drastically when approaching high current density, as it was unable to sustain the increased reaction rate. This trend was observed for all three anodes, validating that untreated carbon-based electrodes are still inferior in terms of electrochemical reactivity and biocompatibility irrespective of configuration (Cai et al., 2013; C. Li et al., 2011).

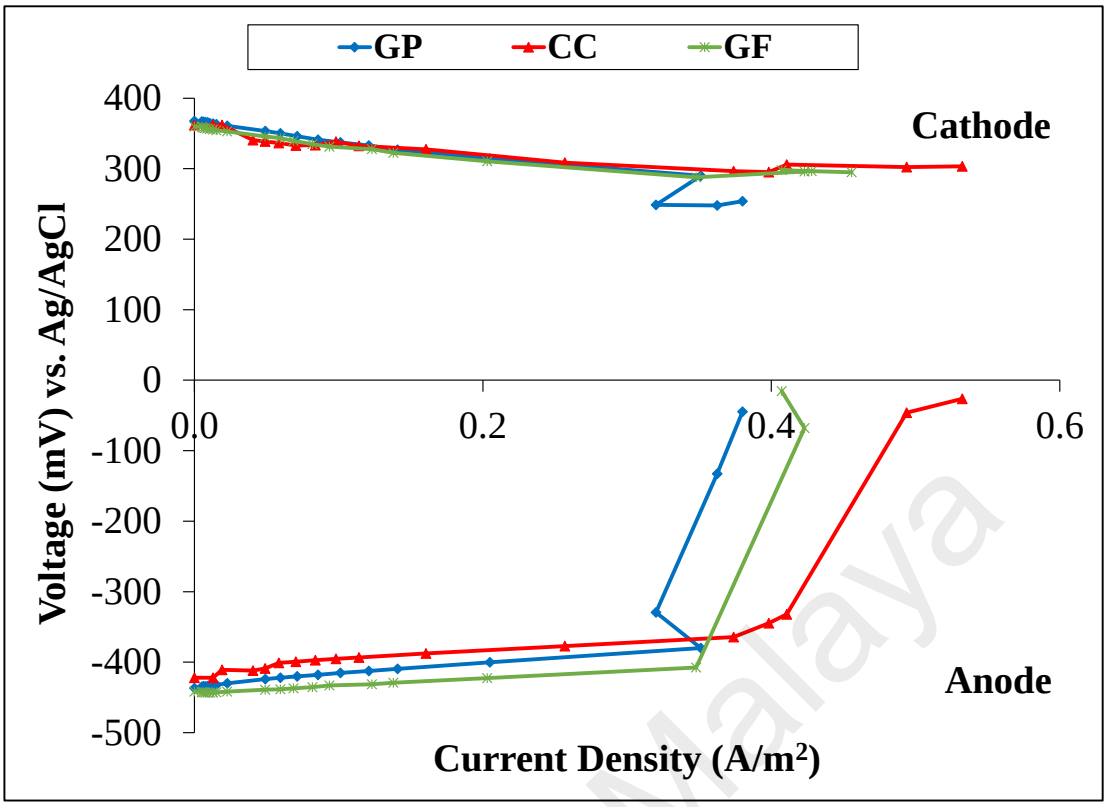

Figure 4.7: Potential of Individual Electrodes of Control Anodes

4.1.2.5 COD Removal and Efficiency

The COD removals of the three types of control anodes were similar and fell in the range of ~79 to 85% as displayed in Figure 4.8. GF anode achieved the highest CE at 45.4%, which is consistent with high voltage generated. GP and CC both attained CE of 39.0% and 31.0% respectively. In summary, the performance of the anodes are in the order of GF > CC > GP due to the influence of their physical configuration and surface morphology as all other factors are kept constant.

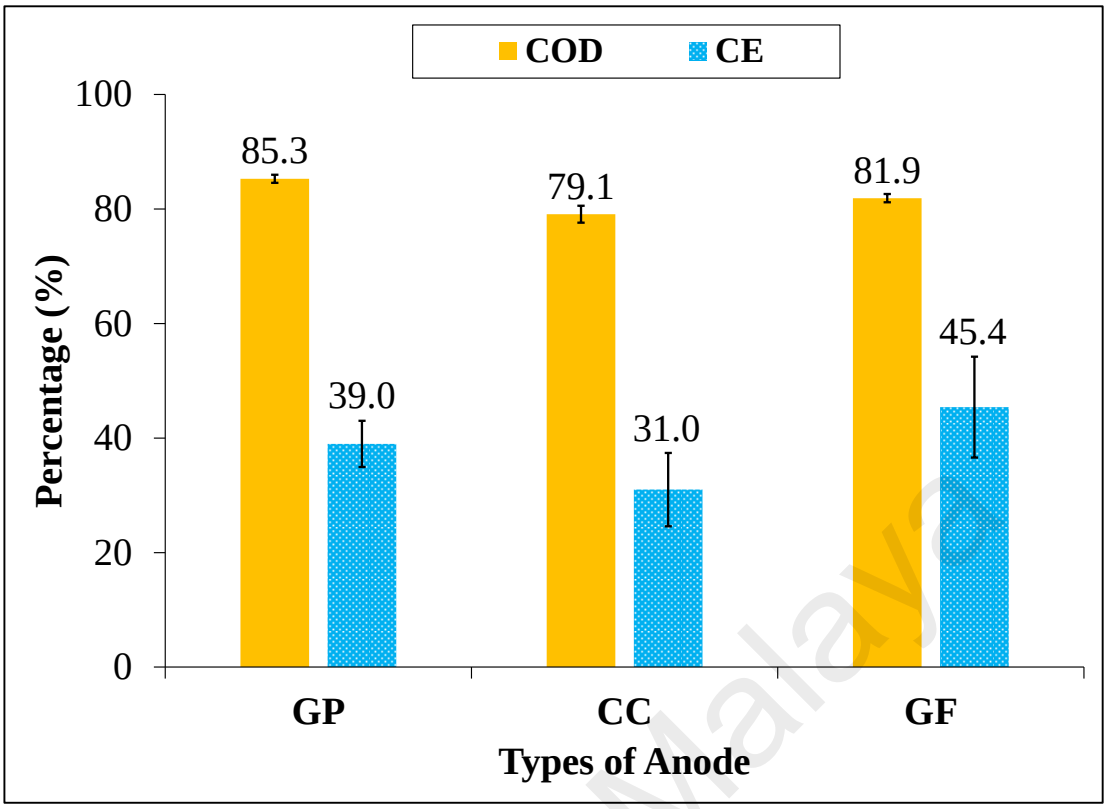

Figure 4.8: COD Removal and CE Percentage of Control Anodes

Evidently, anode component is the limiting factor in this MFC system as established from all the analyses deliberated above. Thus, attention must be given on the improvement of anodes in order to enhance further the performance of MFC. Hence, the present study aims on overcoming the anodic overpotential by modifying these anodes by incorporating PEDOT, a conductive polymer known for its high conductivity and stability.

4.2 Characterization of Synthesized PEDOT

4.2.1 Functional Group and UV–Visible Analysis

The FTIR spectrum for the synthesized PEDOT was carried out to confirm the polymerization of EDOT and is illustrated in Figure 4.9. The spectrum is consistent with the functional groups present in PEDOT, verifying the successful synthesis of the material (Q. Zhao, Jamal, Zhang, Wang, & Abdiryim, 2014). Peaks around 1458 cm^{-1} and 1273 cm^{-1} are attributed to C=C and C-C stretching vibrations of the heteroaromatic thiophene ring respectively. Peaks ranging from 1000-1200 cm^{-1} (1159, 1125 and 1070 cm^{-1}) are indicative of C-O-C bond arising from dioxane. The peaks around 947, 865 and 666 cm^{-1} signifies the presence of C-S-C bonds present in the thiophene ring.

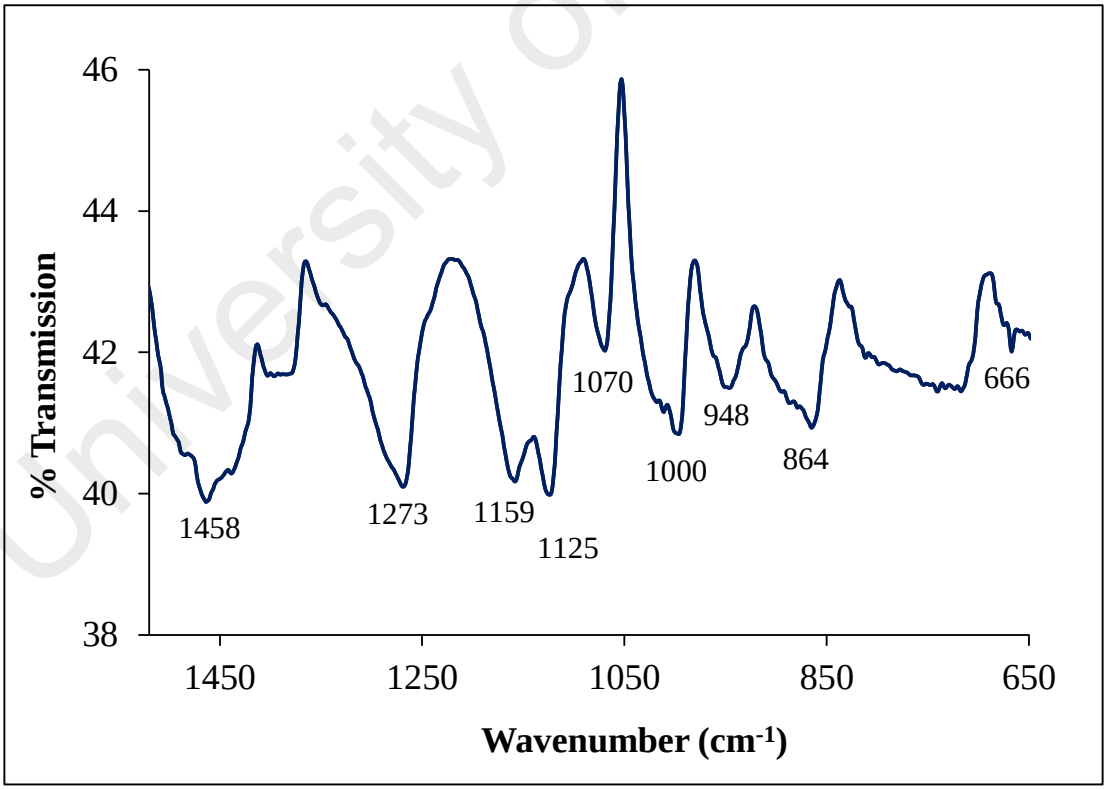

Figure 4.9: FTIR Spectrum of Synthesized PEDOT

The UV-Vis absorption spectrum of the synthesized PEDOT is shown in Figure 4.10. The broad peak ranging from 450 to 700 nm is designated to the π-π* transitions of the thiophene ring (Nie, Zhang, Xu, Lu, & Bai, 2014).

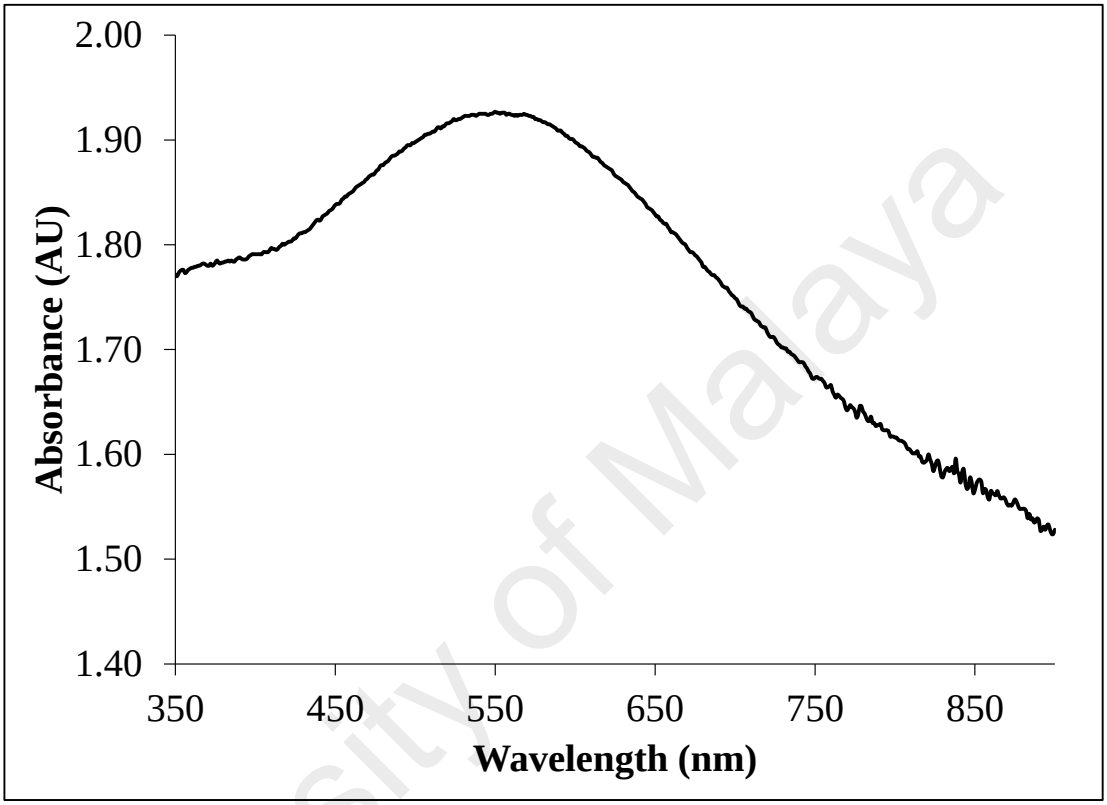

Figure 4.10: UV-Vis Spectrum of Synthesized PEDOT

4.2.2 Crystalline Phase Analysis

The crystallographic analysis of the synthesized PEDOT is depicted in Figure 4.11. The analysis reveals broad peaks that denote the amorphous nature of the synthesized PEDOT (Selvaganesh, Mathiyarasu, Phani, & Yegnaraman, 2007). The spectrum exhibits two distinct peaks at 2Θ = 12.8°and 26°. The peak at ~26° is ascribed to the inter-chain planar ring stacking (C. Jiang, Chen, & Wang, 2012; Q. Zhao et al., 2014). The reflection at 12.8° corresponds to the (2 0 0) polymer backbone.

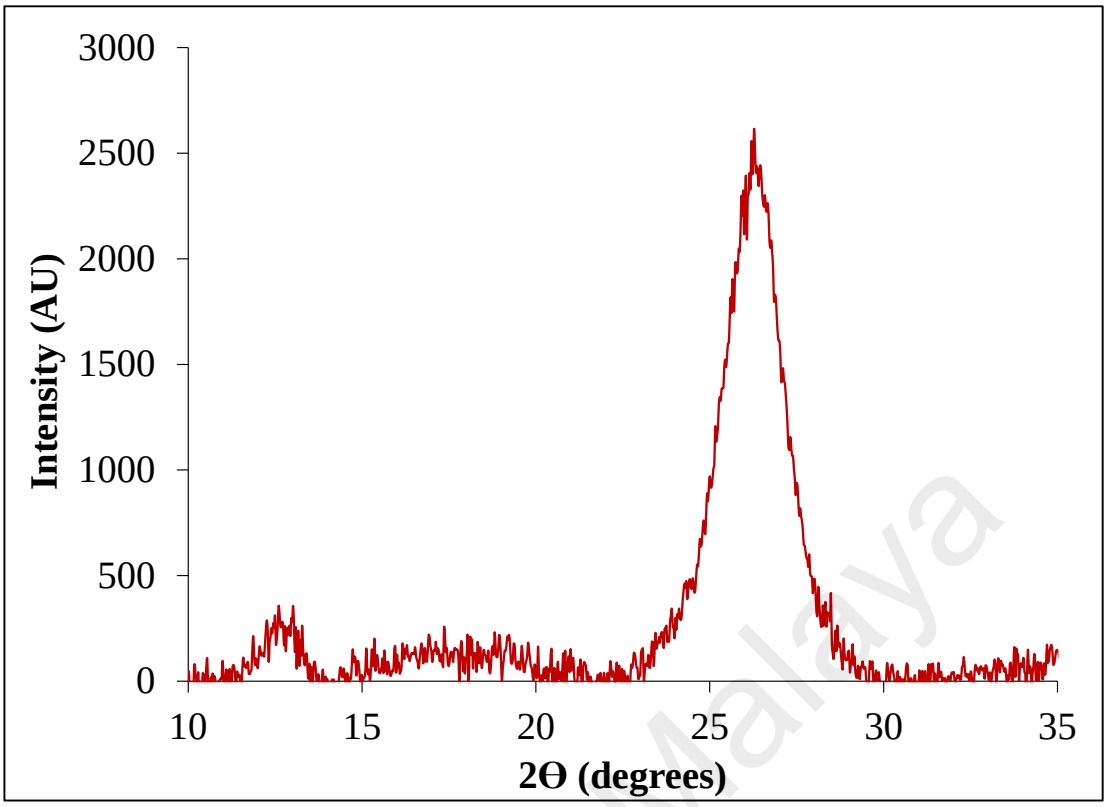

Figure 4.11: XRD Graph of Synthesized PEDOT

4.2.3 Thermal Stability Analysis

The thermal stability of PEDOT was studied with TGA and the obtained curve is shown in Figure 4.12. The weight decreased at the initial phase of ~100°C was related to the evaporation of solvent and moisture from PEDOT. The conductive polymer was stable up to 250°C before a sharp decline was observed at the temperature zone of 300 to 400°C. This was due to the decomposition of the main chains in PEDOT (Shin, Jeon, & Im, 2011).

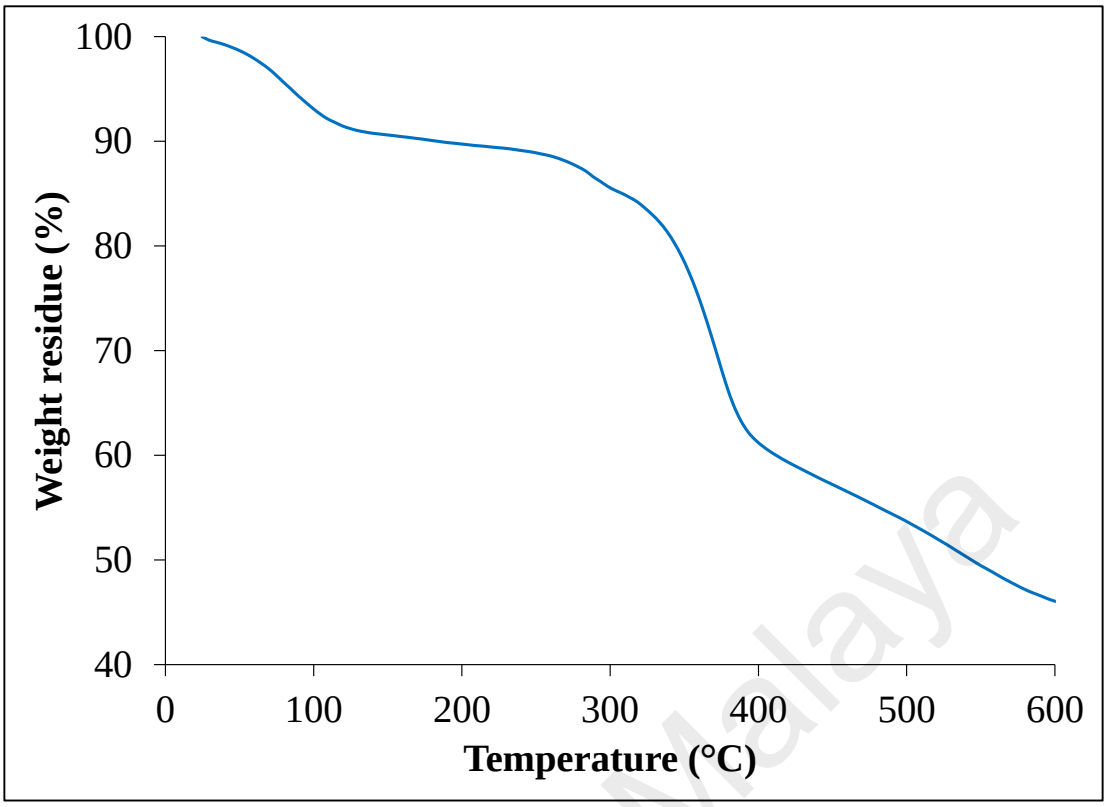

Figure 4.12: TGA Plot of Synthesized PEDOT

4.2.4 Morphology and Composition

Synthesized PEDOT particles were observed using SEM and is shown in Figure 4.13. The morphology of PEDOT had both flake and granules-like structure. The rapid propagation of PEDOT chains that forms nano-fibrous oligomers in the incipient stage of polymerization results in granular formation. The prolonged polymerization caused these nanofibers to attach to each other and consequently led to flake morphology (Q. Zhao et al., 2014). The particles did not have any distinguished shape and size as clearly seen in the SEM image of higher magnification.

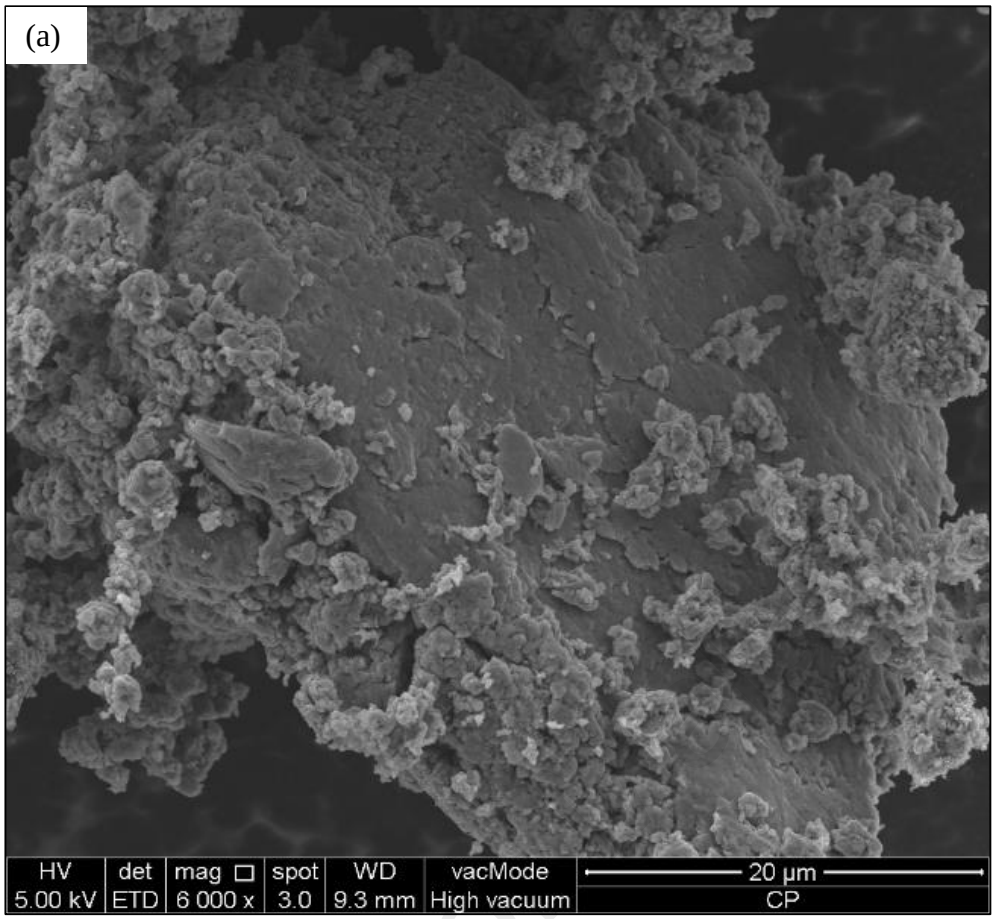
(a)
HV
5.00 kV
det
ETD
mag
6 000 x
spot
3.0
WD
9.3 mm
vacMode
High vacuum
20 µm
CP

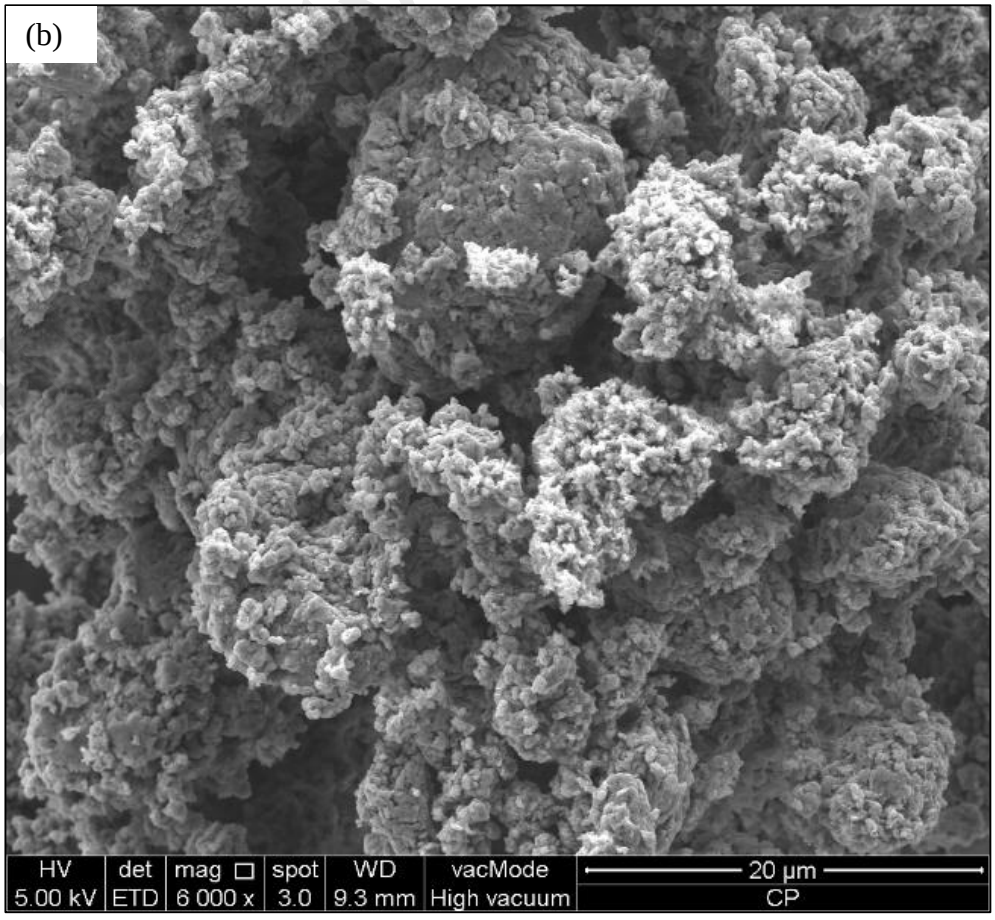
(b)
HV
5.00 kV
det
ETD
mag
6 000 x
spot
3.0
WD
9.3 mm
vacMode
High vacuum
20 µm
CP

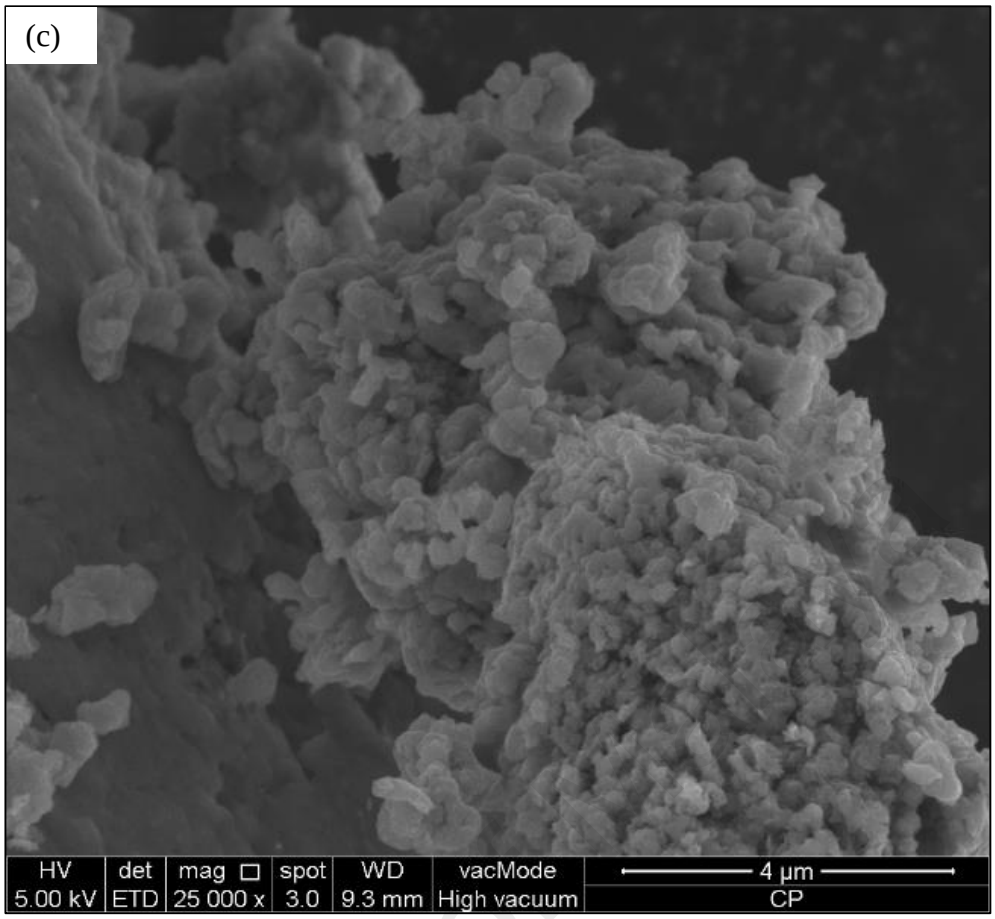

Figure 4.13: Morphology of Synthesized PEDOT at Different Magnifications

The elemental compositions of the PEDOT particles were confirmed with EDS analysis and are presented in Figure 4.14 and Table 4.2. The detected elements (carbon, oxygen and sulphur) are consistent with its linear formula of [$(C_6H_4O_2S)n$]. Traces of iron (Fe) and chlorine (Cl) were identified and were contributed by the oxidizing agent, $FeCl_3$.

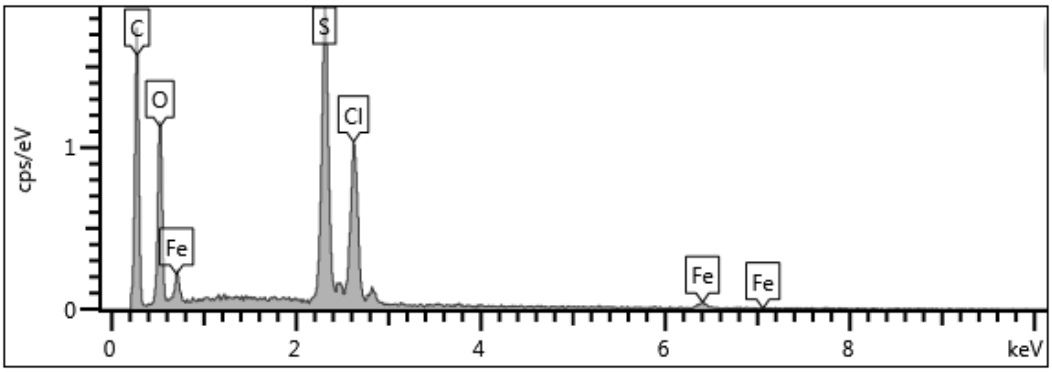

Figure 4.14: EDS Spectrum of Synthesized PEDOT

Table 4.2: Elemental Composition of Synthesized PEDOT

Element	Wt.%	Mol	Approximate Ratio
C	47.94	4.00	7.1
O	13.93	0.87	1.6
S	18.03	0.56	1.0
Cl	13.25	0.37	3.1
Fe	6.84	0.12	1.0
Total:	100.00		

The insight into the characterization analyses revealed the successful synthesis of PEDOT through a facile chemical polymerisation procedure. Thus, the synthesized PEDOT was used as a coating onto the different anode configurations.

4.3 Characterization and Application of PEDOT Functionalized Graphite Plate Anodes

4.3.1 Characterization

4.3.1.1 Surface Morphology

The SEM images of GP and its modified anodes are portrayed in Figure 4.15 (a-d). GP has a smooth planar surface as discussed previously. The image for GP-P disclosed that the surface of the electrode was partially covered with PEDOT particles with uneven coating. For GP-2P sample, the surfaces were uniformly covered with PEDOT particles although minor cracks were visualised. A denser coating was achieved by GP-3P with the surface completely filled with PEDOT particles. However, due to the increased weight and thickness, the surface attachment of PEDOT onto the plate weakened and was susceptible to dislodge easily.

(a)

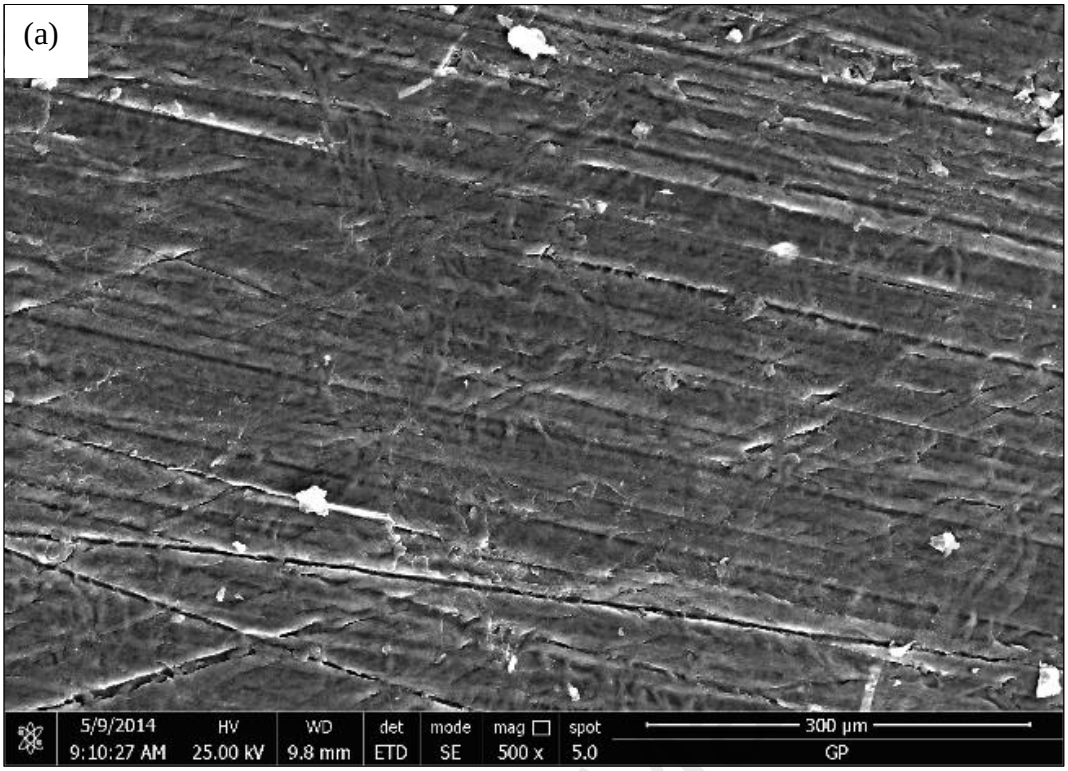
5/9/2014
9:10:27 AM
HV
25.00 kV
WD
9.8 mm
det
ETD
mode
SE
mag
500 x
spot
5.0
300 µm
GP

(b)

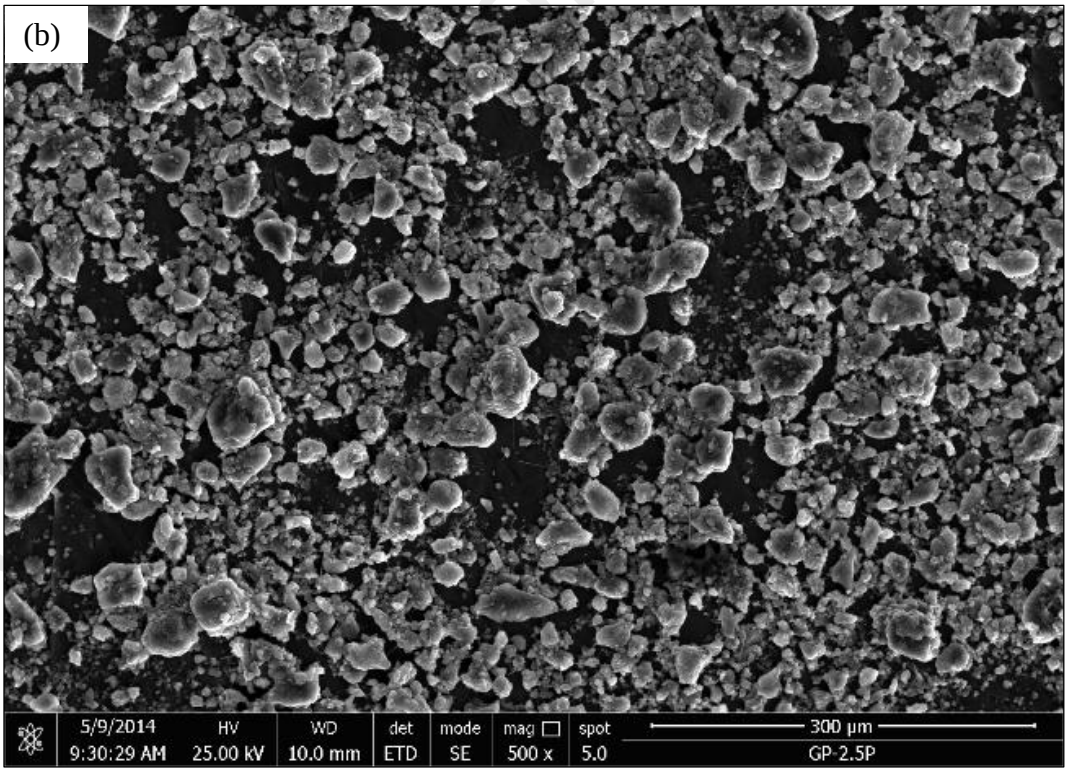
5/9/2014
9:30:29 AM
HV
25.00 kV
WD
10.0 mm
det
ETD
mode
SE
mag
500 x
spot
5.0
300 µm
GP-2.5P

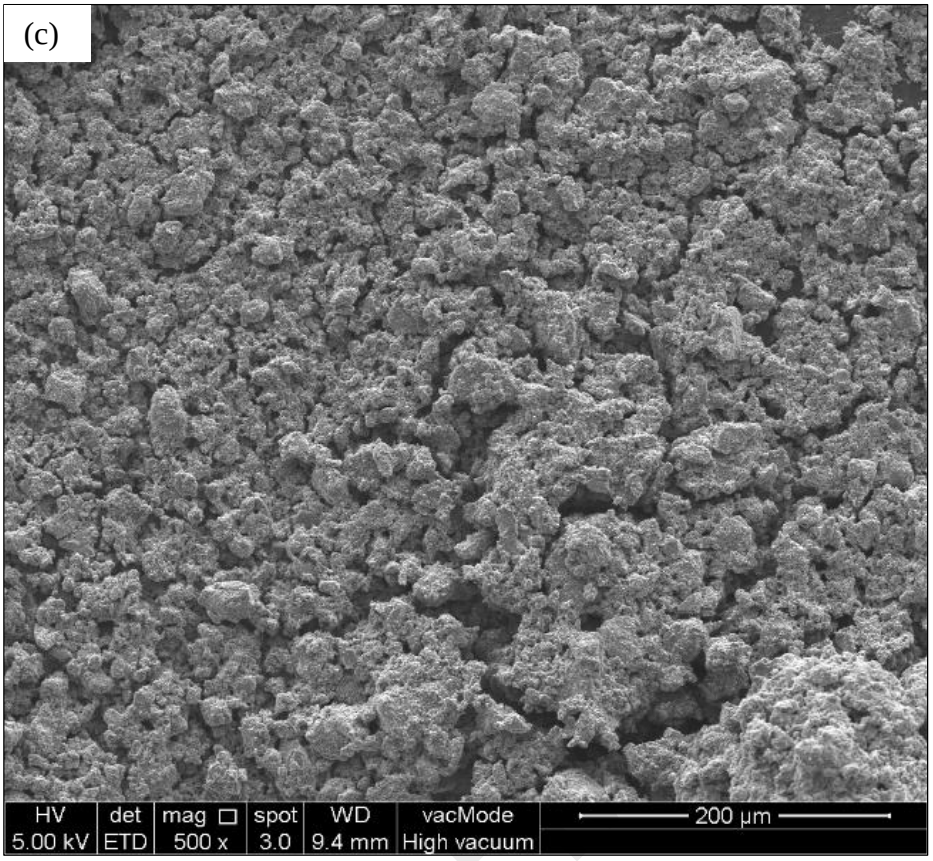

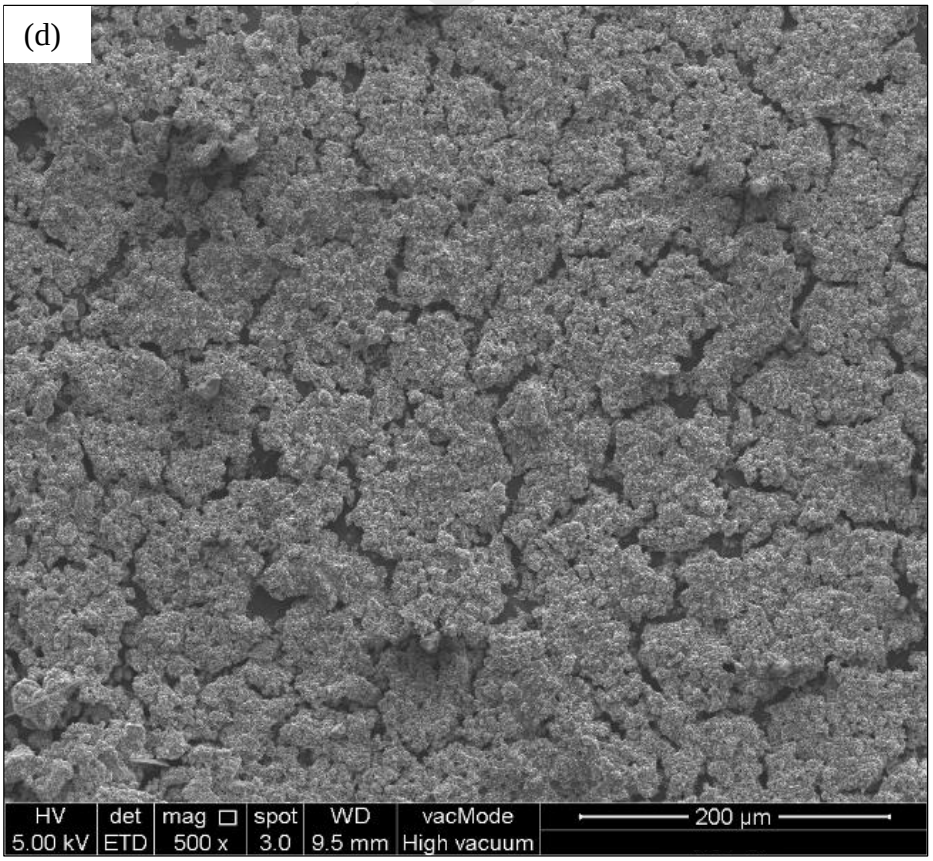

Figure 4.15: SEM Images of Plate Anodes; (a) GP, (b) GP-P, (c) GP-2P and (d) GP-3P

4.3.1.2 Electrochemical Analysis

The CV profile of the functionalized plate anodes is dispalyed in Figure 4.16. The plot revealed the enhancment of electrochemical activeness of the anodes with increased PEDOT loading. In general, the area under voltammogram represents the integration of the potential and current. The total charge involved in the redox reaction can then be quantified if the area under the curve is divided by scan rate. As the CV was carried out with a fixed scan rate, electrolyte concentration and projected surface area for all the samples, the larger the area under the curve is indicative of greater charge transfer involved in the reaction. Hence, the area of the CV curve gives an approximate assessment of the electrochemical reactivity and efficiency of electron transfer of the electrode materials.

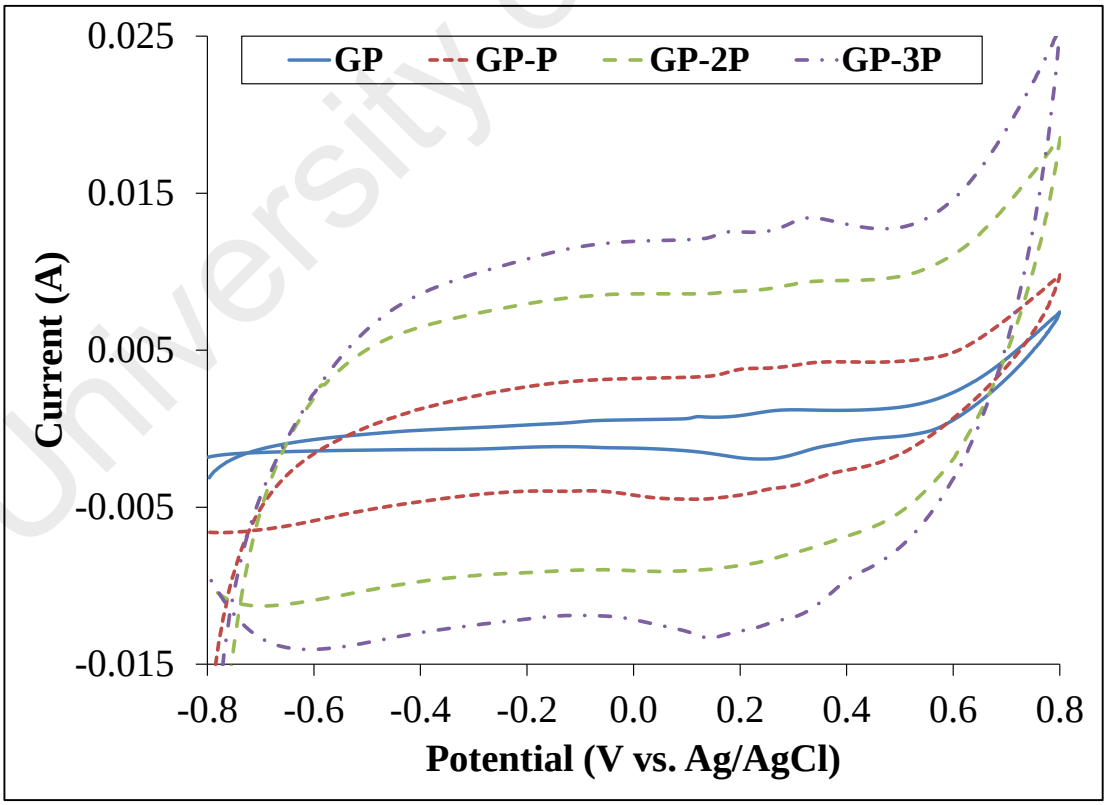

Figure 4.16: CV of Plate Anodes in 1 mM $K_3[Fe(CN)_6]$ and 0.5 M KNO_3 electrolyte at a scan rate of 10 mV/s.

An opposite trend was observed from Figure 4.17 for the EIS analysis as the charge transfer resistance, R_{ct} increased with increasing loading of PEDOT. The initial R_{ct} of GP was ~19 Ω and increased to ~33 Ω for GP-P. The escalation of this resistance becomes more prominent for higher PEDOT loading as the R_{ct} of GP-2P and GP-3P were fitted at 234 Ω and 240 Ω respectively. This surge in R_{ct} were contributed by the Nafion solution used as binder in the functionalized plate anodes. Literatures have demonstrated that these binders reduced the conductivity and hampered the electron transfer on the surface of anodes, increasing their resistance (Lv et al., 2013). As higher PEDOT loading requires higher amount of Nafion binder, the R_{ct} of the modified plate anodes increased as well.

The opposing trends of electrochemical analyses attained by these plate anodes could only be verified by applying them in MFC reactors to evaluate their actual capabilities as various factors govern the efficiencies of MFC anodes.

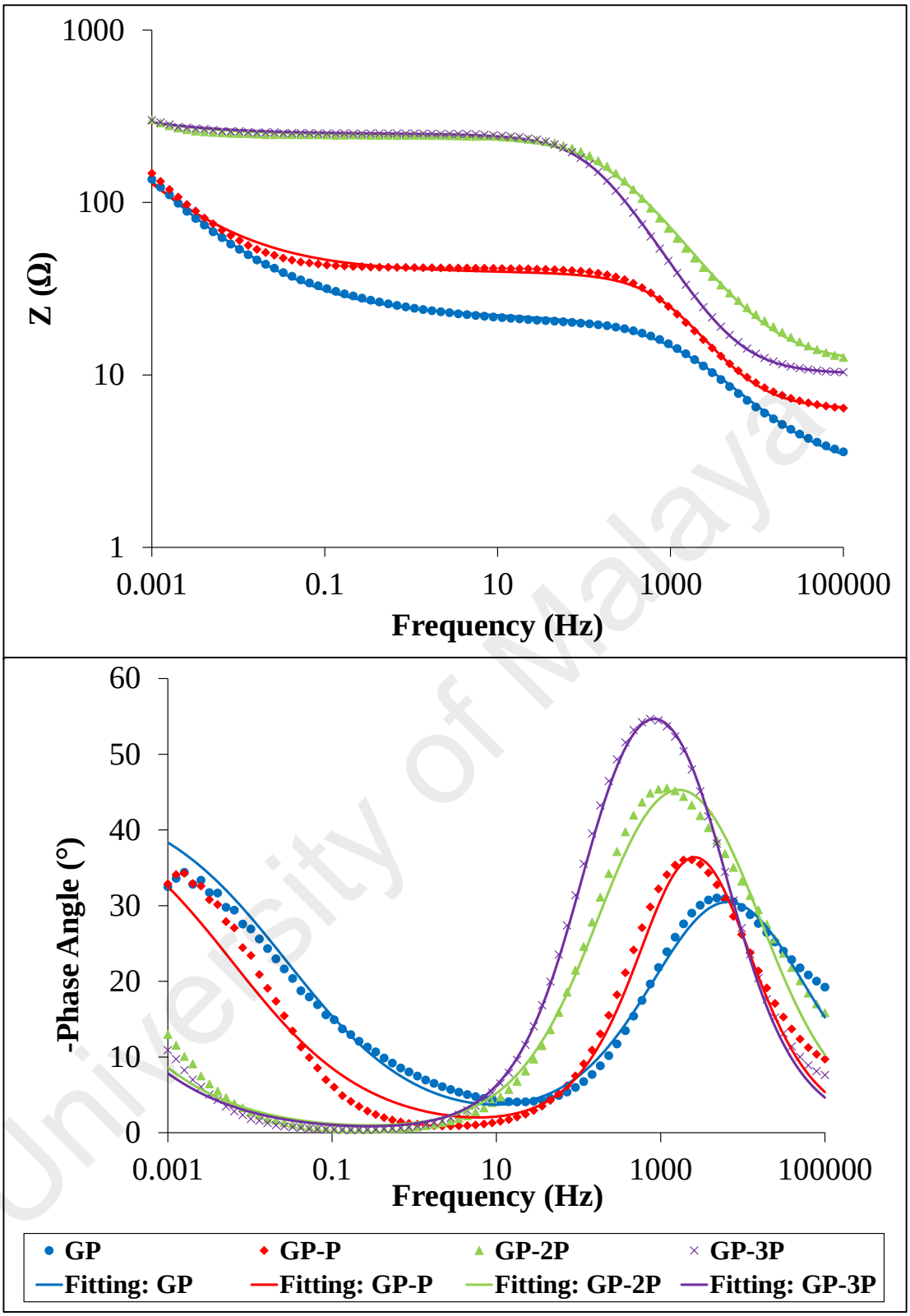

Figure 4.17: Bode Impedance Modulus Plot and Its Corresponding Phase Angle of Plate Anodes in 2.5 mM $[Fe(CN)_6]^{3-/4-}$ and 0.5 M KNO_3 as electrolyte.

4.3.2 MFC Performance

4.3.2.1 Voltage Generation

The voltage generation across 1 kΩ resistor for GP, GP-P, GP-2P and GP-3P for three consecutive cycles are illustrated in Figure 4.18. The maximum voltages for these anodes varied considerably. GP-P displayed highest voltage of 660.0 ± 7.2 mV with significantly improvement of 48% as compared to GP (444.5 ± 12.3 mV). However, with further increase of PEDOT loading, the voltage generation decreased as GP-2P documented a slight drop, achieving 647.3 ± 7.4 mV. GP-3P recorded the lowest voltage at 266.1 ± 12.7 mV, which is less than the control anode. It is evident that GP-3P anode was incapable of generating a promising voltage and the observed voltage was contributed by the cathode compartment of the system. It can be deduced that high loading of PEDOT was detrimental to anode productivity and hindered its MFC performance. Further analyses and verification on the cause of this condition were discussed in the later sections.

In terms of anode stability and durability, all three cycles for the plate anodes demonstrated consistent cycle duration and voltage generation. This elucidates that the anodes did not suffer any degradation or breakdown throughout the experiment, establishing the stability of the PEDOT functionalization and biofilm formation on the anodes.

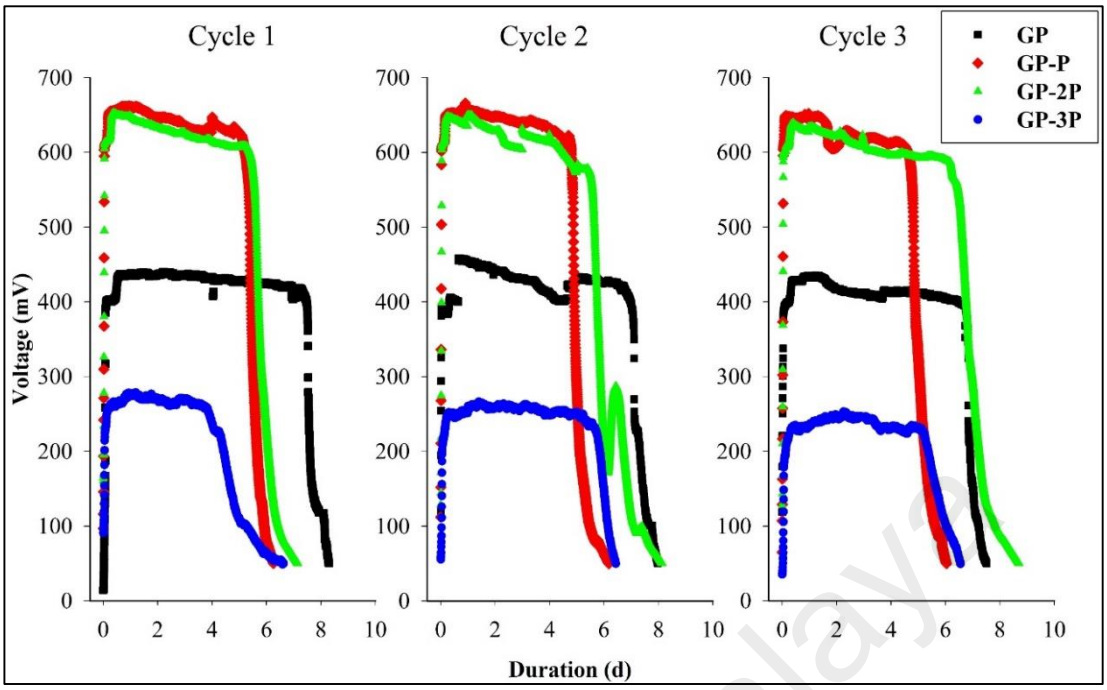

Figure 4.18: Voltage Generation for Three Consecutive Cycles of Plate Anodes

4.3.2.2 Current and Power Density

The polarization and power curve for plate anodes is shown in Figure 4.19. The I_{sc} and maximum power density of the GP-P and GP-2P anodes experienced a significant surge compared to the GP anode. GP-P exhibited an increase of six folds in I_{sc} with a magnitude of 2.74 A/m^2 while GP-2P (4.11 A/m^2) improved almost 10 times compared to GP. However, for GP-3P, the I_{sc} and power density plunged drastically to 0.27 A/m^2, which is below the I_{sc} of the control anode (0.44 A/m^2). This ratify that the functionalization of PEDOT onto plate anodes improved the maximum sustainable current density by increasing the substrate degradation rate, electron transfer and biofilm formation (B. E. Logan & Regan, 2006b).

The power density curves gave the correlation between power and current density of the tested systems. The maximum power density achieved by GP-P and GP-2P are 0.64 W/m^2 and 0.83 W/m^2 respectively, which are 4 and 5 times greater than that of GP (0.16W/m^2). GP-3P demonstrated an inconsequential power density of 0.04 W/m^2.

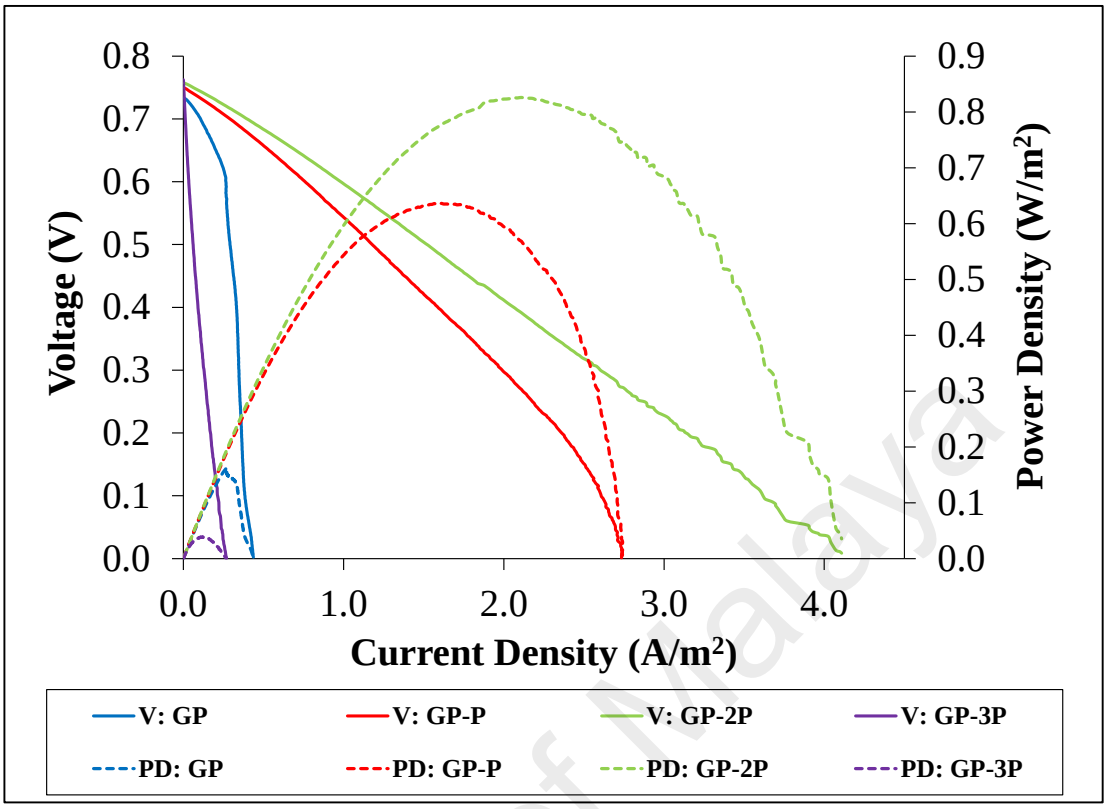

Figure 4.19: Polarization (V) and Power Density (PD) Curves of Plate Anodes

4.3.2.3 Internal Resistance and Overpotential

The EIS analysis for the whole cell under stable working condition is presented in Figure 4.20 accompanied by the fitting plot. The values extracted from the plots are tabulated in Table 4.3. In general, the internal resistance of the overall system decreased considerably with the incorporation of PEDOT onto the plate anodes. The R_Ω of all the modified anodes were in the range of 11-14 Ω as the anolyte and catholyte concentration were kept constant throughout the experiment. The higher R_Ω for GP was due to membrane fouling as discussed previously. The R_a of all the PEDOT modified anodes decreased by ~10 times than that of control anode. It should be noted that all the modified anodes recorded higher R_{ct} before MFC operation compared to the control anode. However, R_a of the modified plate anodes reduced significantly compared to GP. This

reduction was attributed to functionalization of PEDOT where it promoted stable biofilm formation and electron transfer. The R_c of these systems ranged from 5 Ω to 23 Ω and are not the dominant factor limiting the efficiency of the MFC systems.

It should be noted that the low R_a of GP-3P is inconsistent with the low voltage generation exhibited from the system. The current and power density of GP-3P was also inferior compared to both GP-P and GP-2P. This contradicts the inference that lower R_a brings about higher power generation ability. The low R_a exhibited by GP-3P is due to the intrinsic characteristic of the anode itself and was not due to the electron transfer by microorganism. A plausible explanation is due to the invasion of aerobic microorganism in the anodic biofilm contributed to the failure of GP-3P anode to produce improved power generation.

Table 4.3: Components of Internal Resistance for Plate Anodes

Anode	R_Ω	R_a	R_c	R_{int}	χ^2
GP	39.7	440.9	18.1	498.7	0.5806
GP-P	14.2	48.3	22.4	84.9	0.0460
GP-2P	11.2	50.0	7.9	69.1	0.0452
GP-3P	13.2	28.0	4.7	45.9	0.0240

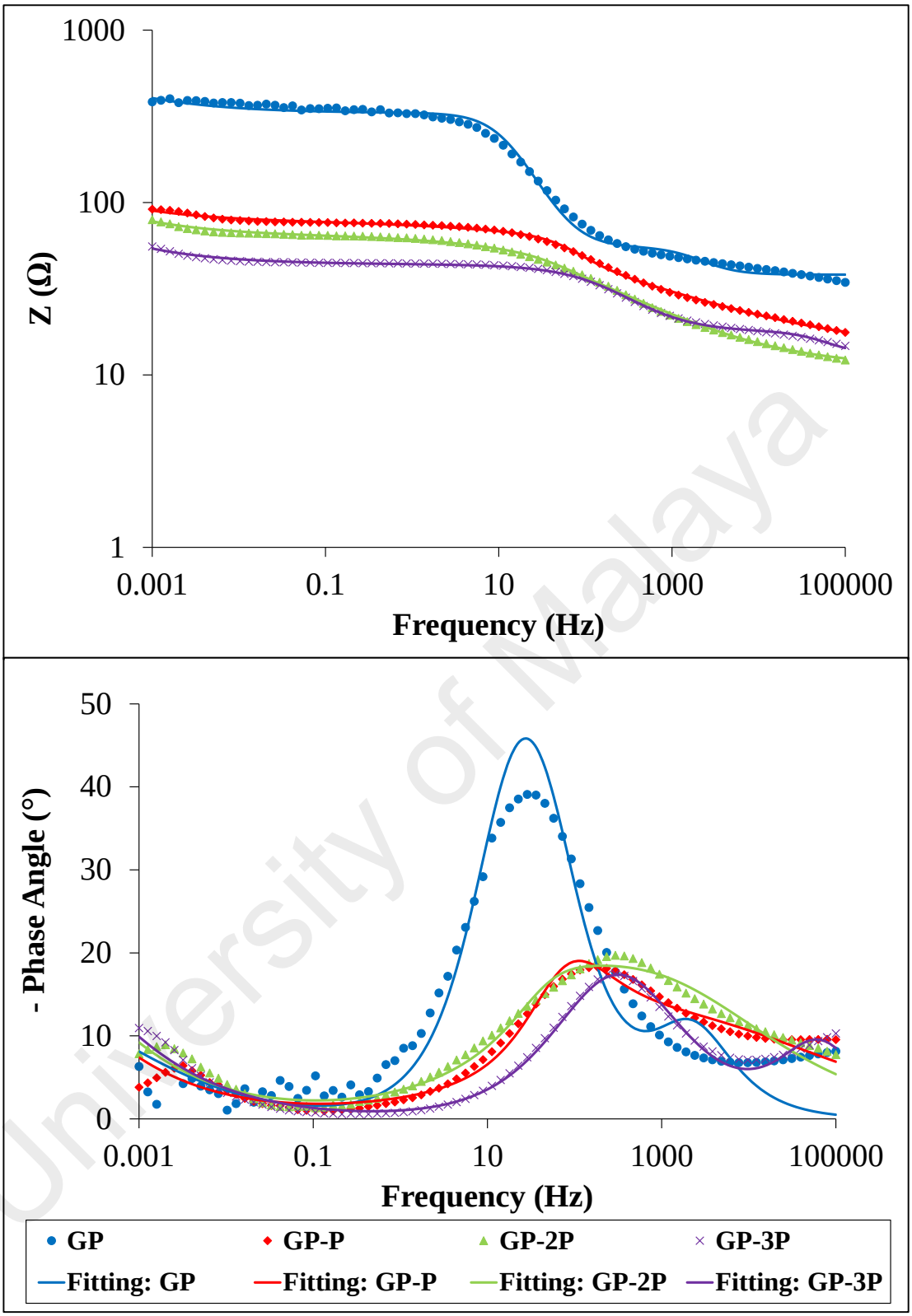

Figure 4.20: Bode Impedance Modulus Plot and Its Corresponding Phase Angle under 1 kΩ condition of Plate Anodes

4.3.2.4 Individual Electrode Potential

The individual electrode potential curve of GP and its modified anodes are illustrated in Figure 4.21. The potential of cathodes remained constant for the range of current density tested for GP-P and GP-2P systems while marginal drop was observed for GP and GP-3P systems. Overall, significant decrease in anodic potentials were observed for all the plate anodes as current density increases. GP and GP-3P anodes experienced drastic plunge when approaching their maximum current density while GP-P and GP-2P underwent more gradual decrease as observed from the figure. It is apparent that drop in anodic potentials are more extensive compared to cathode potentials, indicating that anodes are again the limiting factor in the present systems.

The OCP recorded for all the anodes were consistent with the acetate oxidation values except for GP-3P. The anode potential at OCP for GP-3P was lower than the other anodes at -372 mV. The high R_{ct} and thick PEDOT layer of GP-3P caused the electron transfer from the microbes to the anode to experienced more exertion and consequently reduced the potential (B. E. Logan, 2008). The anodic potential of this sample also changed from negative to positive potential at low current density. Positive potentials are more favourable for aerobic microrganisms, indicating that the anodic bifilm are populated by non electrochemically active bacterias. Hence, the acclimitization of GP-3P anodic biofilm with exoelectrogens was unsuccessful and impeded the electricity generation of the GP-3P system.

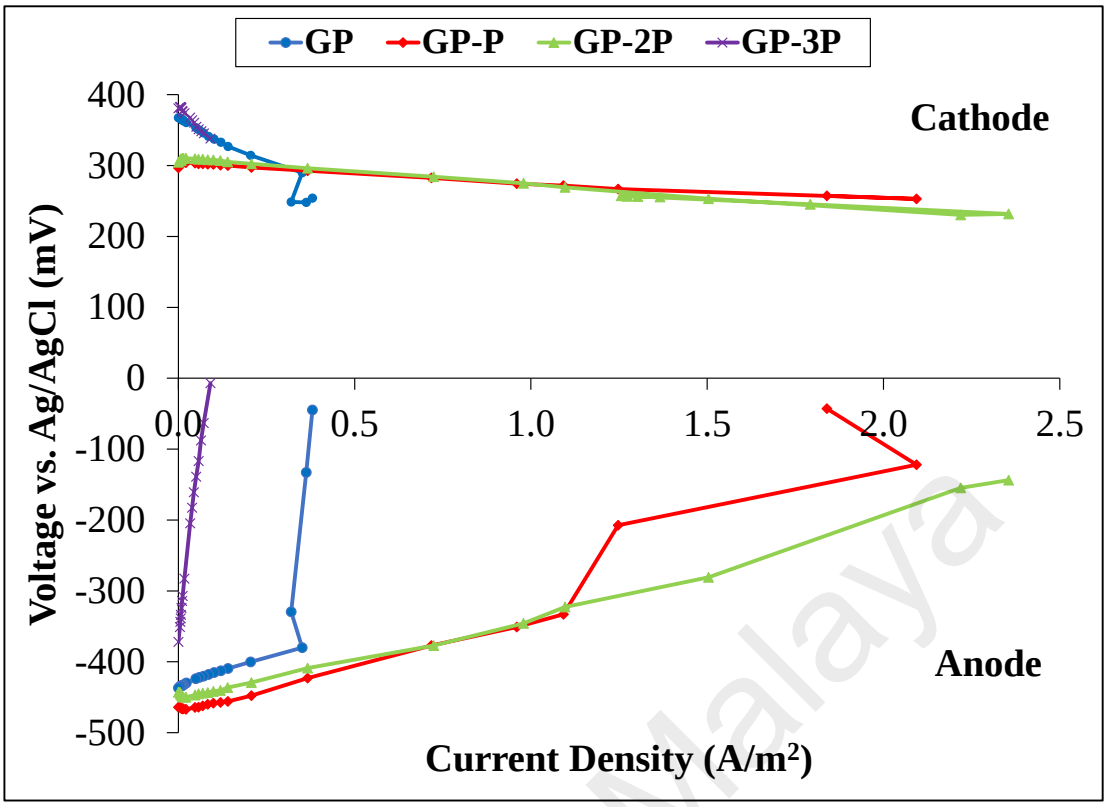

Figure 4.21: Potential of Individual Electrodes of Plate Anodes

4.3.2.5 COD Removal and Efficiency

The COD removals of the all the plate anodes are almost comparable and fall in the range of ~85 to 89% as shown in Figure 4.22. GP-2P exhibited the highest CE at 44.6% followed by GP-P at 40.1%. Due to low voltage generation, GP-3P resulted in lowest CE (~15%). The high COD removal and low CE of GP-3P showed that non-electrochemically active microorganisms such as aerobic bacteria are utilizing the carbon content in the anolyte (Y. Feng, Lee, Wang, Liu, & He, 2010; Rismani-Yazdi et al., 2013).

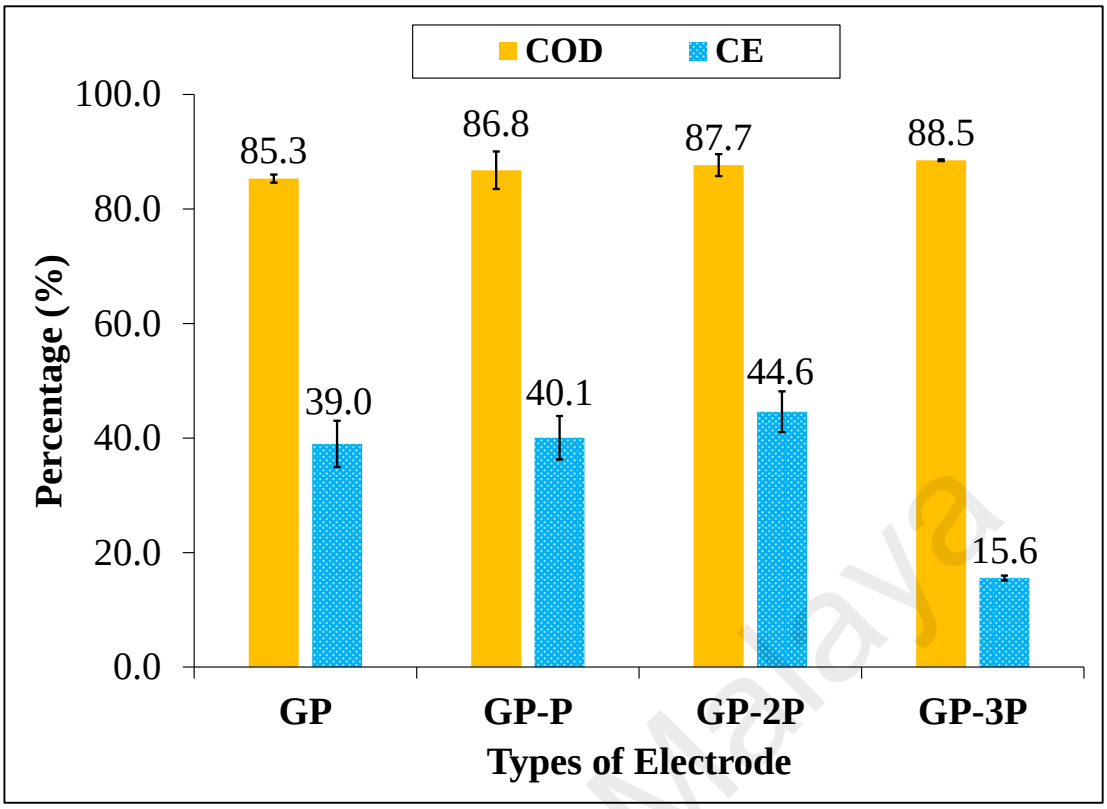

Figure 4.22: COD Removal and CE Percentage of Plate Anodes

The above analyses proved that PEDOT functionalization on plate anodes significantly enhanced their electrochemical reactiveness and these improvements are reflected in their voltage and electricity production. Both GP-P and GP-2P achieved better electron transfer efficiency, maximum current and power density as well as COD removal and CE. However, at the highest PEDOT loading, the overall performance dropped extensively. Although the electrochemical characteristics of the GP-3P indicated substantial enhancement, the inoculation of exoelectrogens onto the anode was unsuccessful and aerobic microbes were cultivated instead as discussed in the analyses above. This phenomenon attested that the overloading of PEDOT onto plate anodes is detrimental to their biofilm selection and consequently MFC performances.

4.4 Characterization and Application of PEDOT Functionalized Carbon Cloth Anodes

4.4.1 Characterization

4.4.1.1 Surface Morphology

The synthesized PEDOT particles were successfully loaded onto the carbon fibres as depicted from the SEM analysis shown in Figure 4.23. CC-P and CC-2P had reasonably uniform coverage of PEDOT across the surface of the anodes with the latter obtaining a thicker coating. However, for CC-3P, the PEDOT coating grew denser and heavier, causing the layer to crumble. The coating on CC-3P was no longer uniform and only fragments of PEDOT particles were seen attached to the fibres.

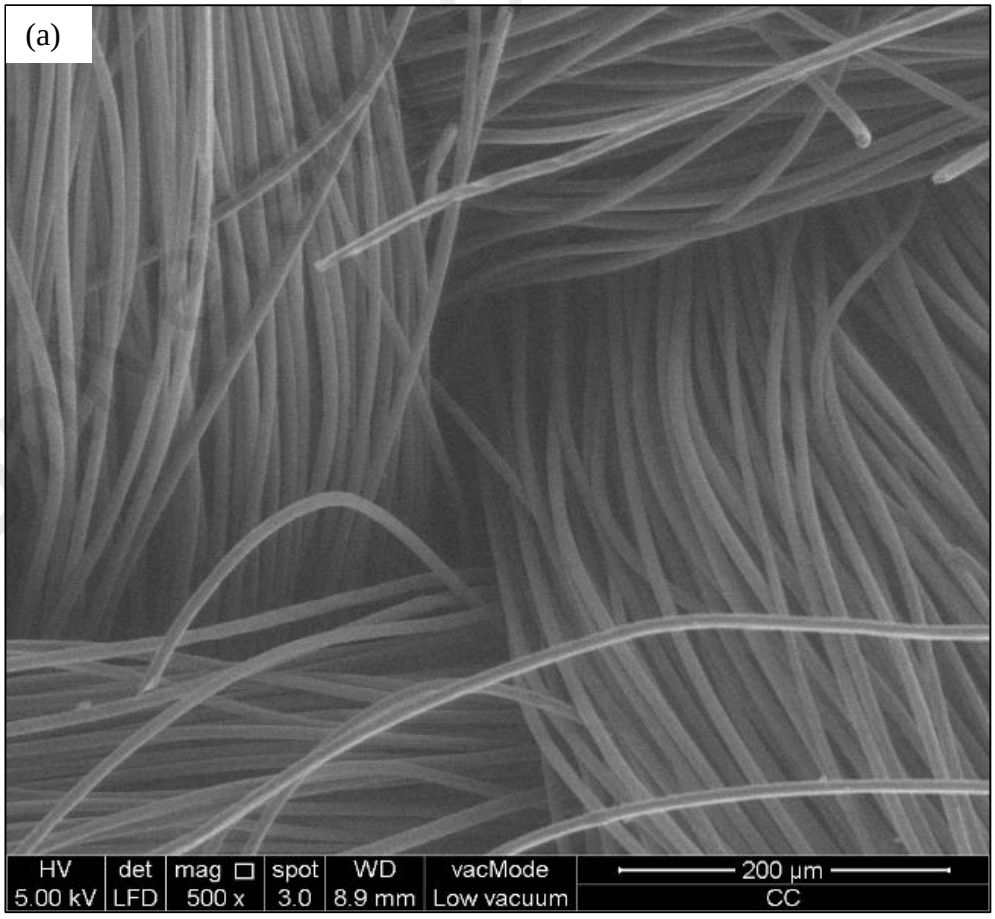

(b)

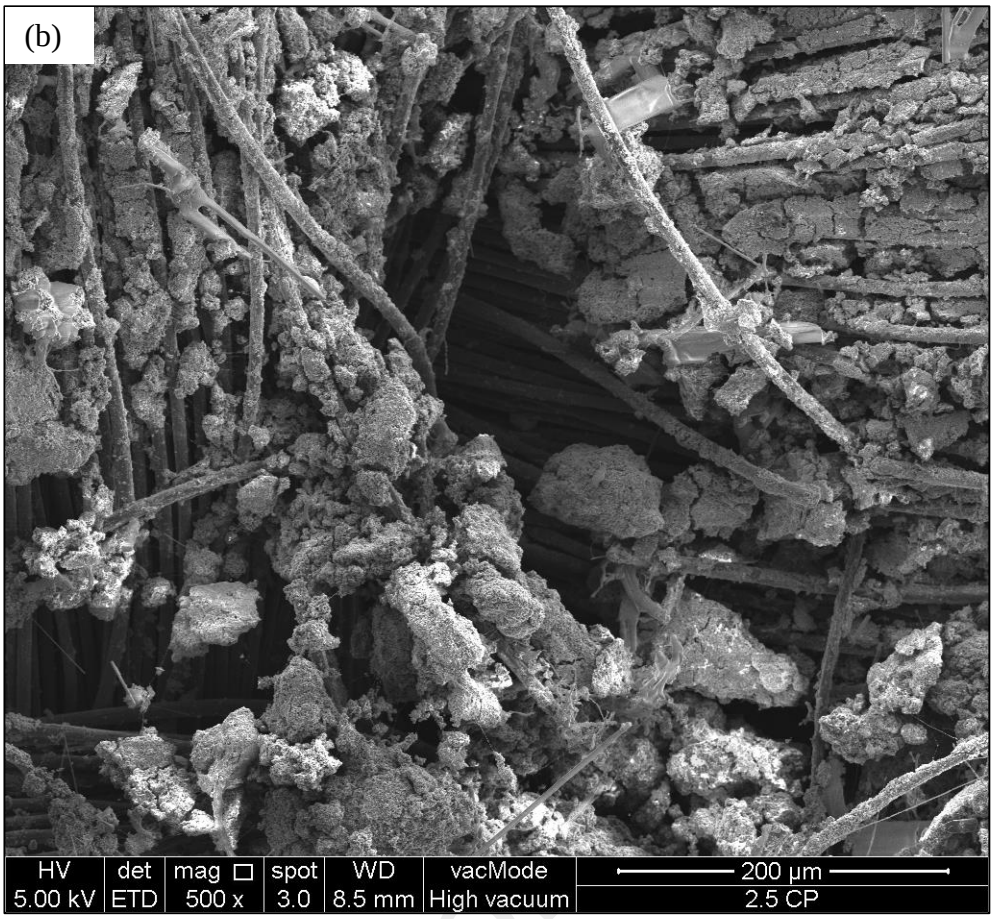
HV
5.00 kV
det
ETD
mag
500 x
spot
3.0
WD
8.5 mm
vacMode
High vacuum
200 µm
2.5 CP

(c)

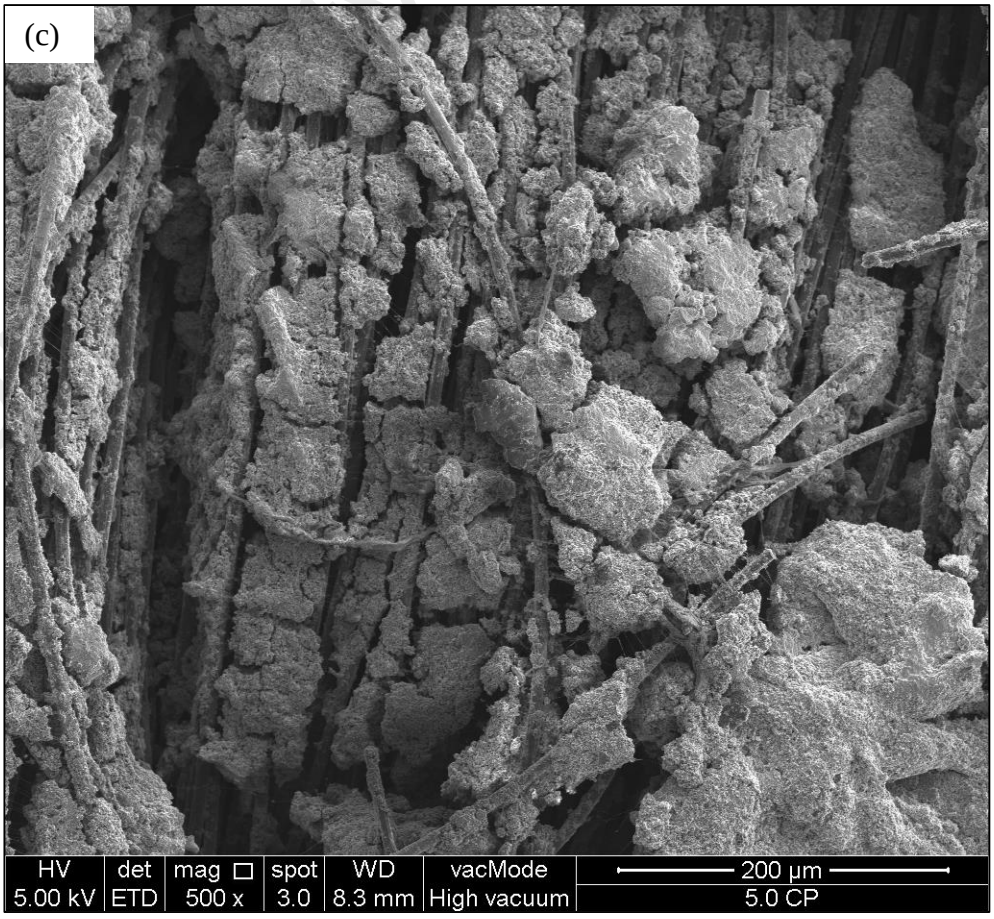
HV
5.00 kV
det
ETD
mag
500 x
spot
3.0
WD
8.3 mm
vacMode
High vacuum
200 µm
5.0 CP

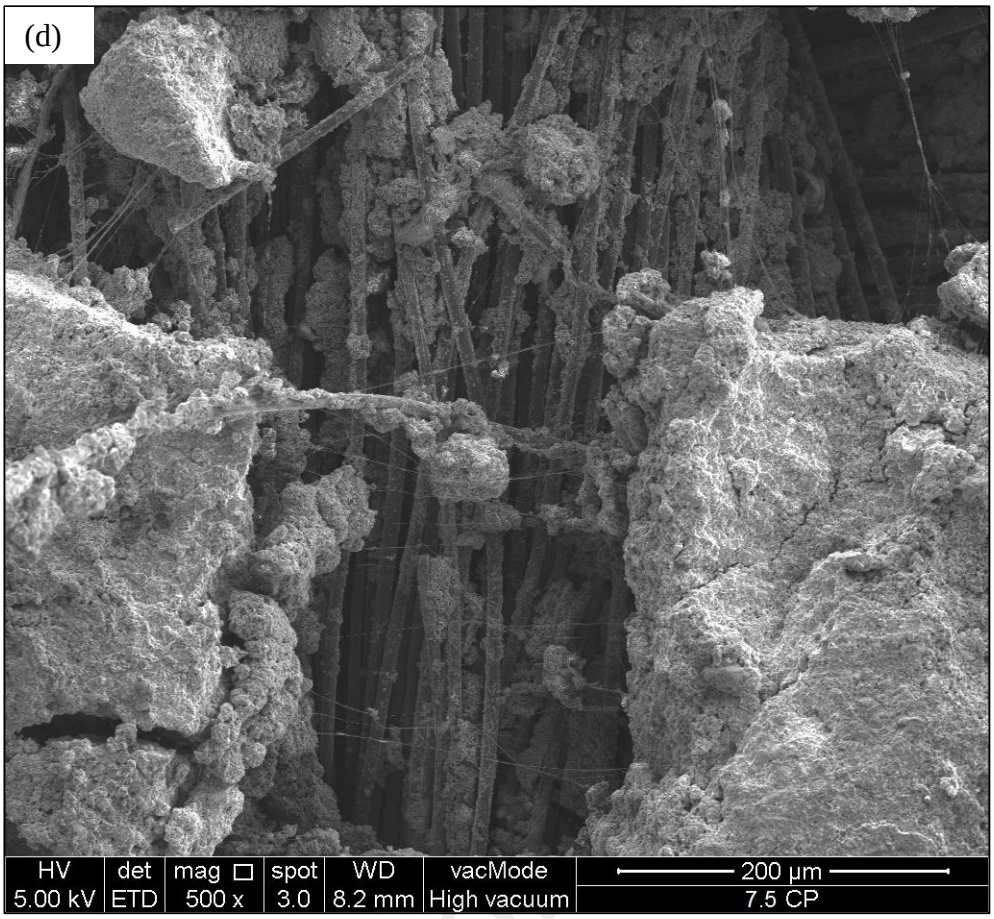

Figure 4.23: SEM Images of Cloth Anodes; (a) CC, (b) CC-P, (c) CC-2P and (d) CC-3P

4.4.1.2 Electrochemical Analysis

The CV analysis of the cloth anodes is shown in Figure 4.24. All the PEDOT functionalized cloth anodes exhibited larger curve area compared to the control anode. The smallest PEDOT loading (CC-P) increased the electrochemical activity of the cloth anodes significantly and further increase in PEDOT on CC-2P intensified the effect. However, this effect reached saturation condition at CC-3P (7.5 mg/cm^2 PEDOT) as the CV showed no improvement between CC-2P and CC-3P. This indicates that the optimum PEDOT loading on carbon cloth anodes is 5.0 mg/cm^{2,} as further addition did not enhance the electrochemical activity of the anodes.

The EIS analysis of the modified cloth anodes revealed the charge transfer resistance decreased with increasing PEDOT loading (Figure 4.25). Furthermore, the R_{ct} of the modified cloth anodes decreased by more than 10 times compared to control anode. The values of the R_{ct} of CC, CC-P, CC-2P and CC-3P are 150.0 Ω, 12.8 Ω, 9.8 Ω and 3.3 Ω respectively.

These electrochemical analyses clearly demonstrated the role of PEDOT in enhancing and improving the electroactivity of carbon cloth anodes. The performances of the cloth anodes in MFC systems are discussed in following section.

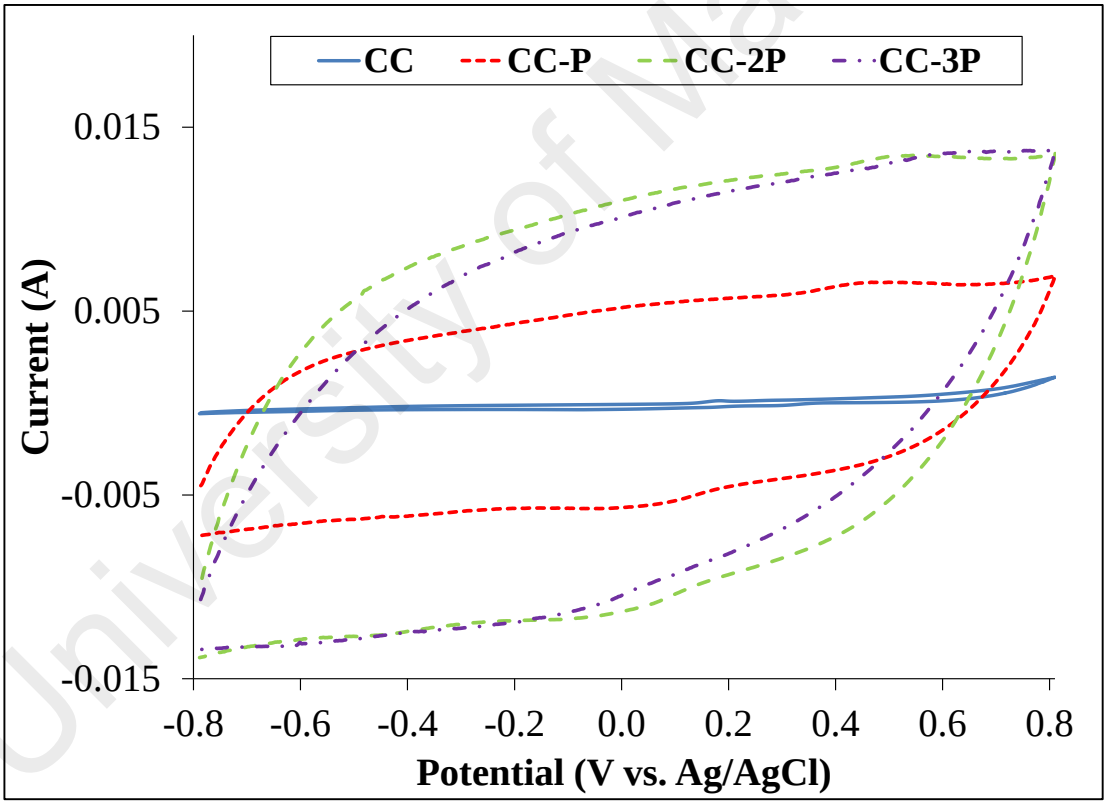

Figure 4.24: CV of Cloth Anodes in 1 mM $K_3[Fe(CN)_6]$ and 0.5 M KNO_3 electrolyte at a scan rate of 10 mV/s.

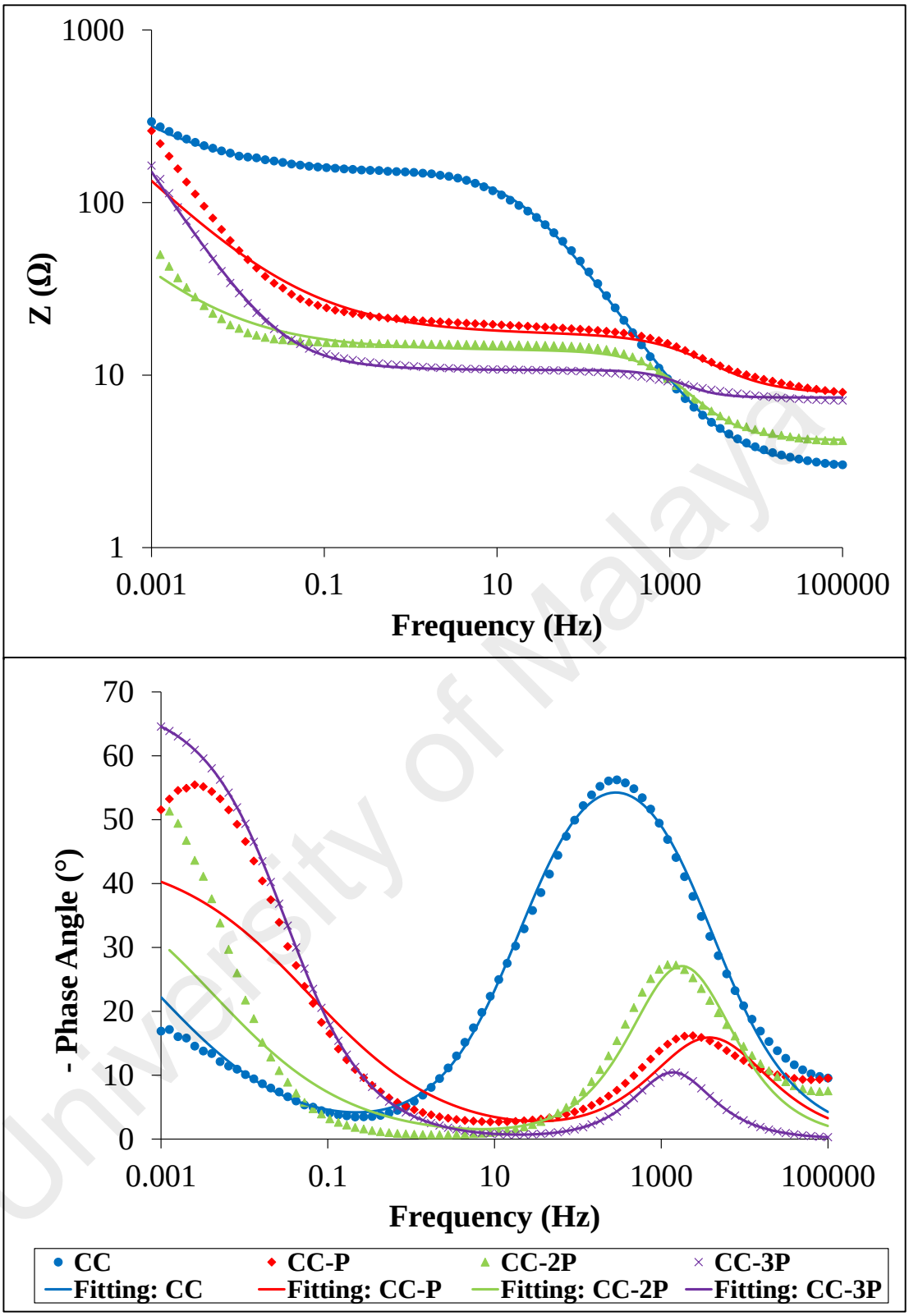

Figure 4.25: Bode Impedance Modulus Plot and Its Corresponding Phase Angle of Cloth Anodes in 2.5 mM $[Fe(CN)_6]^{3-/4-}$ and 0.5 M KNO_3 as electrolyte.

4.4.2 MFC Performance

4.4.2.1 Voltage Generation

Voltage generation of the control and modified cloth anodes varied both in terms of cycle duration and voltage production as observed in Figure 4.26. The voltage generation of CC-2P recorded the highest voltage (695.0 ± 15.9 mV) and longest cycle with each lasting for more than a week. In comparison with the control anode CC, both CC-P (662.3 ± 1.5 mV) and CC-2P recorded higher voltage generation while CC-3P recorded a voltage slightly below that of the control anode at a value of 543.4 ± 8.6 mV. Thus, the optimal cloth anode for voltage generation is the CC-2P.

The stable and repeatable voltage generation of the modified cloth anodes indicated the stability of the PEDOT and that it did not undergo any deterioration during the MFC operation. Control anode showed slightly unsteady voltage generation and variation in cycle period caused by unstable biofilm activity. These changes were attributed to the transformation of microbial community during the operation period where non-electrochemically active microbes compete with exoelectrogens for substrate.

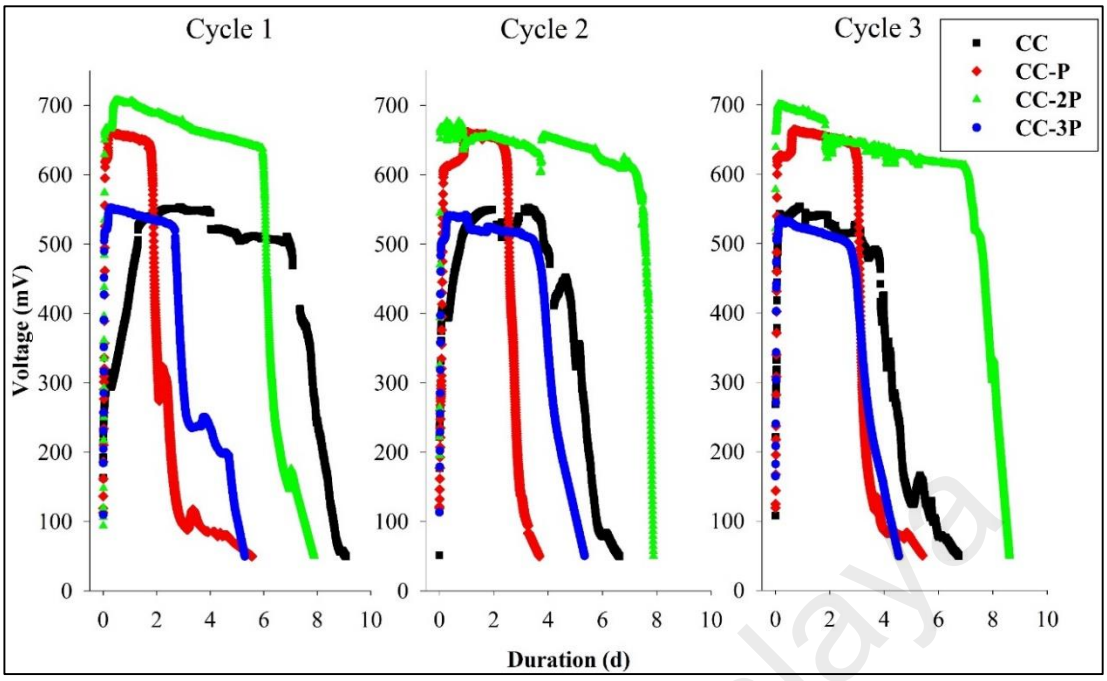

Figure 4.26: Voltage Generation for Three Consecutive Cycles of Cloth Anodes

4.4.2.2 Current and Power Density

The polarization and power density curve for CC and its modified anodes were shown in Figure 4.27. Optimum I_{sc} among the modified anodes was demonstrated by CC-2P at 4.79 A/m^2 followed by CC-P at 3.49 A/m^2 whereas the highest PEDOT loading (CC-3P) resulted in the least at 1.62 A/m^2. Irrespective of loading, all the modified anodes outperformed the control anode (0.76 A/m^2). The voltage overshoot present in the control anode was absent for all the modified cloth anodes, verifying that PEDOT functionalization enhanced the electron transfer properties and biofilm colonization of the anodes. The power density curves calculated from the polarization curve revealed the maximum power density delivered by these systems. The calculated power density of CC-P and CC-2P accomplished twice the control anode (0.35 W/m^2), achieving 0.79 W/m^2 and 0.82 W/m^2 respectively while CC-3P achieved the lowest power density at 0.22 W/m^2.

The anode with 5.0 mg/cm^2 PEDOT emerged as the better candidate among the cloth anodes and the highest loading (7.5 mg/cm^2) again was ascertained to be detrimental. Irregularities were observed between the electrochemical reactivity and electricity generation for the CC-3P anode. CC-3P anode recorded good electrochemical reactiveness and low R_{ct} before being applied into the reactor but exhibited low voltage generation and power density during MFC operation. This is due to poor biofilm formation and electron transfer between the biofilm and anode. Hence, it is well portrayed that 5.0 mg/cm^2 to be the ideal loading condition for this configuration.

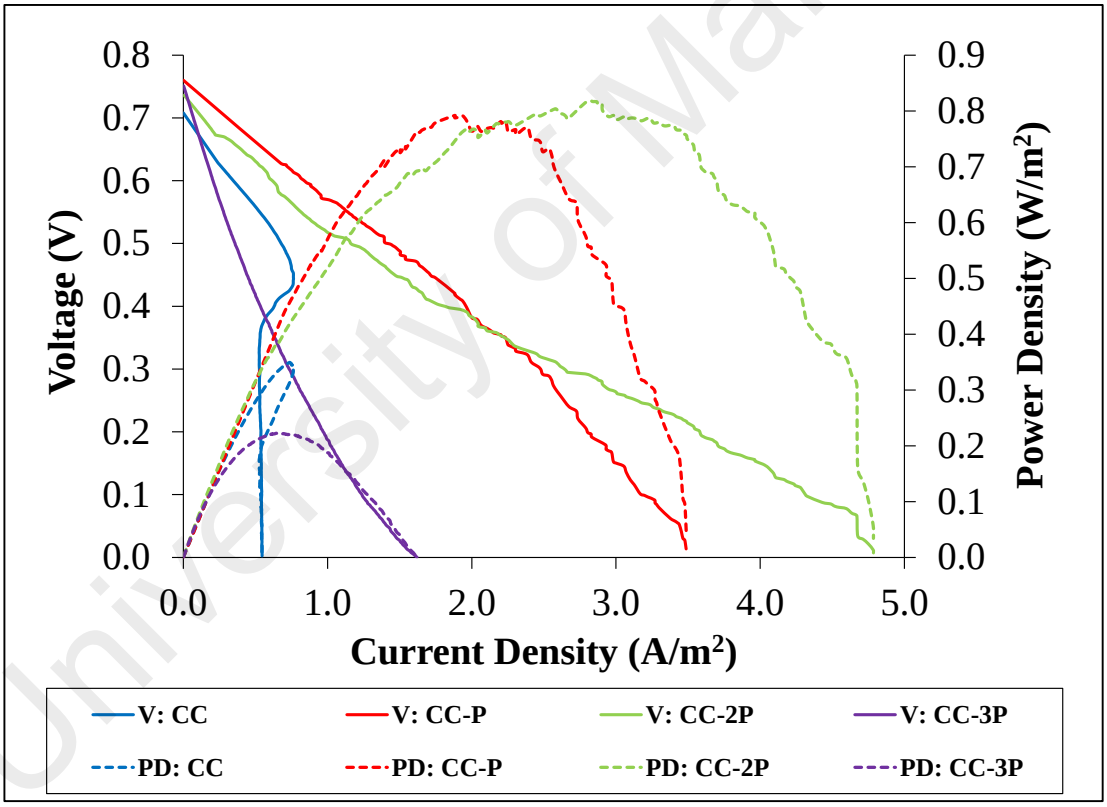

Figure 4.27: Polarization (V) and Power Density (PD) Curves of Cloth Anodes

4.4.2.3 Internal Resistance and Overpotential

The investigation of internal resistance components were carried out by means of in-situ EIS analysis. The Bode plots and its fitting to appropriate equivalent circuit are shown in Figure 4.28. The values of these overpotentials are tabulated in Table 4.4. The R_Ω of all the tested anodes were consistent (8.9 Ω to 12.5 Ω) as the electrolyte concentrations used were similar. The narrow range of the R_Ω also demonstrated that the membranes did not undergo severe fouling or blockage. The R_a of the CC was found to be 98.7 Ω and the least addition of PEDOT (CC-P) decreased the R_a by 12.6 %. Further increase in PEDOT concentration reduces the R_a by 63.7% with respect to control anode. However, the highest concentration of PEDOT brought an opposing effect on the R_a, causing a drastic rise to 225 Ω. The trends of R_a for the modified anodes were clearly reflected by their maximum power density. The high power generation of CC-P and CC-2P were attributed to the low R_a that enabled better anodic electron transfer. An interesting note on this analysis is that the R_{ct} of the CC-3P was the lowest among the modified anodes before MFC operation but recorded highest R_a after stable MFC operation. This inconsistency was due to deterring effect exhibited by the dense layer of PEDOT on the electron transfer capabilities of the biofilm. Although the high PEDOT loading enhanced the inherent electrochemical activity of the anode, it considerably impeded the biological component of the system such as biofilm formation and mobility of electrons from the microbes.

The R_c of the cloth anode systems ranged from 6 Ω to 66 Ω. The irregularities in catholyte concentration might contribute for the variation.

Table 4.4: Components of Internal Resistance for Cloth Anodes

Anode	R_Ω	R_a	R_c	R_{int}	χ^2
CC	9.3	98.7	53.7	161.7	0.0125
CC-P	8.9	86.1	19.4	114.4	0.0348
CC-2P	12.2	35.4	65.3	112.9	0.0057
CC-3P	12.5	225.0	6.2	242.7	0.0295

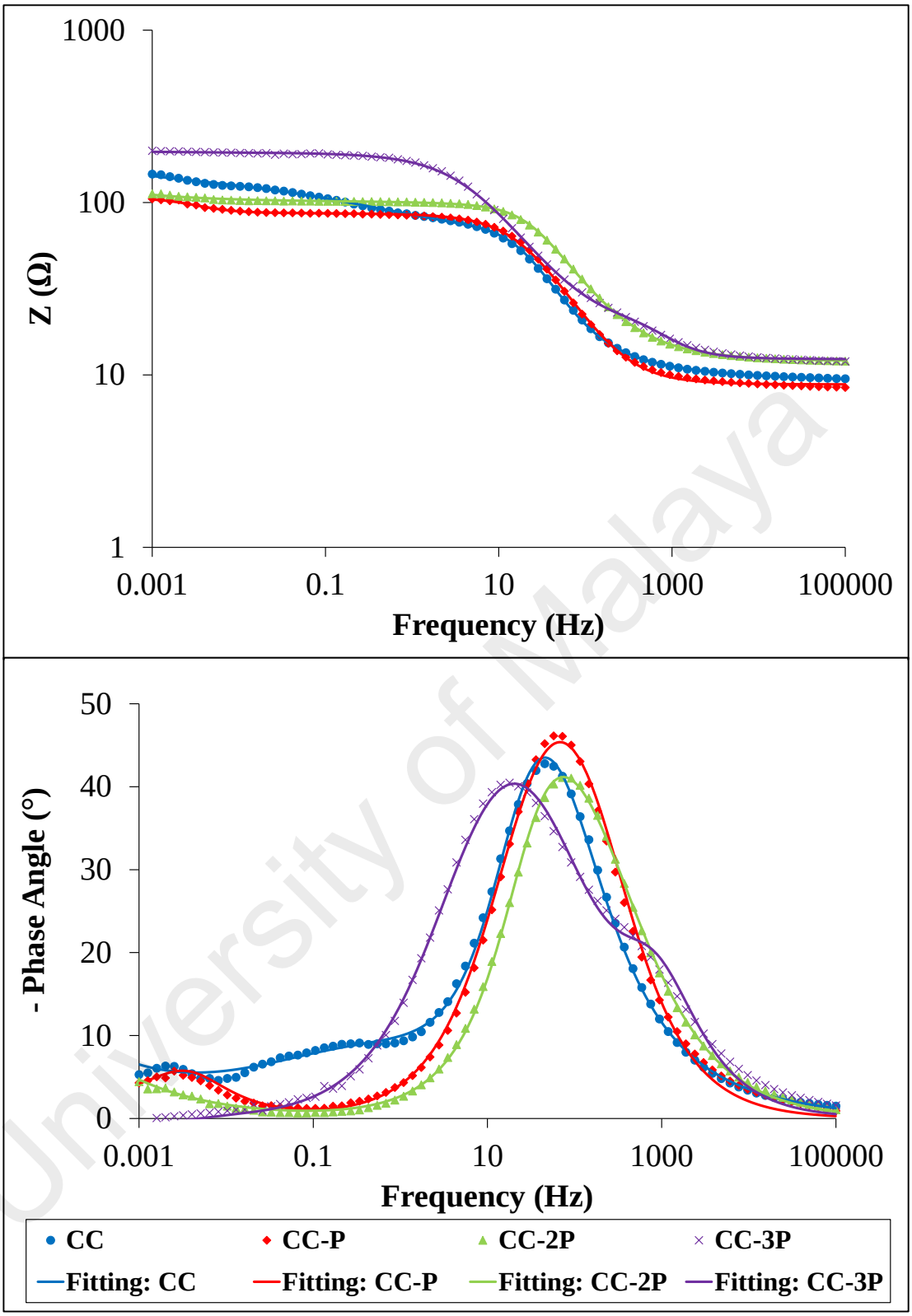

Figure 4.28: Bode Impedance Modulus Plot and Its Corresponding Phase Angle under 1 kΩ condition of Cloth Anodes

4.4.2.4 Individual Electrode Potential

The contribution of voltage by individual electrodes were evaluated and is shown in Figure 4.29. The voltage of both cathode and anode experienced overpotential as current density increases. However, the anodic potentials suffered more severe decline compared to the cathodes particularly when appproching high current densities. It is a clear indication that anode is the limiting factor restricting the performance of the MFC systems. The OCP of the anodes recorded are also consistent with the potential obtained from oxidation of acetate. The more acute cathodic potential reduction for CC-2P system is consistent with the higher cathodic overpotential observed (R_c = 65.3 Ω).

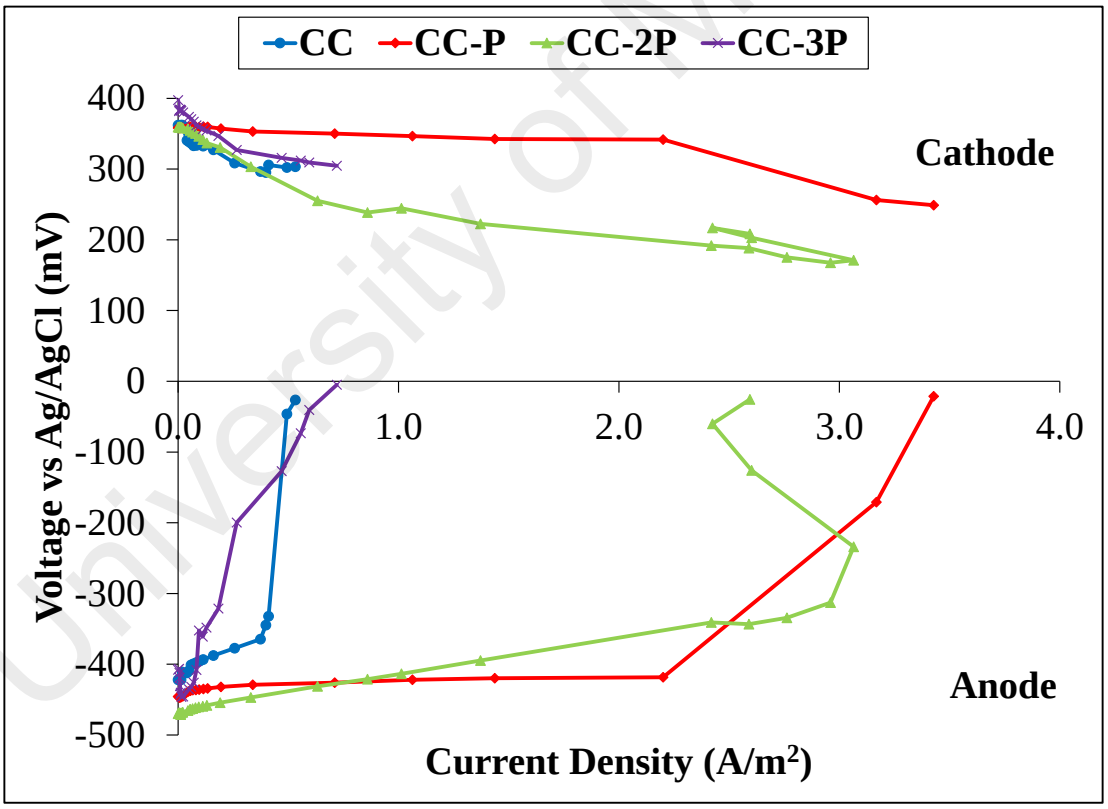

Figure 4.29: Potential of Individual Electrodes of Cloth Anodes

4.4.2.5 COD Removal and Efficiency

All the anodes recorded high COD removal ranging from 79-86 %. However, the CE values fluctuate considerably among the cloth anodes as observed from Figure 4.30. The CC-2P documented the highest CE at 58.2%, which is in line with the high voltage generation and prolonged cycle period. The CC-3P anode has high COD removal accompanied by low CE is due to the invasion of non-electrochemically active microorganism such as methanogens (Y. Feng et al., 2010; Rismani-Yazdi et al., 2013).

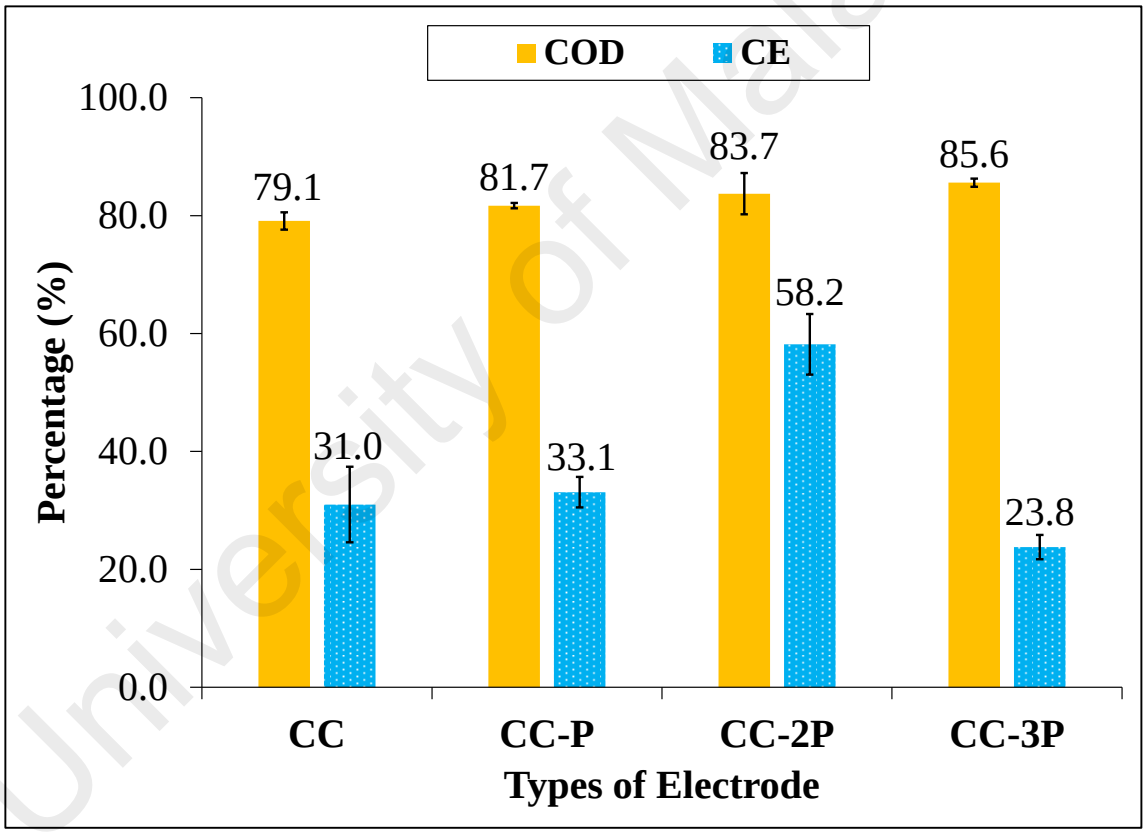

Figure 4.30: COD Removal and CE Percentage of Cloth Anodes

4.5 Characterization and Application of PEDOT Functionalized Graphite Felt Anodes

4.5.1 Characterization

4.5.1.1 Surface Morphology

Figure 4.31 shows that all the functionalized felt anodes experienced changes in morphology attributed to the addition of PEDOT. For the GF-P sample, most particles were confined between the fibres while minority of them was directly immobilized on the fibres. However, at higher loading rate of PEDOT (GF-2P and GF-3P), the particles were found to be very closely integrated with the felt fibres. The high amount of PEDOT led to the individual graphite fibres to form a bunch, wrapping most of the pores and restricted the open structure of the felt anodes.

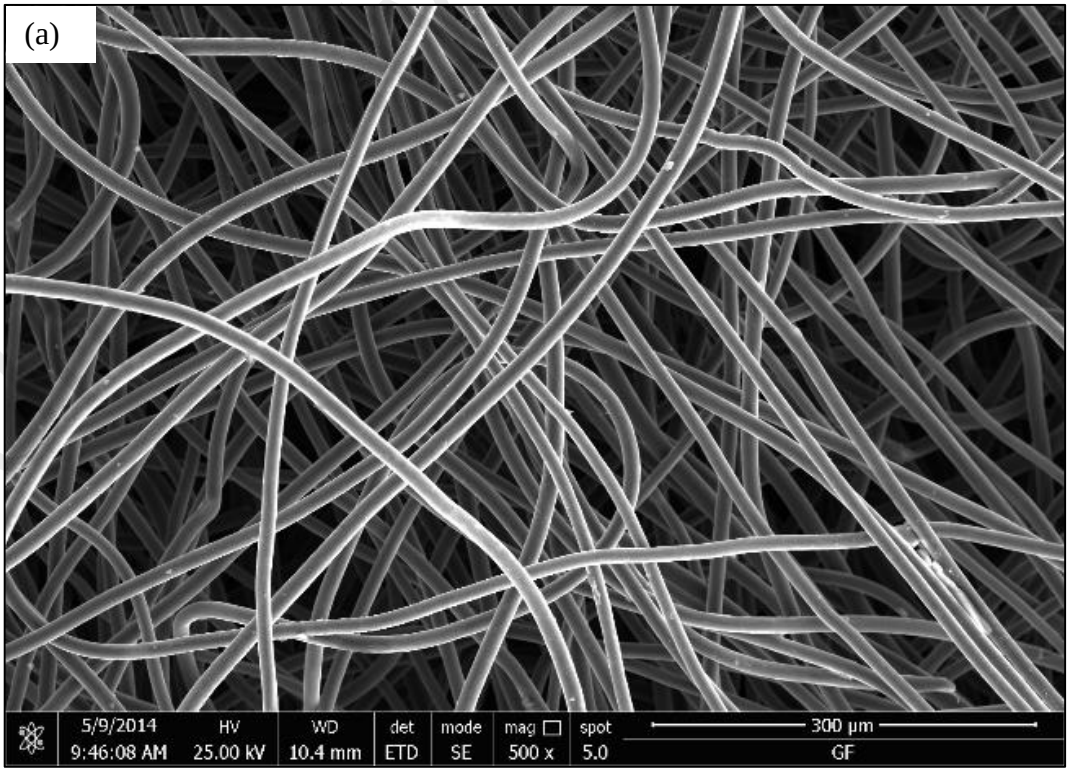

(b)

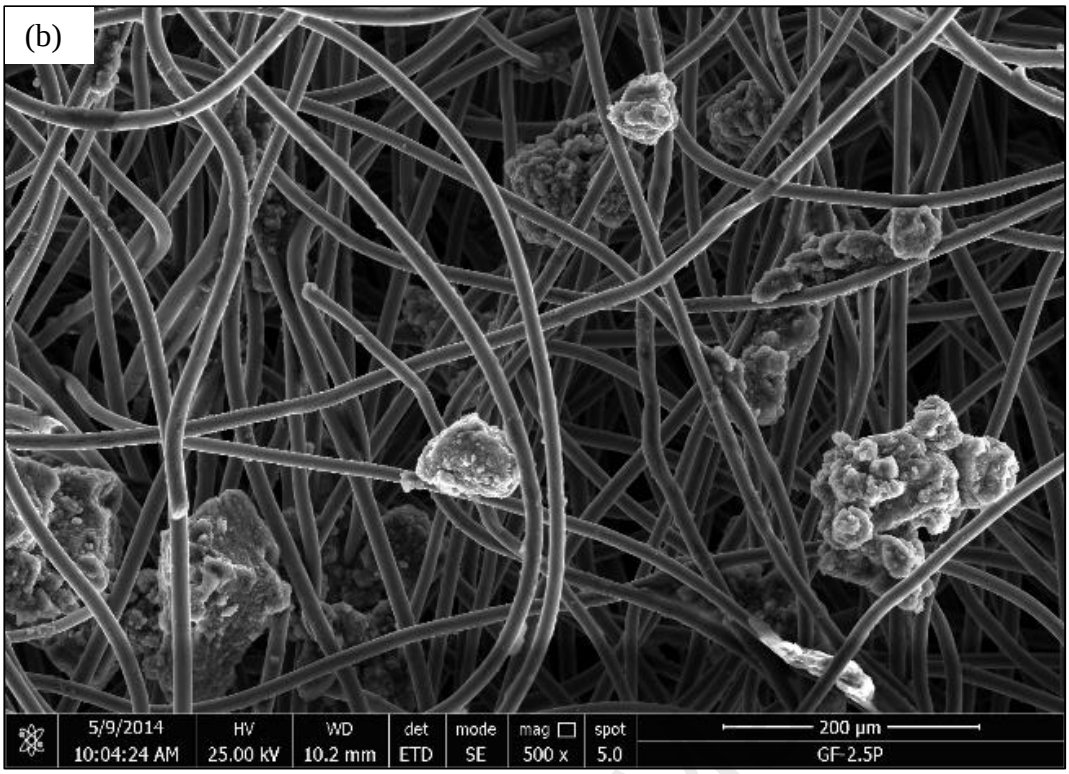
5/9/2014
10:04:24 AM
HV
25.00 kV
WD
10.2 mm
det
ETD
mode
SE
mag
500 x
spot
5.0
200 µm
GF-2.5P

(c)

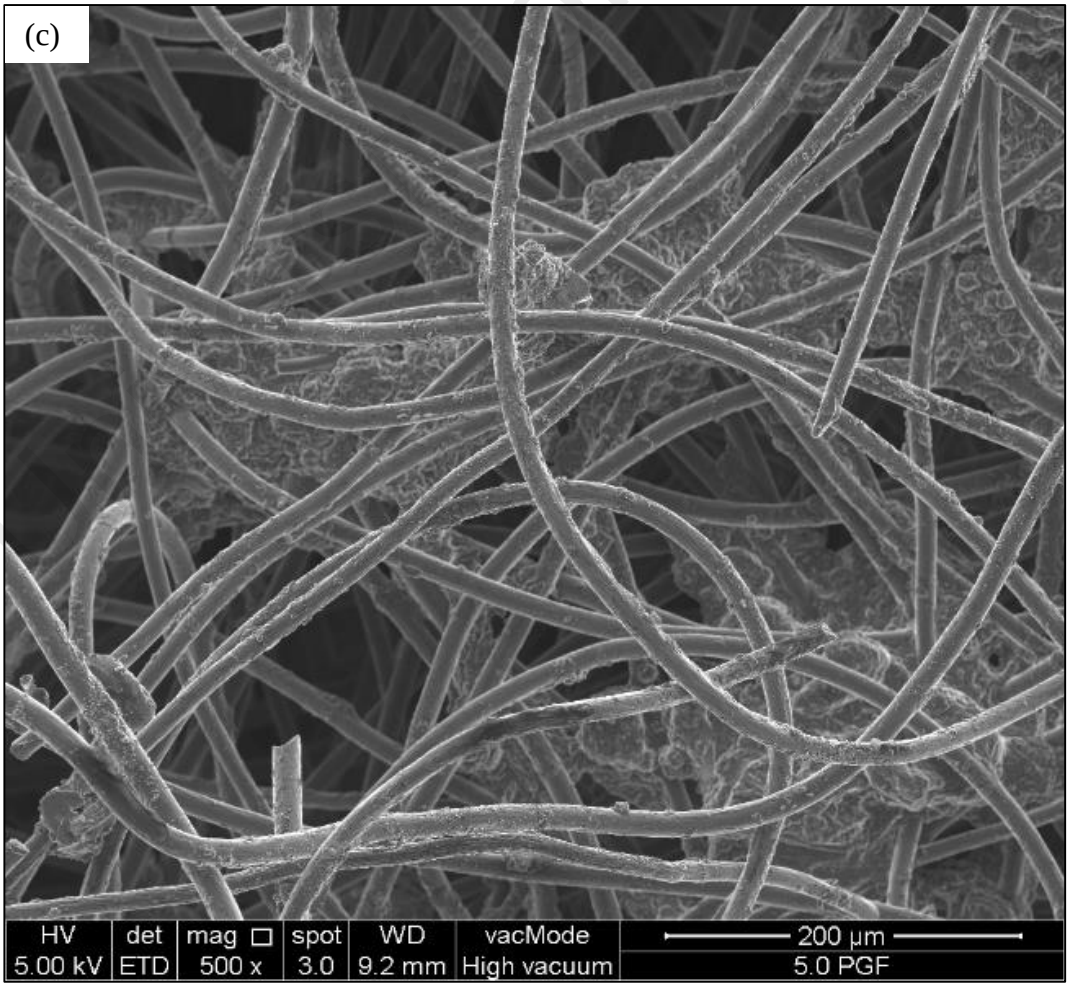
HV
5.00 kV
det
ETD
mag
500 x
spot
3.0
WD
9.2 mm
vacMode
High vacuum
200 µm
5.0 PGF

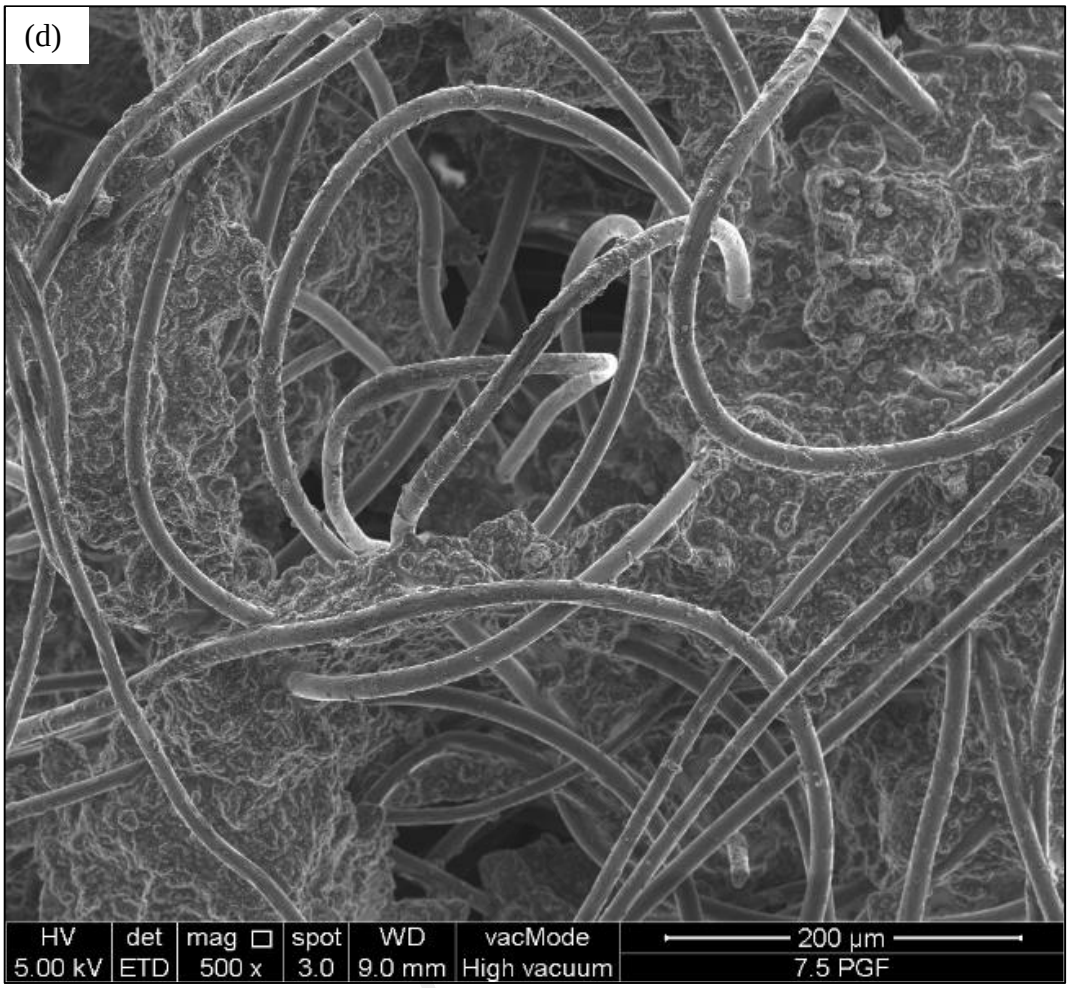

Figure 4.31: SEM Images of Felt Anodes; (a) GF, (b) GF-P, (c) GF-2P and (d) GF-3P

4.5.1.2 Electrochemical Analysis

The CV depicted in Figure 4.32 established that incorporation of PEDOT onto felt anodes surged the electrochemical activity drastically and resulted in larger peak current and area under the curve. This demonstrated that PEDOT aid in amplifying the electrochemical reactiveness of these materials. From the CV assessment, it can be postulated that the optimum anode is the GF-3P as it exhibited the most enhanced electrical conductivity and electron transfer capabilities. Redox peaks denoting graphite was also inferred from the voltammogram for all the felt anodes (Tang et al., 2015). However, the redox peak separation intensified with higher PEDOT loading. These shifts

are attributed by lag in current response against the applied voltage (Bard & Faulkner, 2001). This phenomenon illustrates that the presence of PEDOT particles inhibits the diffusion of the electrolyte into the felts and the effect is more prominent with increasing PEDOT loading (I. H. Park et al., 2014).

EIS analyses were performed to evaluate the internal resistance components of the anodes. Bode plots presented in Figure 4.33 were fitted into a modified Randle's equivalent circuit. It is evident from the plot that the GF anode demonstrated highest R_{ct} (18.3 Ω) and subsequent addition of PEDOT reduces its R_{ct} significantly. Both GF-P and GF-2P recorded a drop of 36.1 % and 86.9 %, reducing their R_{ct} to 11.7 Ω and 2.4 Ω respectively. Further increase in PEDOT loading (GF-3P) marginally increased the R_{ct} to 5.6 Ω. Thus, this established GF-2P as the optimum felt anode with the lowest R_{ct} as further increase in PEDOT loading resulted in the impairment of felt anodes by increasing the internal resistance.

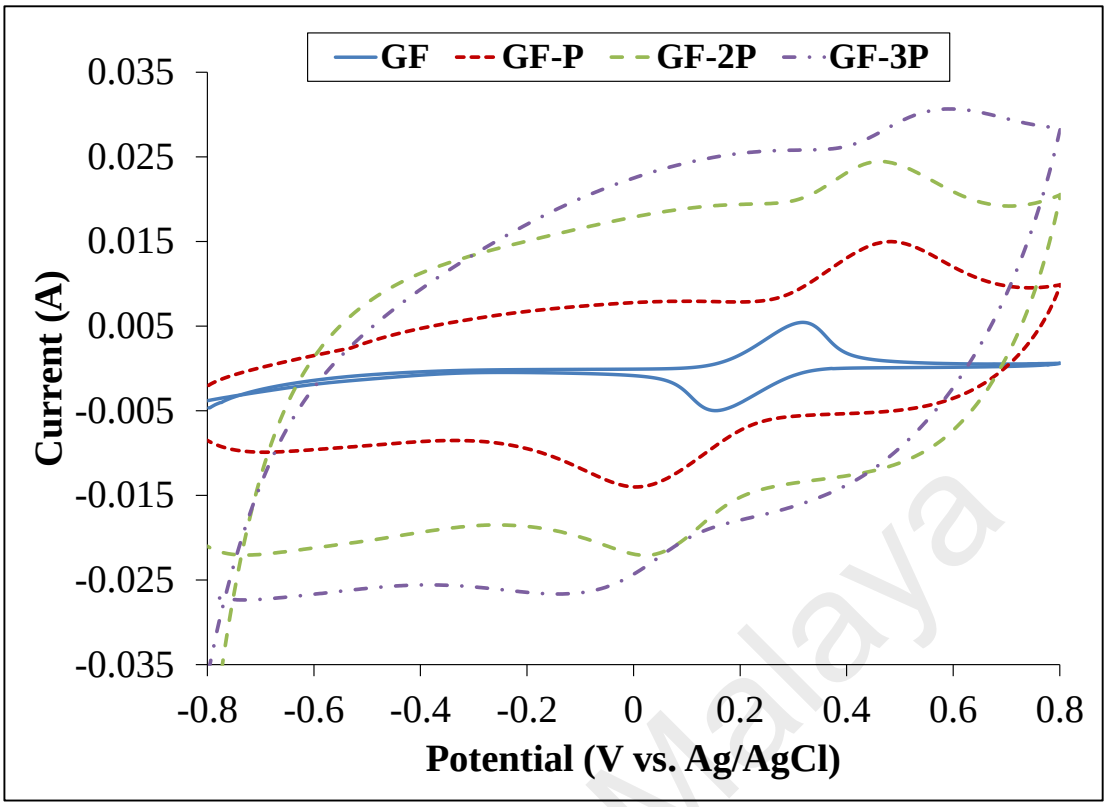

Figure 4.32: CV of Felt Anodes in 1 mM $K_3[Fe(CN)_6]$ and 0.5 M KNO_3 electrolyte at a scan rate of 10 mV/s.

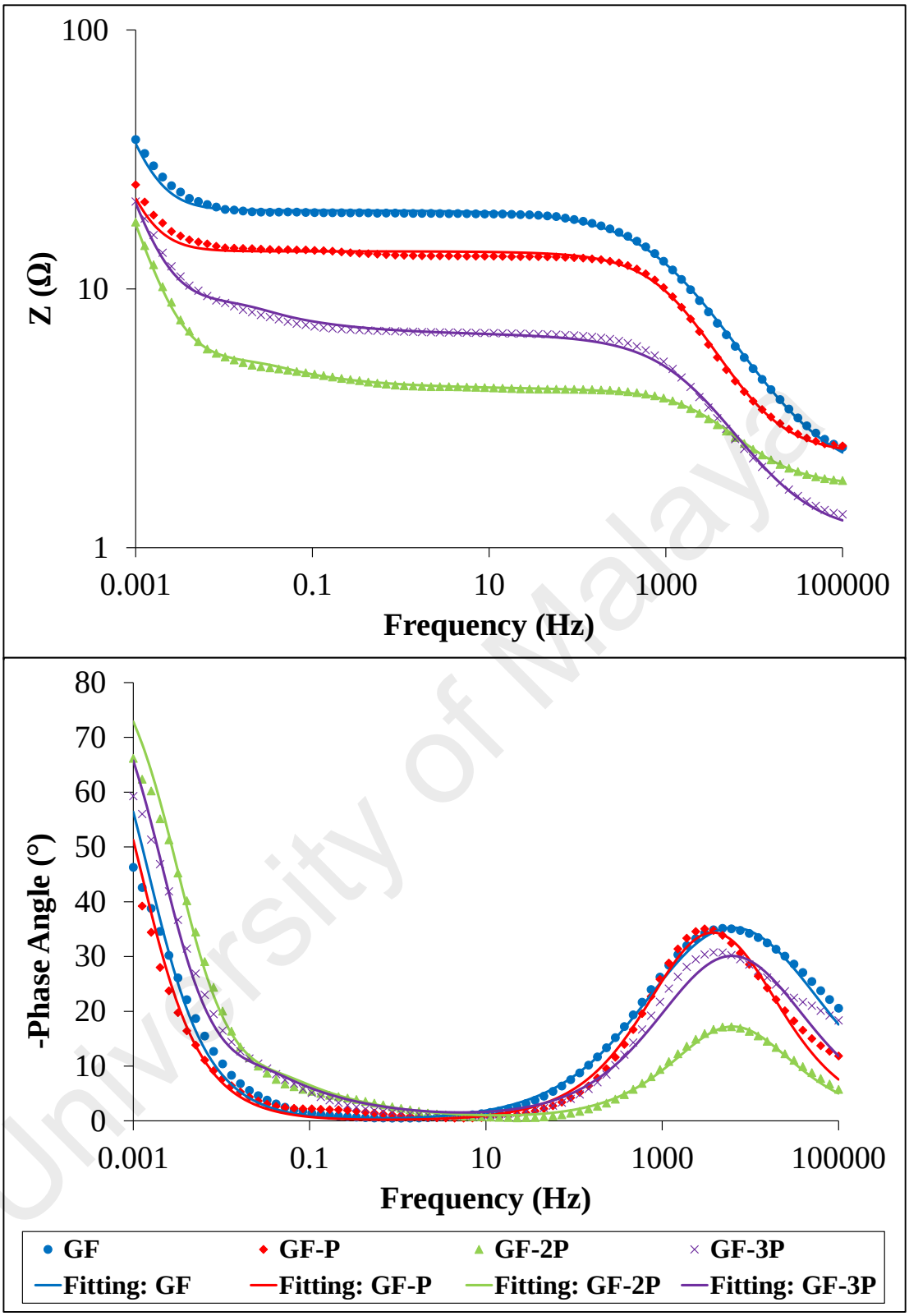

Figure 4.33: Bode Impedance Modulus Plot and Its Corresponding Phase Angle of Felt Anodes in 2.5 mM $[Fe(CN)_6]^{3-/4-}$ and 0.5 M KNO_3 as electrolyte.

4.5.2 MFC Performance

4.5.2.1 Voltage Generation

The voltage generation across 1 kΩ for the GF and its modified anodes are demonstrated in Figure 4.34. The maximum voltage generated by GF anode is 637.0 ± 25.9 mV while modified anodes achieved slightly higher average voltage of ~709 mV. Although GF-P, GF-2P and GF-3P recorded almost similar voltages (710.0 ± 2.6 mV, 711.0 ± 3.6 mV and 705.3 ± 10.3 mV respectively), the duration of each cycle differs drastically. GF-P proved to be the most efficient as it was able to maintain the voltage for approximately 6 days while GF-2P and GF-3P were only able to record peak plateau voltage for 4 and 2 days correspondingly. The dense presence of PEDOT blocked the macropores of the felt configuration, obstructing the diffusion of substrate into the core of felt. This condition led to microbial fouling at the inner section of the anode as starving microbes died off and accumulated. The blockage caused significant reduction in specific surface area for electrochemical reaction and biofilm formation, contributing to the deterioration in anode lifespan and voltage production (Chou et al., 2014).

All the modified felt anodes managed to generate almost similar voltage for three successive cycles, pointing to stable biofilm formation and PEDOT coating. The high standard deviation of GF potential was due to the lower voltage recorded on the 1st cycle. After better acclimatization, the 2nd and 3rd cycles managed to generate almost similar voltage trend.

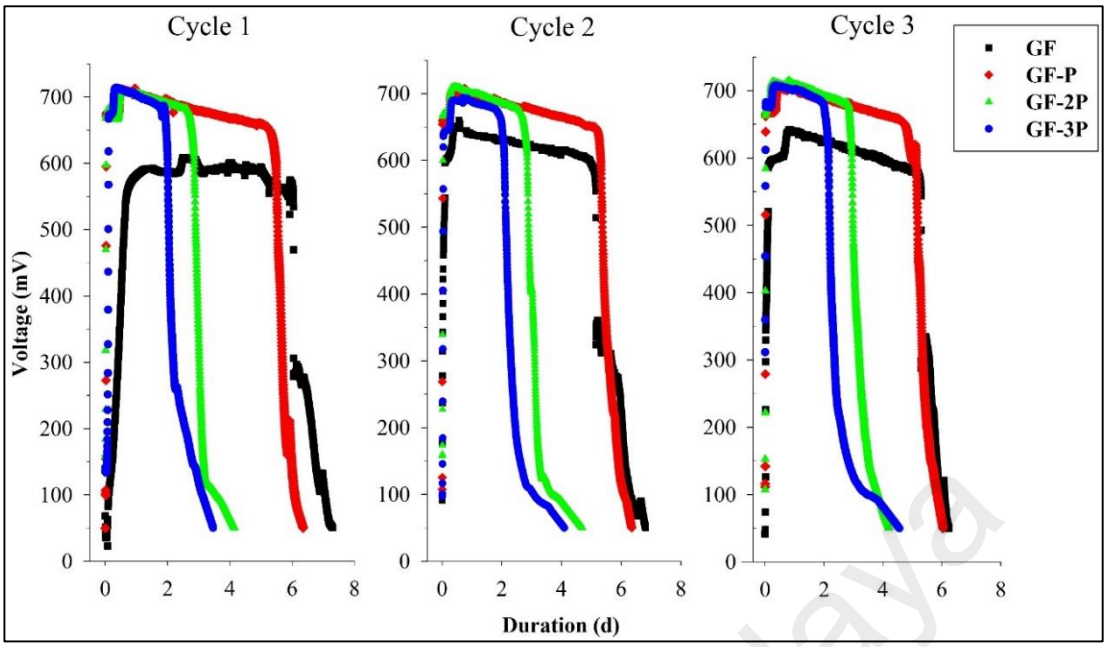

Figure 4.34: Voltage Generation for Three Consecutive Cycles of Felt Anodes

4.5.2.2 Current and Power Density

Polarization and power density curves are computed to obtain in depth analysis of felt anodes and are presented in Figure 4.35. The control anode (GF) recorded I_{sc} of 0.48 A/m^2 and considerable increment was perceived by all the modified anodes. The least addition of PEDOT (GF-P) increased the I_{sc} to 3.50 A/m^2, which is 7.3 times greater than GF. Subsequent increment of PEDOT loading elevated the I_{sc} up to 4.11 A/m^2 and 4.57 A/m^2 for GF-2P and GF-3P respectively.

Mild voltage overshoot were observed for both the control and modified felt anodes. This observation is distinctive for the felt anodes, as both the planar anodes do not experience such overshoot after functionalization of PEDOT. It should also be noted that the range of current density for modified cloth anodes were comparable to that of the felt systems. Hence, the probable explanation for the recurrence of this phenomenon is due to the configuration of the felt. The significant thickness of the felt anodes impeded the diffusion of substrate in and out of the core compared to the planar anodes, causing

mass transfer limitation. The coating of PEDOT particles onto felt aggravated this effect as the gaps between the fibres were blocked by PEDOT as observed in SEM analysis. Thus, felt anodes irrespective of modification experienced voltage overshoot as demonstrated by the polarization curve analysis.

A vast improvement in maximum power density was achieved by all the modified anodes (GF-P, GF-2P and GF-3P), ranged between 1.56 W/m^2 and 1.62W/m^2. The asymmetrical power density curve ratifies the internal resistance of these systems are not dominated by ohmic resistance. A better quantification of the components of internal resistance for these systems was carried out through EIS analysis.

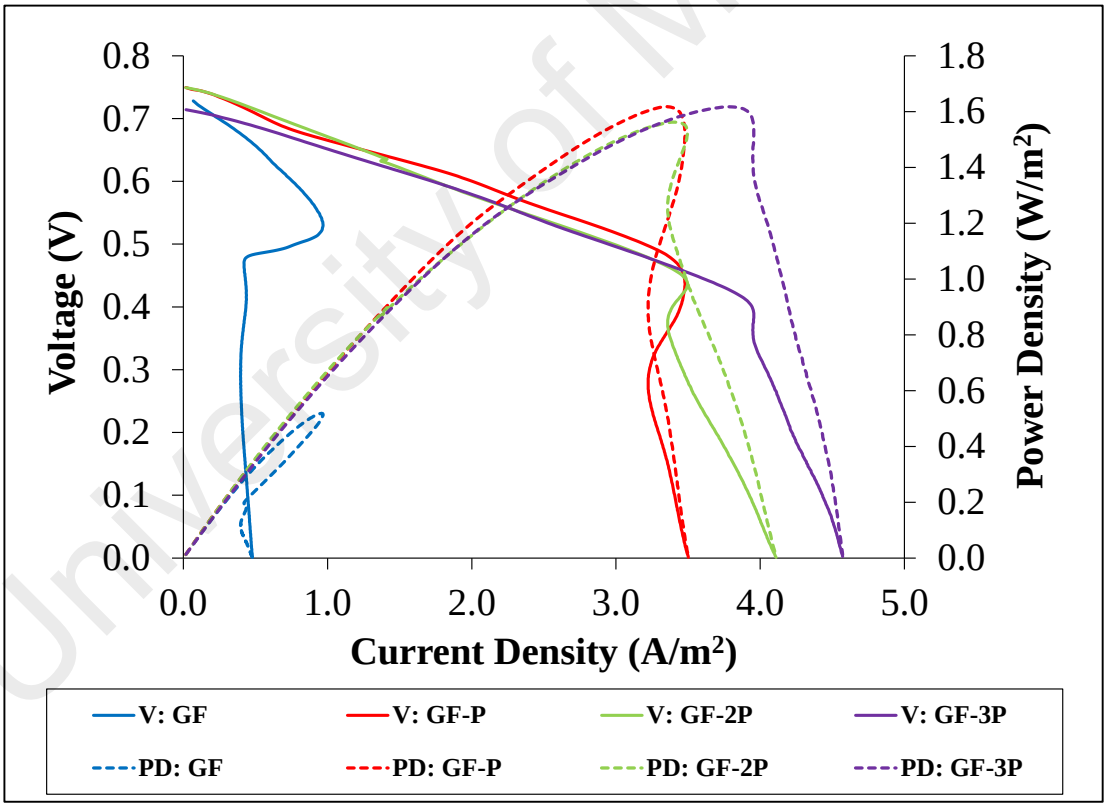

Figure 4.35: Polarization (V) and Power Density (PD) Curve of Felt Anodes

4.5.2.3 Internal Resistance and Overpotential

The EIS analysis was executed to compute the elements of internal resistance of the felt anodes. The bode plot and its corresponding fitting are plotted in Figure 4.36 and tabulated in Table 4.5. Generally, PEDOT loading brought about significant reduction in the overall R_{int} as seen from the ~50% reduction in R_{int} exhibited by the functionalized felt anodes. Additionally, all the modified anodes yielded almost similar R_a ranging from ~14 – 18 Ω, which clarified the similar voltage and maximum power density achieved.

The R_Ω of GF, GF-2P and GF-3P were in the range of 9 Ω to 13 Ω. However, the decline of membrane quality due to prolonged operation increased the membrane resistance for GF-P system, causing the exceptionally high R_Ω. The R_c of the systems ranged from 10 - 59 Ω. All felt anodes exhibited R_d although it is not the dominant resistance in this study. The presence of R_d is consistent with other 3D anodes as reported by literatures (J. Hou et al., 2014; Hutchinson et al., 2011). This is further verified by the voltage overshoot seen from the polarization curves.

Table 4.5: Components of Internal Resistance for Felt Anodes

Anode	R_Ω	R_a	R_c	R_d	R_{int}	χ^2
GF	13.2	27.7	58.6	27.1	126.6	0.0075
GF-P	33.8	13.7	9.8	1.1	58.4	0.0129
GF-2P	8.8	17.7	13.5	5.0	45.0	0.0909
GF-3P	9.0	14.1	14.8	6.2	44.1	0.0827

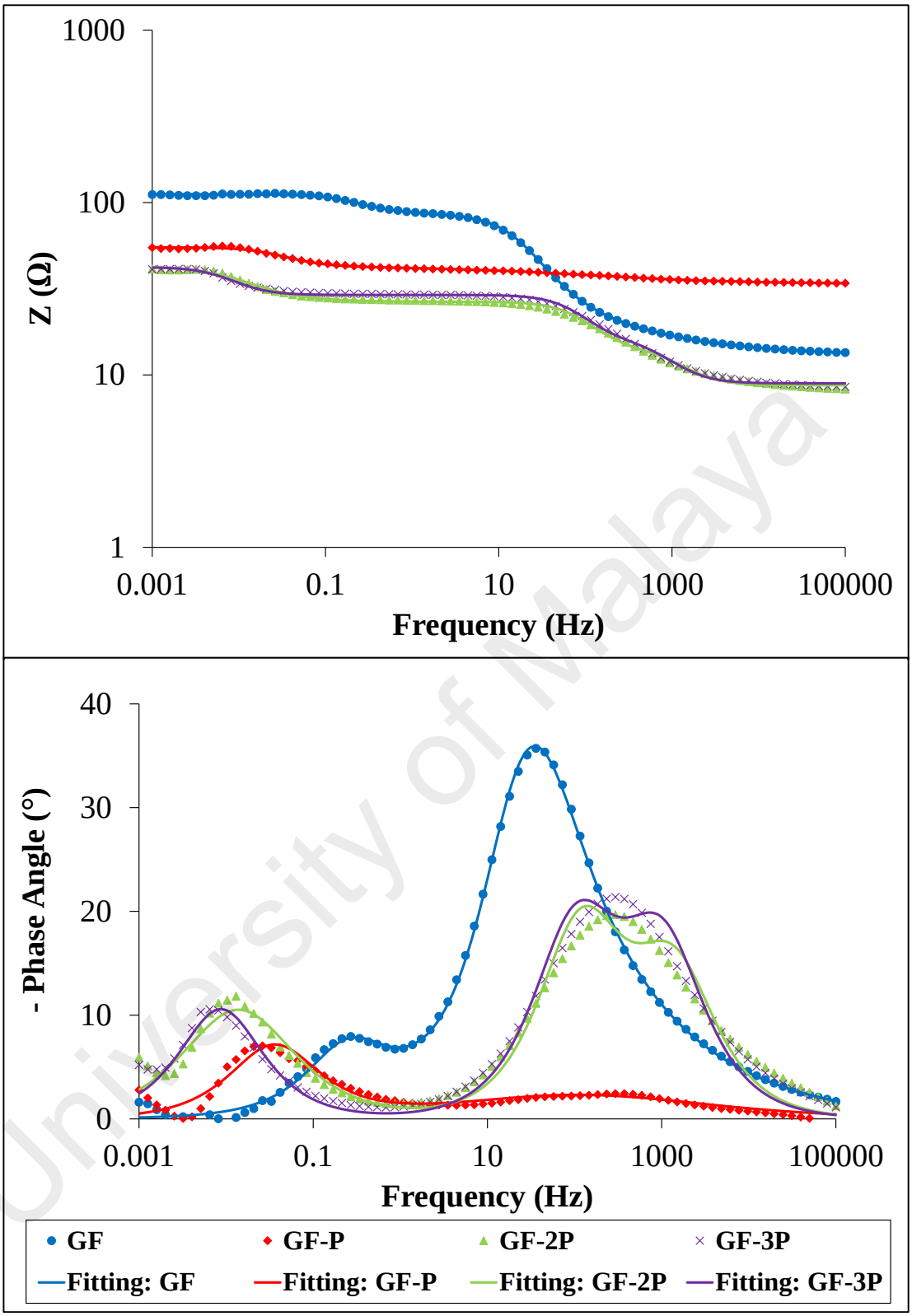

Figure 4.36: Bode Impedance Modulus Plot and Its Corresponding Phase Angle under 1 kΩ condition of Felt Anodes

4.5.2.4 Individual Electrode Potential

Individual polarization curves for both anode and cathode were recorded by varying the external resistance. This establishes the relationship between current density and the potential of the anode and cathode separately as shown in Figure 4.37. All the tested samples revealed anodic potential around -440 mV vs. Ag/AgCl, which were analogous to acetate oxidation. The anodic potential of GF plunged drastically while reaching high current density, revealing anode as controlling factor in such system. The modified felt anodes were able to sustain higher current density before its potential drops due to the improved electron transfer capabilities enhanced by the addition of PEDOT. The potential of cathode remained fairly stable throughout the range of current density for all the felt system.

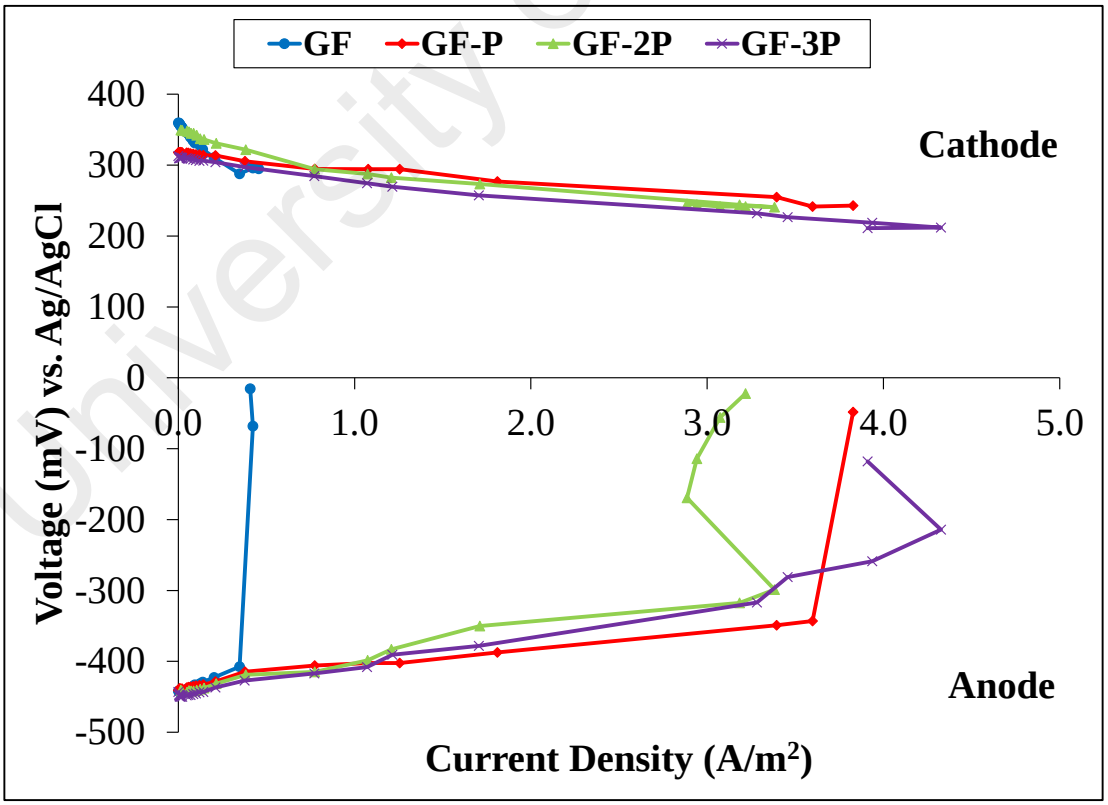

Figure 4.37: Potential of Individual Electrodes of Felt Anodes

4.5.2.5 COD Removal and Efficiency

The COD removal and CE of the tested anodes are presented in Figure 4.38. The COD removals of the felt anodes ranged from 65.6% to 86.3% while the CEs were between 26.3 % and 51.0%. The highest COD removal and CE was achieved by GF-P. The CE is considerably lower for GF-2P and GF-3P due to the ephemeral nature of cycle although they recorded almost similar voltage. It is evident that high loading of PEDOT on felt anodes were detrimental to the efficiency of the system in terms of both substrate degradation and electricity generation.

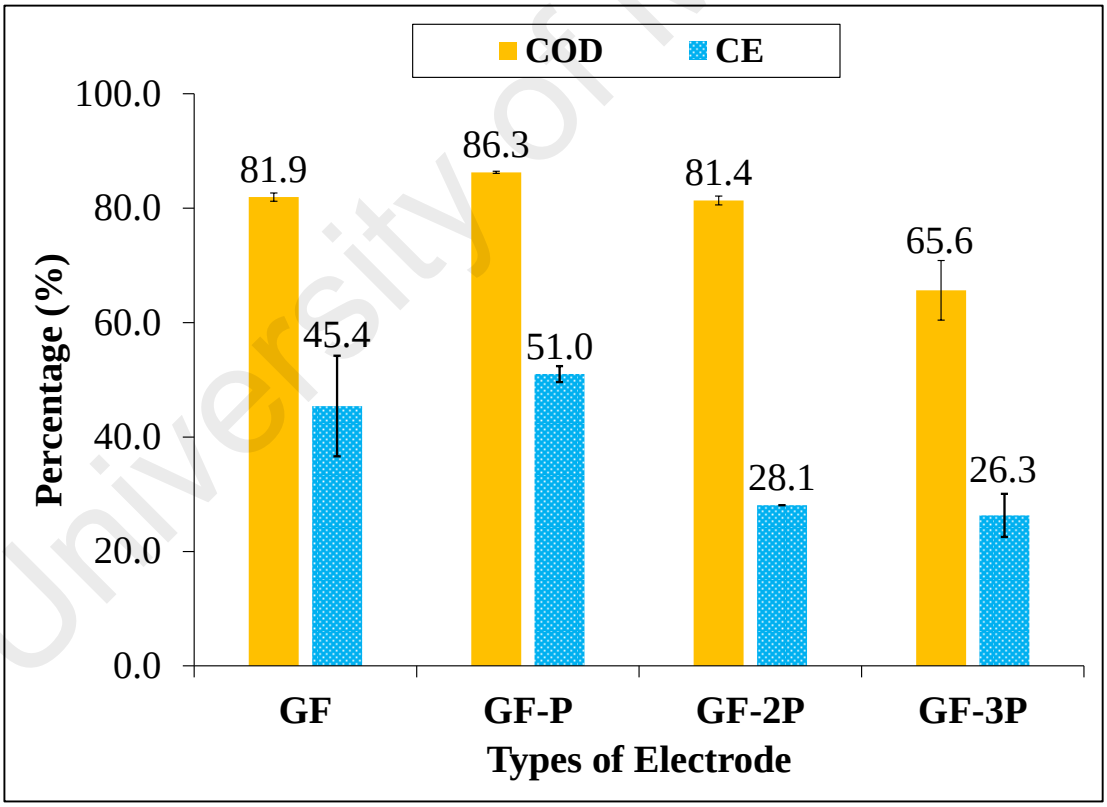

Figure 4.38: COD Removal and CE Percentage of Felt Anodes

4.6 Summary of MFC Performance for the Studied Anodes

The structural configuration of anodes influenced MFC performance greatly as seen from Table 4.6. GF anode achieved the best performance both in electricity generation (0.52 W/m^2) and CE (45.4%) compared to both GP (0.16 W/m^2; 39%) and CC (0.35 W/m^2; 31%) anodes. Additionally, PEDOT functionalized anodes for the three configurations demonstrated significant improvement on their MFC performance. The optimum loading of PEDOT varies with each configuration where 5.0 mg/cm^2 was ideal for both plate (GP-2P) and cloth (CC-2P) anodes while 2.5 mg/cm^2 was sufficient for felt anode (GF-P). Among the modified anodes, GF-P attained the highest power density of 1.62 W/m^2 while CC-2P is the most efficient with 58.2%. Increased concentrations of PEDOT were found to be detrimental to anode performance.

Table 4.6: Summary of Power Density and CE of All Tested Anodes

Anode	Power Density (W/m^2)	CE (%)
GP	0.16	39.0
GP-P	0.64	40.1
GP-2P	0.83	44.6
GP-3P	0.04	15.6
CC	0.35	31.0
CC-P	0.79	33.1
CC-2P	0.82	58.2
CC-3P	0.22	23.8
GF	0.52	45.4
GF-P	1.62	51.0
GF-2P	1.56	28.1
GF-3P	1.62	26.3

Overall, the study established the feasibility of chemical polymerized PEDOT as an anode enhancer and its performance is on par, if not superior to electrochemically polymerized PEDOT as compared in Table 4.7.

Table 4.7: Comparison between MFC Performances of Electrochemically Synthesized PEDOT Anode and the Current Study

PEDOT Coating on Electrode	Operating Conditions	Maximum Power Density	References
Electro-polymerized PEDOT on carbon cloth	Marine broth, *Shewanella loihica* strain PV-4, Two chamber	▪ Modified: 140 mW/m^2 ▪ Control: 98 mW/m^2	X. Liu, Wu, and Gu (2015)
GN/PEDOT on carbon paper	Glucose, *Escherichia coli*, Two chamber	▪ Modified: 873 mW/m^2 ▪ Control: 55 mW/m^2	Y. Wang, Zhao, Sun, Zhang, and Zhu (2013)
In-situ chemical polymerization PEDOT coated onto graphite plate (GP), carbon cloth (CC) and graphite felt (GF)	Acetate, mixed culture, Two chamber	▪ GP-2P: 826 mW/m^2 ▪ Control GP: 161 mW/m^2 ▪ CC-2P: 818 mW/m^2 ▪ Control CC: 349 mW/m^2 ▪ GF-P: 1618 mW/m^2 ▪ Control GF: 519 mW/m^2	Current study

4.7 Distribution of Exoelectrogen in MFC System

The study was carried out to reveal the proportion of anodic biofilm and planktonic cells contribution to the voltage generation and system efficiency. The batch-mode operation adopted in the study retained the grown planktonic cells in the anolyte for the duration of each cycle. Thus, the combined anodic biofilm and planktonic cells could contributed to the system performance and efficiency. However, if a continuous mode is implemented, these planktonic cells are constantly flushed out and are not sustained in the system (Du, Li, Tong, Li, & Li, 2008). Thus, it was concluded that the efficiency of batch mode was higher than continuous system if exoelectrogens were present among the planktonic cells. The significance of this study is to determine whether the results obtained in this research can be replicated when executed onto a continuous MFC system.

4.7.1 GP and GP-P Anodes

GP and GP-P were employed in this experiment to denote the control and PEDOT modified plate anodes respectively, and the results are shown in Figure 4.39. For both samples, the biofilm experiments were able to achieve peak voltage instantaneously and sustained the voltage for 48 h.

A surge in voltage at the initial stage of the planktonic cell experiment for GP anode was observed but the voltage was not sustained. It cannot be verified that this voltage is contributed either by abiotic factors or by planktonic cells. Hence, the contribution of planktonic cells on GP anode was not definitive from this experiment. There was no significant voltage recorded for the first 36 h from the planktonic cell for the GP-P anode and a slight voltage was recorded from the 36^{th} to 48^{th} hour. This confirms that planktonic cell contributed little or insignificantly to the voltage generation. Thus, it

can be deduced from the above experiments that anodic biofilm governs the voltage generation for both the control and modified plate anodes.

The injection of biocide (1% glutaraldehyde) at the end of 48 h instantly initiated a drastic voltage reduction for both samples in the biofilm experiments. This phenomenon confirms that the voltage produced was through the transfer of electron from exoelectrogens and eliminates the contribution by abiotic factors.

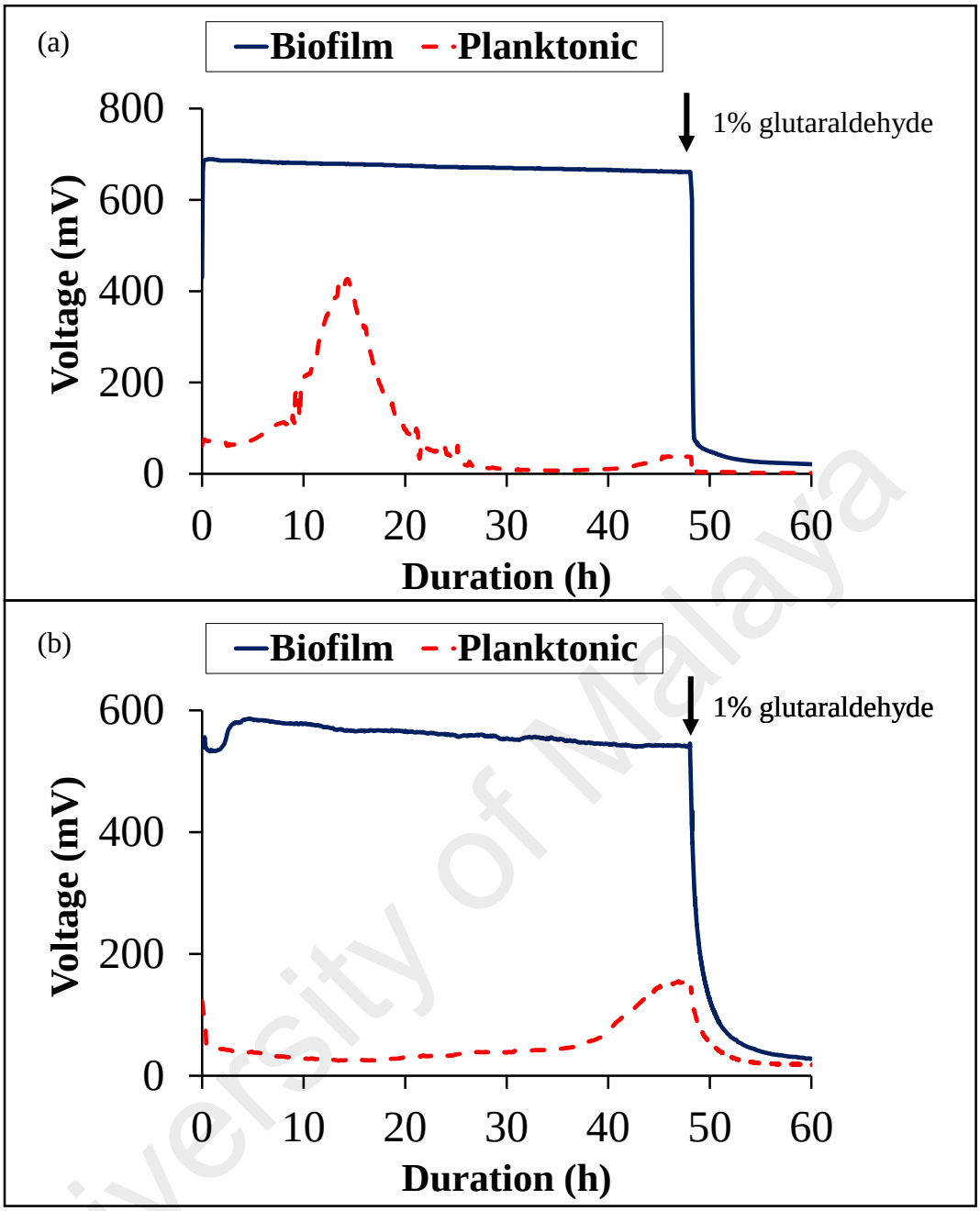

Figure 4.39: Distribution of Anodic Biofilm and Planktonic Cells for (a) GP and (b) GP-P Systems

4.7.2 CC and CC-P Anodes

The contribution of biofilm and planktonic cells from the cloth anodes were represented by the CC and CC-P as shown in

Figure 4.40. The cloth anodes with stable biofilm achieved voltage of ~600 mV after several hours of being inserted into fresh anolyte. The biofilm experiment of both samples managed to achieve maximum plateau voltage in a few hours indicating that majority of the exoelectrogens are immobilised on the anodes.

The planktonic experiment of CC did not display any significant voltage generation throughout the operation, eliminating the contribution of planktonic cells. For CC-P anode, an increase in voltage was observed after 24 h but the condition was not prolonged. The addition of biocide did not caused the voltage to plunge instantly, causing ambiguity towards the contribution of live planktonic exoelectrogen towards the generated voltage.

The introduction of biocide at the end of the experiments again caused the voltage of biofilm experiments for both cloth anodes to plunge severely, verifying the role of electrochemically active microorganism in electricity production.

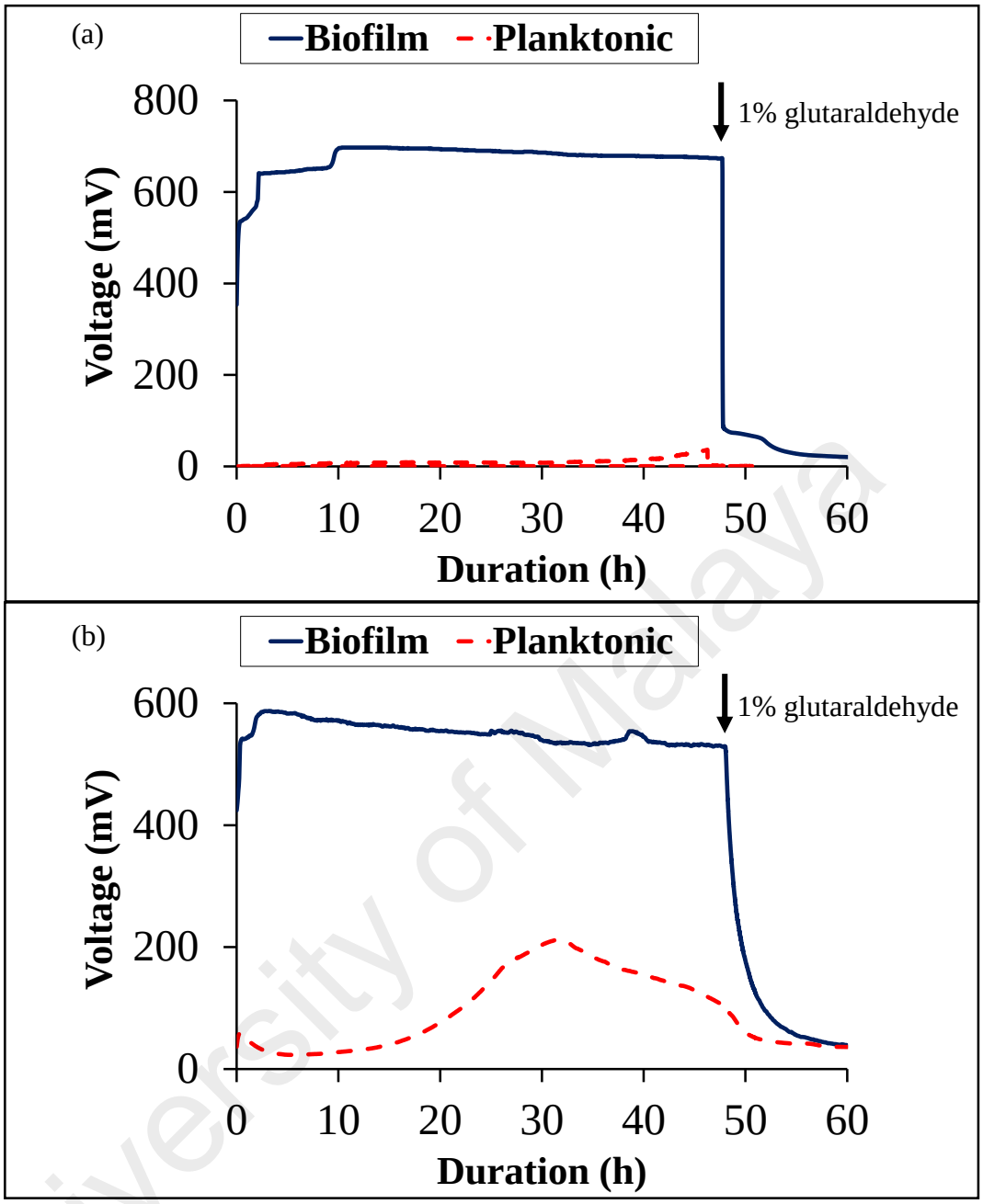

Figure 4.40: Distribution of Anodic Biofilm and Planktonic Cells for (a) CC and (b) CC-P Systems

4.7.3 GF and GF-P Anodes

GF and GF-P were employed to represent the control and PEDOT modified felt anodes respectively. Both the biofilm and planktonic cell experiments for GF recorded almost similar peak voltage after 48 h, as clearly depicted in Figure 4.41(a). However, peak voltage was attained within 3 h by the GF with stable biofilm whereas the latter took

~24 h to achieve the peak value. The obtained result verifies that anodic biofilm dictates the electricity generation of the system (Yamamuro et al., 2014). However, the contribution from planktonic cells cannot be neglected, as it is able to deliver 93% of the peak voltage attained by biofilm. The combined contribution from both biofilm and planktonic cells led to the high CE of GF system (~45%) as compared to other control anodes (~31-39%).

The electricity in GF-P system was solely contributed by anodic biofilm as clearly portrayed in Figure 4.41(b). The biofilm achieved peak voltage in ~1 h whereas there was no significant voltage measured during the planktonic cells study. The voltage plunged to 10% of its peak voltage in the space of 1 h after biocide was injected into the chamber containing GF anode. The steep fall in the peak voltage ascertains the notable contribution of the live microbes for electron transfer and eliminates the contribution by the abiotic factors.

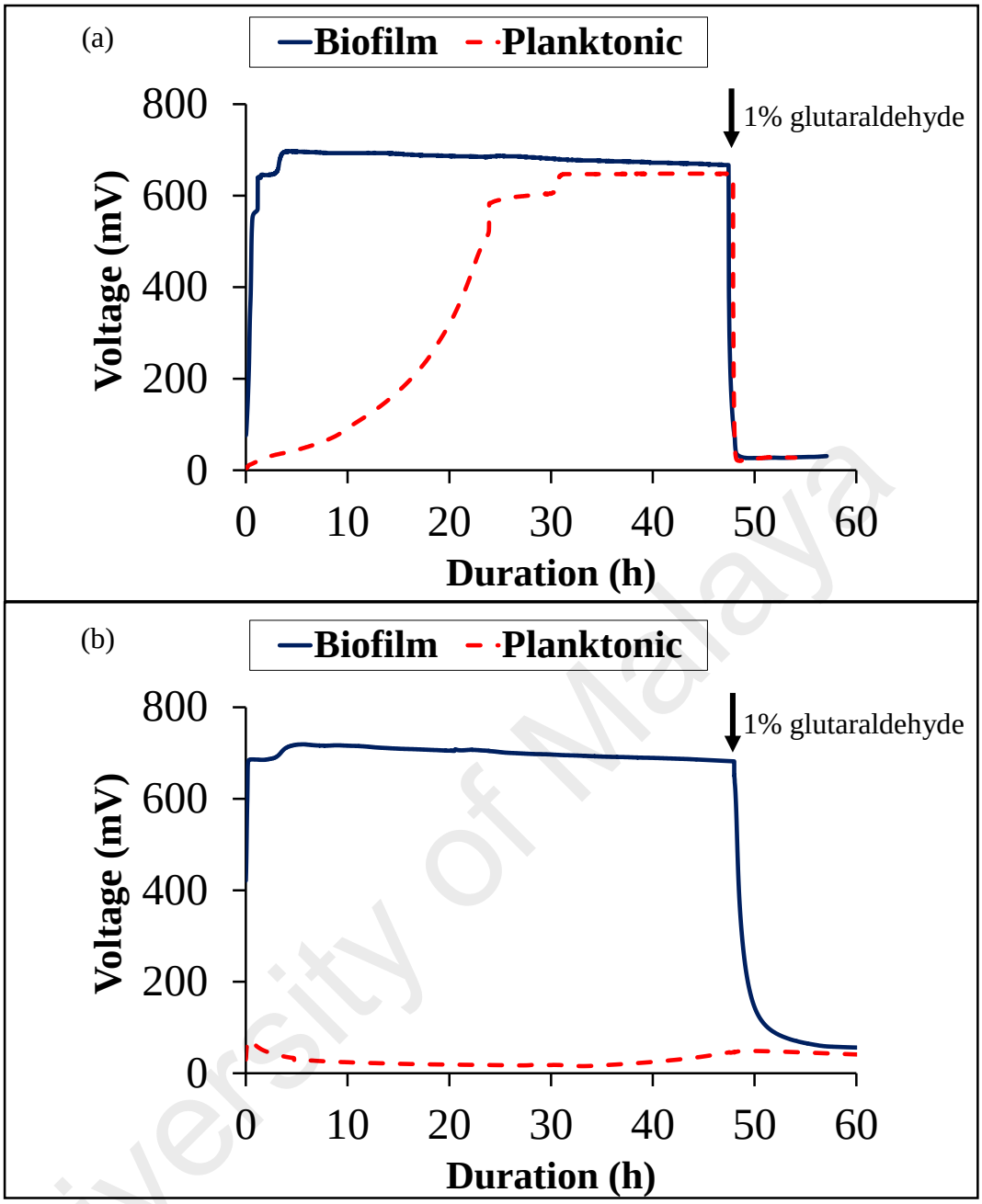

Figure 4.41: Distribution of Anodic Biofilm and Planktonic Cells for (a) GF and (b) GF-P Systems

4.7.4 Summary

The distribution of exoelectrogens experiments for all the tested anodes regardless of configuration and modification elucidates that the electricity generation in all these systems are predominantly contributed by the biofilm immobilised on the anodes. These anodic biofilms were analysed for further comprehensive identification in order to reveal

their characteristics and function in the MFC system. As the contributions of planktonic cells are insignificant, no further analysis on these cells was carried out.

Another observation that can be substantiated from these experiments is that the PEDOT modified anodes took a longer time to achieve voltage reduction once the biocide was added into the electrolyte. While the voltage from the control anodes plunged rapidly once the biocide was injected, all the modified anodes managed a more gradual decrease. This is possibly due to the capacitive effect of the PEDOT (Lei, Wilson, & Lekakou, 2011). Ideally, the voltage is expected to drop instantly after the biofilm was terminated by the biocide; however, the buffer electron stored in the PEDOT resulted in the trailing trend. The other hypothesis is that the PEDOT acts as a protective layer for the biofilm and the diffusion of biocide to the biofilm was delayed.

4.8 Biofilm Characterization

Comprehensive characterization of the biofilm attached onto anodes is imperative to provide information on the interaction between the microbes and the anode. For this purpose, SEM and next generation DNA sequencing were adopted for all control anodes and their corresponding lowest PEDOT loaded anodes.

4.8.1 Morphology of Biofilm

Biofilm morphology on anodes at the end of three stable cycles of voltage generation was captured with SEM and demonstrated immobilised microorganism on the surface of the anodes. Figure 4.42 and Figure 4.43 show the images of the control and PEDOT modified anodes respectively. Generally, the SEM image proves the physical existence of biofilm on the anodes. It is evident from those images that rod-shaped

bacteria were predominant and some cocci were observed sporadically among the consortium.

For the GP anode, microorganisms were seen attached onto the surface of the plate. Higher magnification image showed the clustering of the microbes. In CC and GF anodes, the microorganisms were attached onto their fibres. The agglomeration of these microbes interlinked the fibres as clearly seen for GF anode. Such linkage between the individual fibres promotes better electron transfer system.

The modified anodes also showed the presence of rod-shaped microorganisms. These microbes were attached to the PEDOT particles as well as on the surface of the anodes. The modified anodes had high microbial density compared to their corresponding control anodes. The addition of PEDOT particles on these anodes had considerably increased their surface roughness and area, facilitating better biofilm immobilisation and growth. Furthermore, the electrostatic force between negatively charged cell walls and positively charged polymer backbone of PEDOT regulated more stable biofilm formation (H. S. Park, Ko, Park, Kim, & Song, 2013; Y. Wang et al., 2013).

Although it is evident that there are microorganisms grown on the anodes, not all of them contributed for the electricity generation. Hence, further molecular biology classification by extracting DNA was carried out to identify the diversity and taxonomy of the microbes present in the anodes.

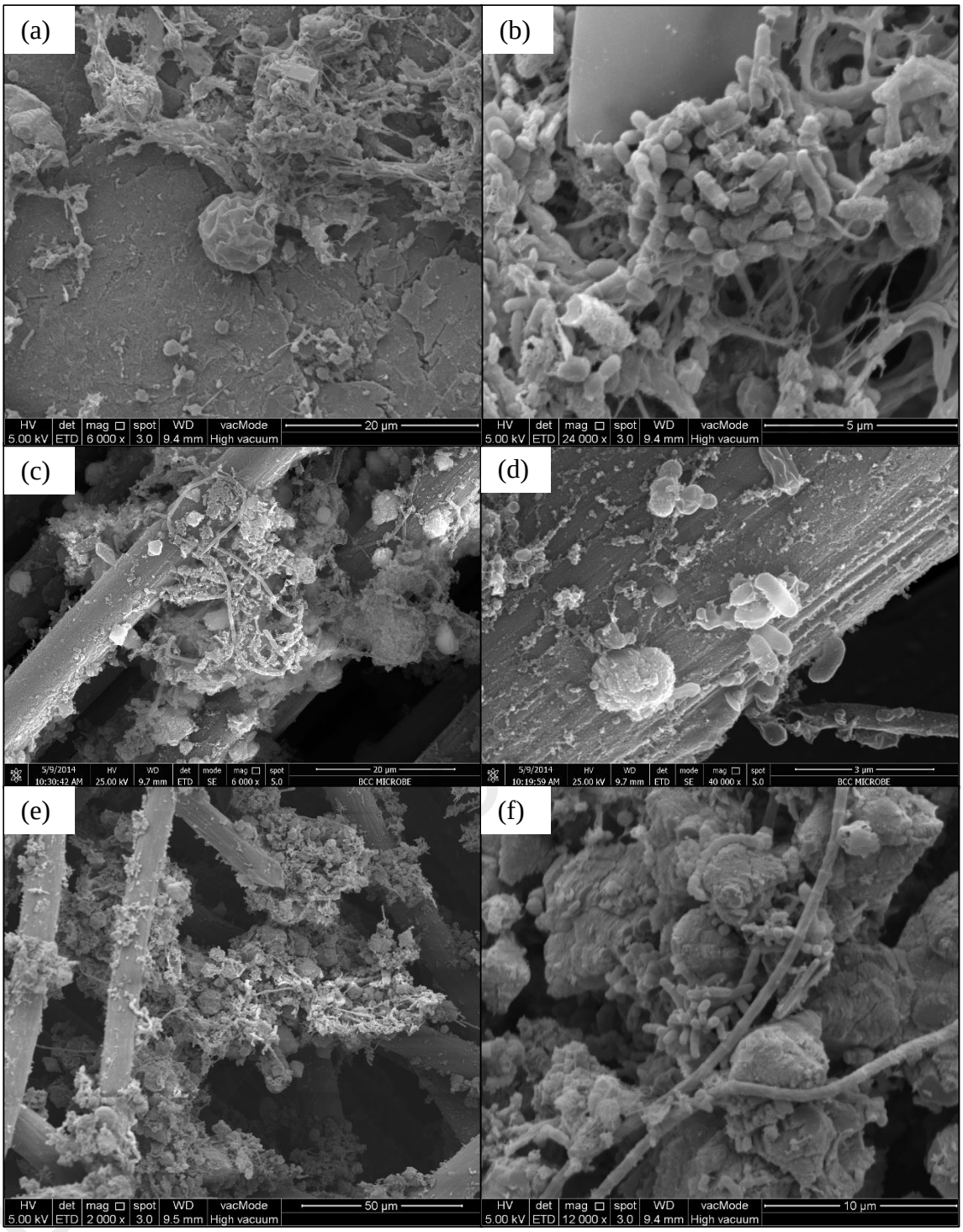

Figure 4.42: SEM Images of Biofilm Attachment on (a-b) GP, (c-d) CC and (e-f) GF Anodes

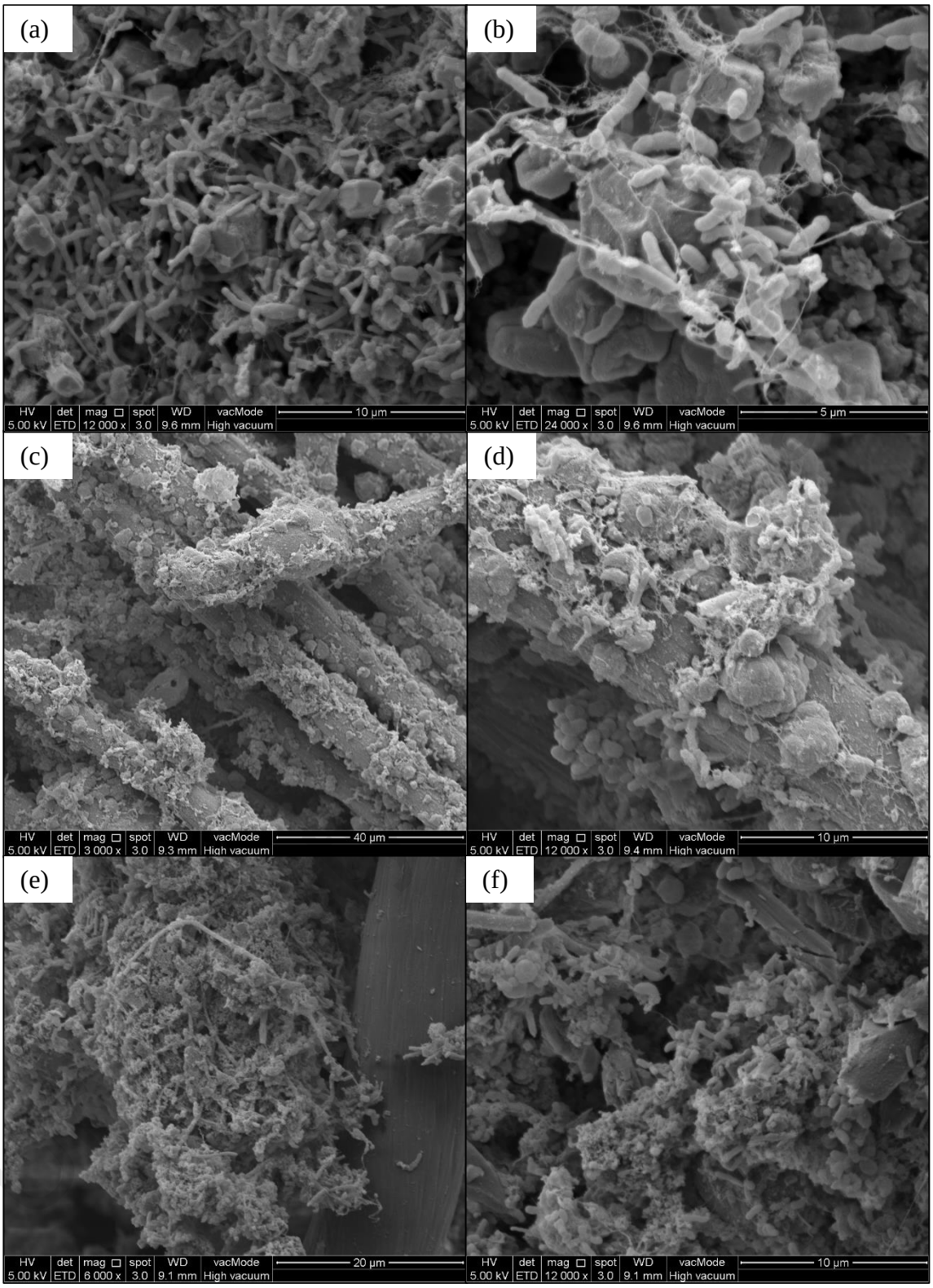

Figure 4.43: SEM Images of Biofilm Attachment on (a-b) GP-P, (c-d) CC-P and (e-f) GF-P Anodes

4.8.2 Biodiversity Sequencing

The inoculum for MFC has expanded from pure to mixed cultures due to the robustness and practicality of the latter (Yang, Du, & Liu, 2012). The vast microbial diversity increased the flexibility of operating conditions and the substrate used in these systems (Kleerebezem & van Loosdrecht, 2007). Therefore, the present study focused on the utilization of mixed culture from POME treatment plant in MFC system without any pre-treatment or isolation. Next Generation Sequencing (NGS) technique was chosen to identify the taxonomy of the seed inoculum and biofilm grown on the anodes. The changes or transformation of taxonomy composition between the anodes also reveals the effect of PEDOT modification on the biofilm formation. The identification of selected exoelectrogens revealed the path and mechanism of electron transfer.

4.8.2.1 Alpha Diversity

An alpha diversity analysis of selected anodes and inoculum is presented in Table 4.8. The number of sequence ranged from ~19,000 to 23,900, providing consistent sequencing depth for all the samples. The richness of the samples are analysed by the number of OTUs and Chao1 index. The table showed that all the anodes have decreased richness compared to the sludge used for inoculation. This was due to the selection of exoelectrogens during acclimatisation phase (Z. Wang, Lee, Lim, Choi, & Park, 2014). The richness index further declined for modified anodes and proved that PEDOT incorporation further developed the selection of anodic biofilm. This was further verified by the beta diversity study. The Shannon index gives an insight on the species richness and diversity, taking into consideration on the abundance of each species. The modified anodes recorded Shannon indices around 4.96 to 4.29 while the control anodes and

inoculum ranged from 5.59 to 5.09, indicating lower diversity among the modified anodes.

The richness rarefaction curve is plotted in Figure 4.44. The curves did not reach plateau even as the sequences exceed 19,000 reads, implying that there are microbes that are not sequenced. However, the effect of this minor absence of additional microbes does not influence the overall understanding of anodic biofilm (Shehab, Li, Amy, Logan, & Saikaly, 2013).

Table 4.8: Summary of Alpha Diversity of the Inoculum and Anodic Biofilm

Sample	No. of Sequence	No. of OTU	Shannon Index	Chao1 Index
Sludge	23899	2848	5.41	8287.58
GP	19317	2733	5.59	6023.00
CC	20007	2614	5.09	5952.39
GF	23504	2516	5.51	5577.07
GP-P	19001	2233	4.66	4891.69
CC-P	21429	2104	4.96	4808.51
GF-P	20675	1914	4.29	4169.40

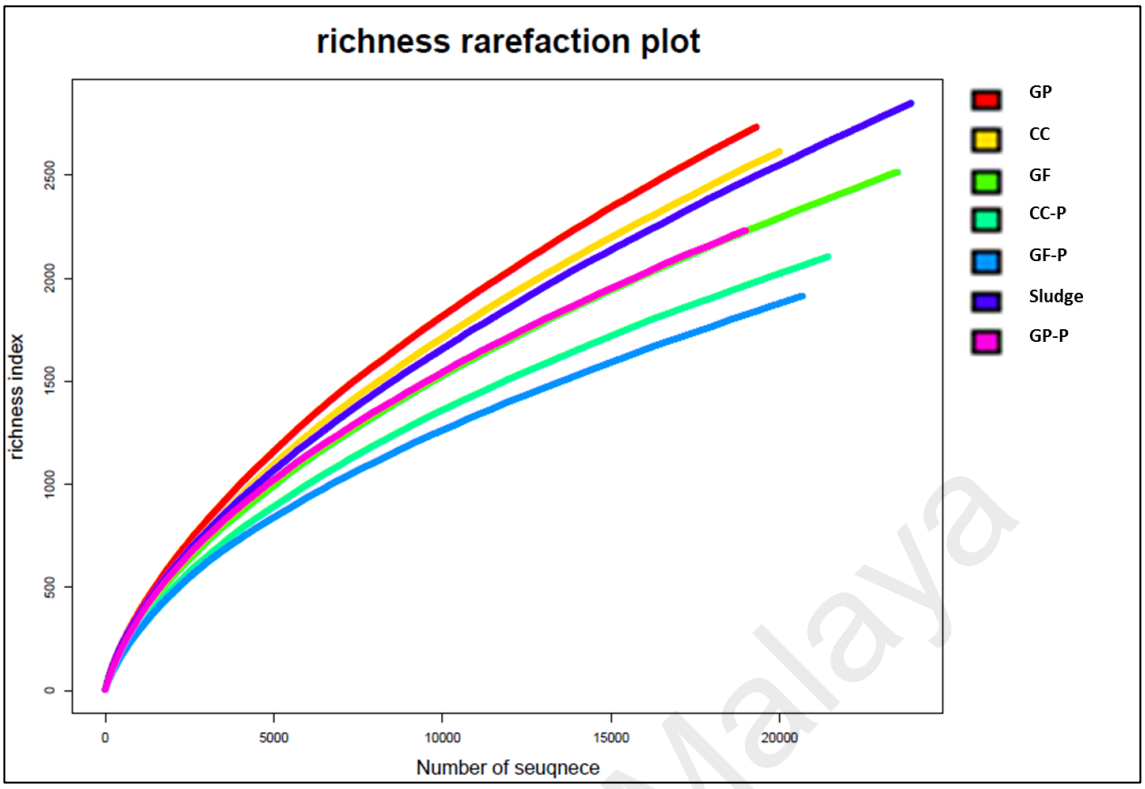

Figure 4.44: Richness Index of the Inoculum and Representative Anodes

4.8.2.2 Beta Diversity

The relative abundance of the anodic biofilm and inoculum community at phylum level was classified and shown in Figure 4.45. The transformation of the microbial community from the inoculum to the anodic biofilm was apparent even at the phylum level. The predominant phylum for the inoculum was the *Firmicutes* (46 %) while all the anodes consist of mainly phylum *Proteobacteria*. This phylum accounted for more than 50% of the anodic biofilm but only 15% for the inoculum. *Proteobacteria* consists of four classes that are the *Alpha*, *Beta*, *Delta* and *Gammaproteobacteria*. Out of these four classes, *Deltaproteobacteria* takes the major percentage in the anodic biofilm community. Phylum *Bacteroidetes* are the second most dominant for all the samples, ranging from 2% to 23%.

The comparison of microbial community representing dominant 50 and 15 genera is demonstrated in Figure 4.46 and Figure 4.47 respectively. The most dominant genus for the sludge community is the *Trichococcus* while all the anodes were dominated by *Geobacter* followed by *Hydrogenophaga*. Identified exoelectrogens such as *Geobaceter*, *Hydrogenophaga* and *Shewamella* were present in most anodic biofilms whereas the same is below detectable level (< 1 %) in the inoculum and is tabulated in Table 4.9. This shows that the anodes were able to cultivate electrochemically active microorganism on their surface. On the contrary, the *Pseudomonas*, an exoelectrogen was reduced or disappeared from the anodic biofilm population although it was detected in the sludge. This strain was less competent compared to the other genera for electron generation and was eliminated from the community (Z. Wang et al., 2014). The acclimatization has significantly increased the exoelectrogens in all the anodes compared to the sludge inoculum. The adopted acclimatisation condition allowed the selection of biofilm with external electron transfer capabilities to achieve a steady-state cell potential (Babauta, Renslow, Lewandowski, & Beyenal, 2012).

The prevalence of *Geobacter* is consistent with most acetate-fed operation as they are able to oxidize acetate and transfer electron directly to the anode (Bond & Lovley, 2003; X. Jiang et al., 2013; H. Zhang, Chen, Braithwaite, & He, 2014). The second majority of exoelectrogens found on the anodic biofilms were the *Hydrogenophaga.* They are hydrogen-consuming exoelectrogens that utilizes the by-product of acetate metabolism by *Geobacter*. Hence, *Hydrogenophaga* established a syntrophic relationship with *Geobacter* and usually found alongside *Geobacter* in MFC systems (Kimura & Okabe, 2013). Table 4.9 also showed the nominal presence of *Shewanella*. However, their contribution to electricity generation cannot be ignored, as predominance of a strain does not necessarily relate to their current production ability (Kiely, Call, Yates, Regan, & Logan, 2010).

Additionally, the frequency of exoelectrogen on PEDOT modified anodes were higher compared to the control anodes. It is evident that the presence of PEDOT supports the growth and development of these exoelectrogens. The robust electrical conductivity of the PEDOT stimulates the biofilm formation as compared to unmodified anodes (Webb et al., 2015). This finding is also evident from the similarity composition plot shown in Figure 4.47, where the similarities of control anodes is closer to the sludge composition compared to the modified anodes.

Methanogens such as *Methanobrevibacter*, *Methanobacterium* and *Methanosaeta* are also detected in the sludge samples as well as in the anodes in very minor percentage (< 1%). The presence of these microbes should be curtailed as they may reduce the efficiency of MFC systems by competing with exoelectrogens for substrate.

Table 4.9: Exoelectrogen Distribution in Sludge Inoculum and Tested Anodes (>1%)

Genus	Sludge (%)	GP (%)	CC (%)	GF (%)	GP-P (%)	CC-P (%)	GF-P (%)
Geobacter	-	18.8	58.8	22.9	86.7	48.4	63.5
Hydrogenophaga	-	16.4	2.3	4.8	-	-	17.2
Shewanella	-	-	4.7	-	-	2.1	2.3
Pseudomonas	3.7	-	-	2.5	1.2	-	-
Total	3.7	35.1	65.8	30.3	87.9	50.5	83.0

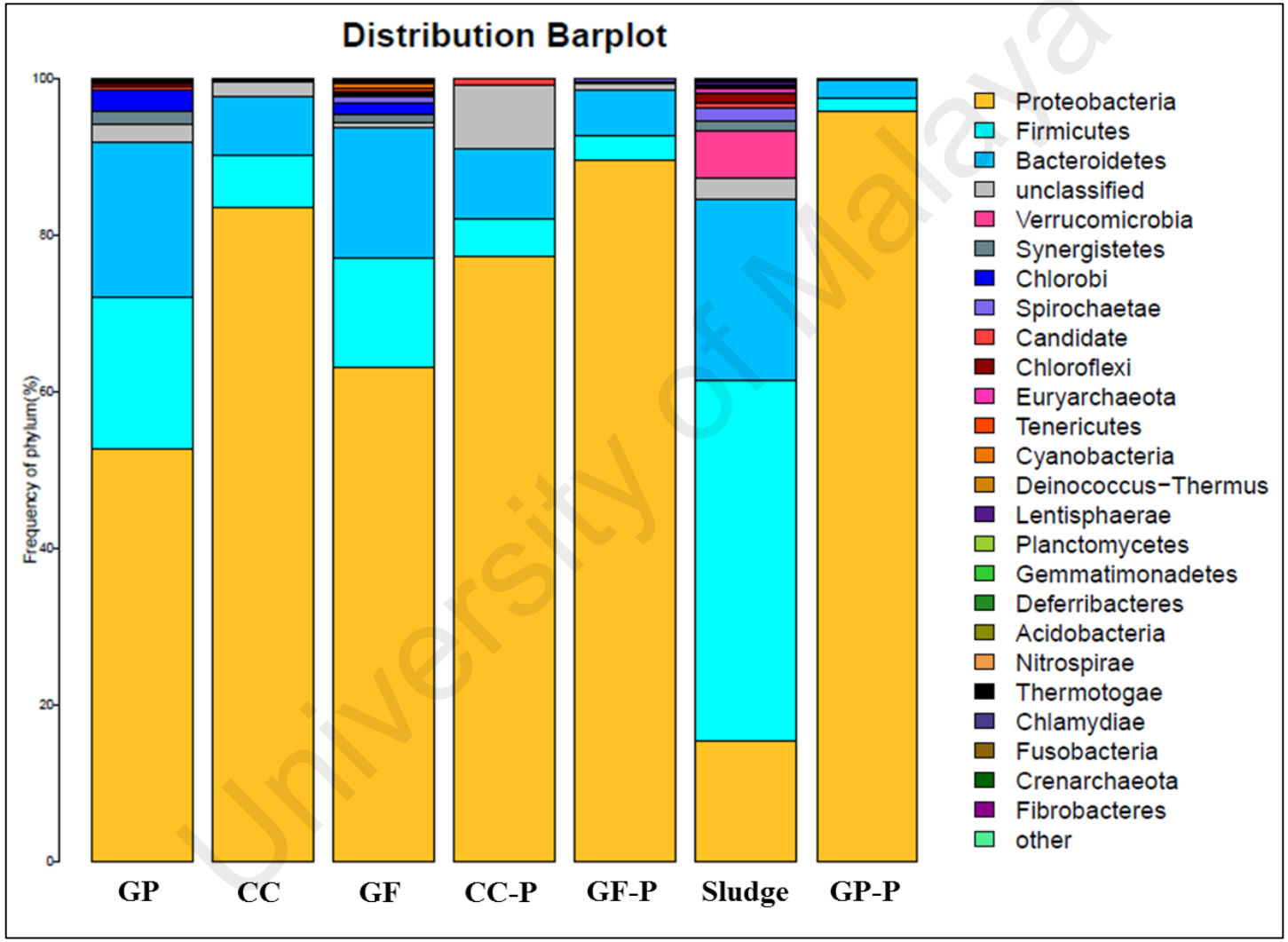

Figure 4.45: Relative Abundance of Microbial Community for the Sludge and Representative Anodes at Phylum Level

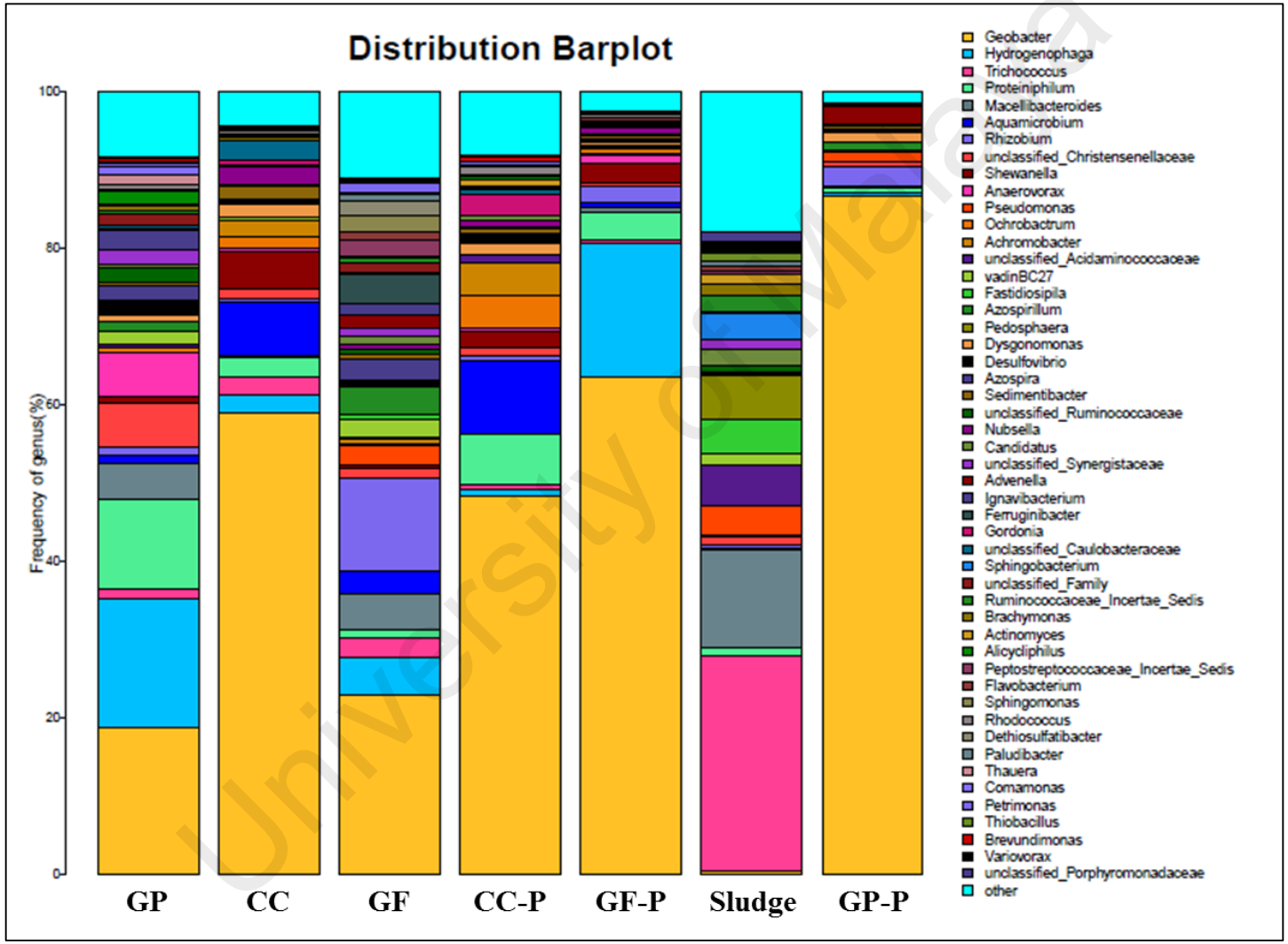

Figure 4.46: Taxonomy Classification of Microbial Community for the Sludge and Representative Anodes (First 50 Genus)

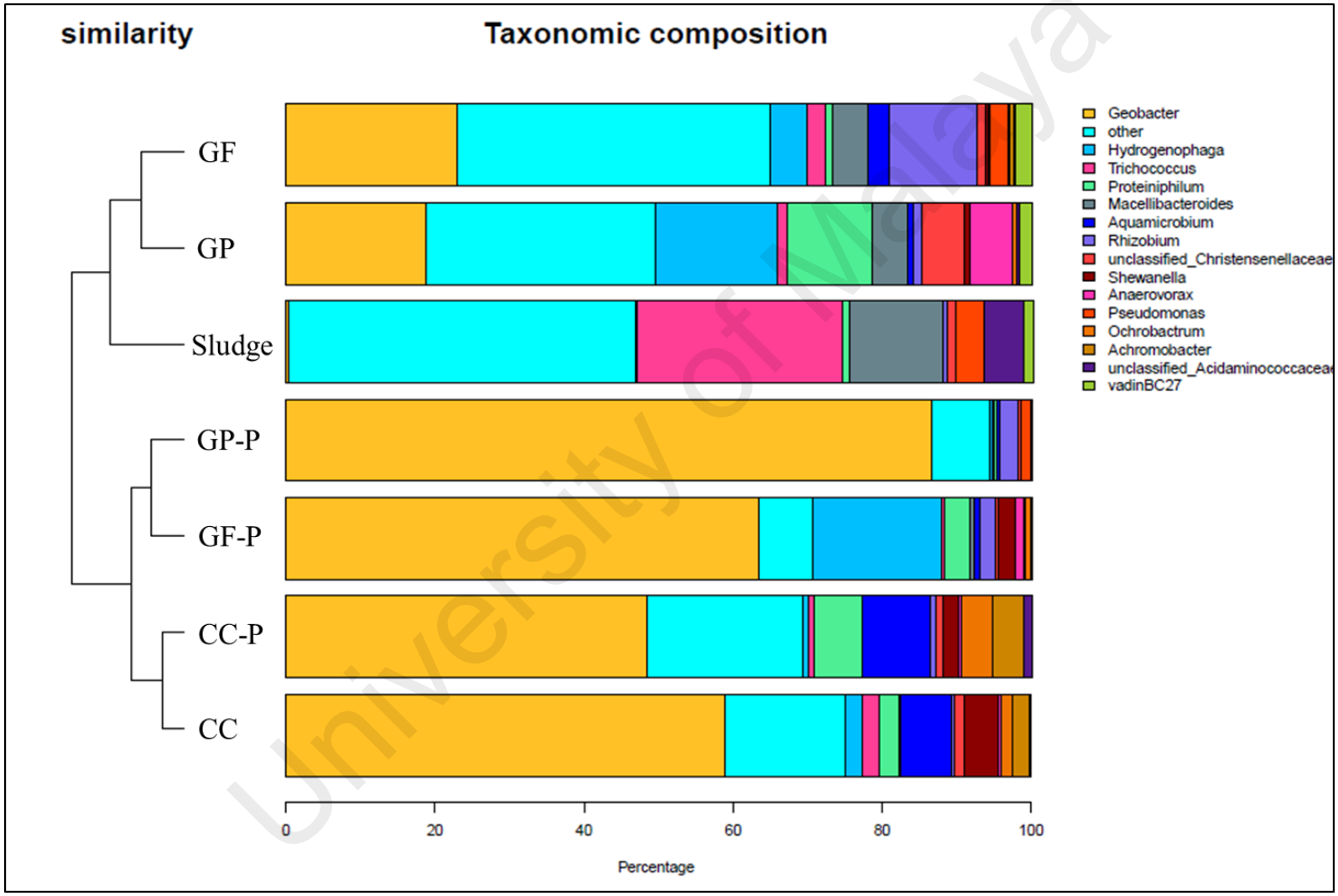

Figure 4.47: Taxonomy Classification of Microbial Community for the Sludge and Representative Anodes (First 15 Genus)

4.9 Wastewater as Substrate for MFC

From the microbiological identification discussed above, the dominant exoelectrogens found for all the tested anodes are the *Geobacter* and *Hydrogenophaga*. *Hydrogenophaga* consumes hydrogen contributed as a by-product of acetate oxidation while *Geobacter* prefers low-molecular substrate like acetate and butyrate (Schroder, 2007). Hence, it is necessary to evaluate the stability of these systems when utilizing complex molecule and rich organic substrates. CC-2P and GF-P, which demonstrated better performance among the studied anodes, were chosen for this study. POME was diluted to ~350 mg/L of COD and introduced gradually to the reactor with acetate of similar COD concentration. Their performances are discussed below.

4.9.1 Performance of CC-2P using POME as Substrate

The voltage generation across 1k Ω resistor was carried out for two cycles in order to investigate the stability of the biofilm towards POME and the obtained results are displayed in Figure 4.48. The obtained results clarified that the generated voltage were not consistent and lower voltage productions were observed regardless of substrate composition. The highest maximum voltage of 676.5 ± 8 mV was achieved by 75% POME followed by 100% POME (661.0 ± 23 mV) and 50% POME (506.0 ± 31 mV). These values were slightly lower than the ~ 695.0 mV demonstrated by the same anode under acetate substrate. The duration of peak voltage plateaus for all wastewater ratios lasted for 1 to 2 days.

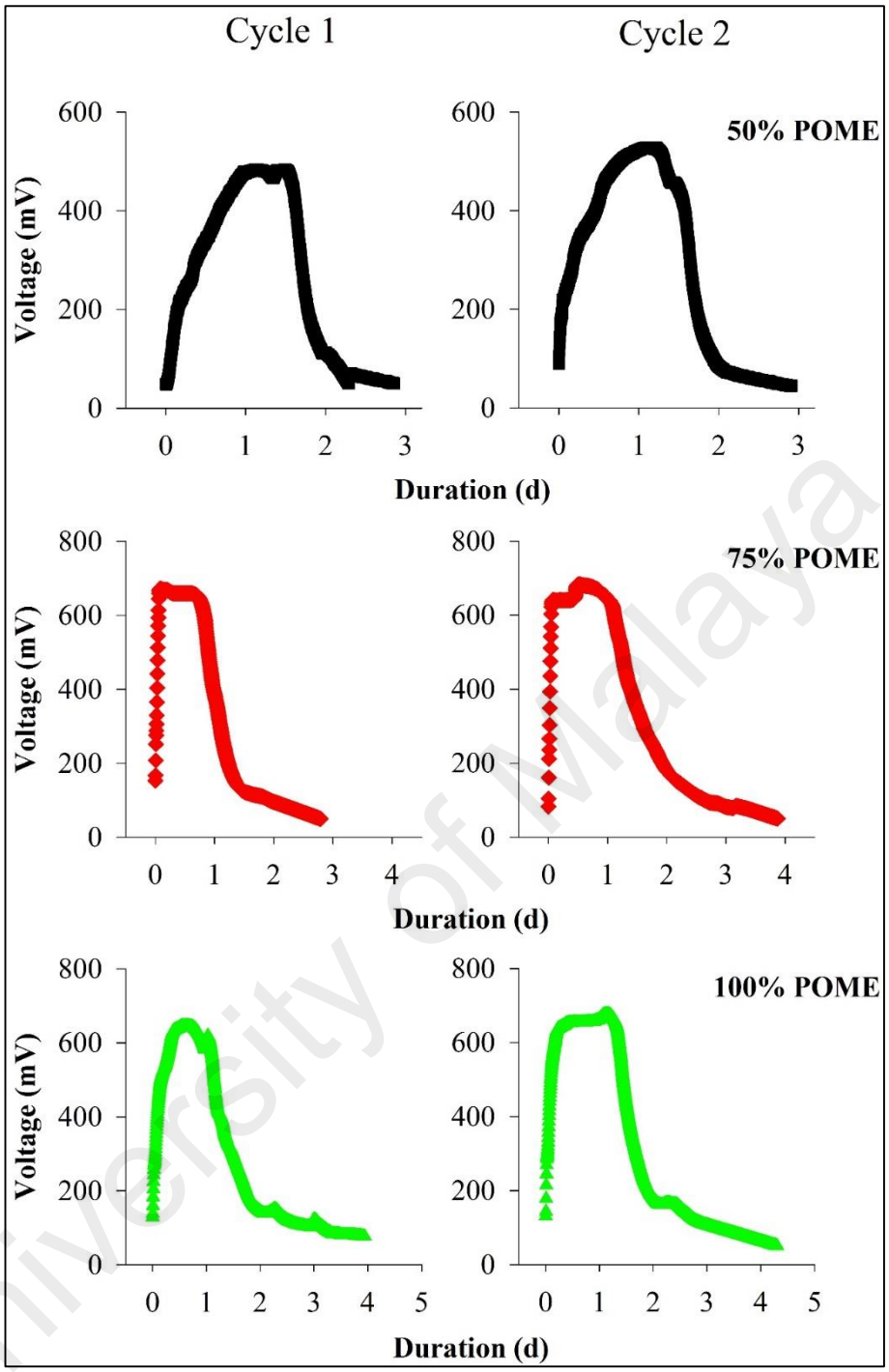

Figure 4.48: Voltage Generation for CC-2P using Different Ratios of POME

The maximum current densities among the three studied ratio of wastewater were found to be 6.0 A/m^2 for 50% POME, 5.0 A/m^2 and 5.4 A/m^2 for 75% and 100% respectively and are illustrated in Figure 4.49. All the obtained current densities are well comparable with the pure acetate condition (4.8 A/m^2). The power density for 50% POME recorded the highest power generation of 1.82 W/m^2, while the 75% POME system

achieved 1.49 W/m^2. The power density bounced back to 1.66 W/m^2 for 100 % wastewater. The lowest POME ratio obtained high power production due to the high amount of acetate, which was easier for the exoelectrogens to oxidize. 75% of POME contains more complex organics that results in the decline of both maximum current and power density.

Conversely, due to better and prolonged acclimatization of the biofilm towards complex POME substrate, the current and power density performances improved marginally when 100% POME was inserted compared to 75% POME.

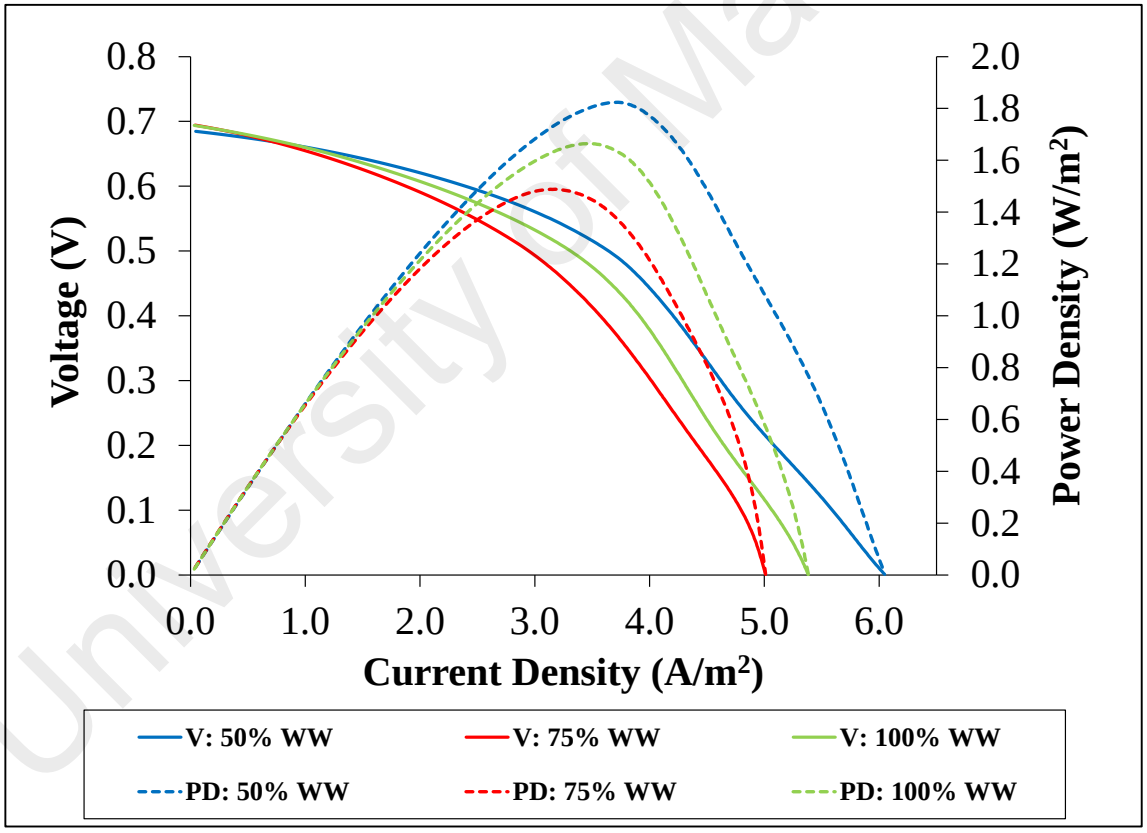

Figure 4.49: Polarization (V) and Power Density (PD) Curves of CC-2P for Different Ratios of POME

The COD removal for these systems decreases with an increase of POME ratio and is shown Figure 4.50. The higher POME content contributed to more complex molecules that are hard to be metabolised by the microbes and caused the COD removal to fall. The CE for all three substrate samples was in the range of ~13 % to 30%. The obtained CEs were found be significantly lower compared to pure acetate condition (58%). The lag in adaptation of the biofilm to the environment resulted in the extremely low CE for 50% POME.

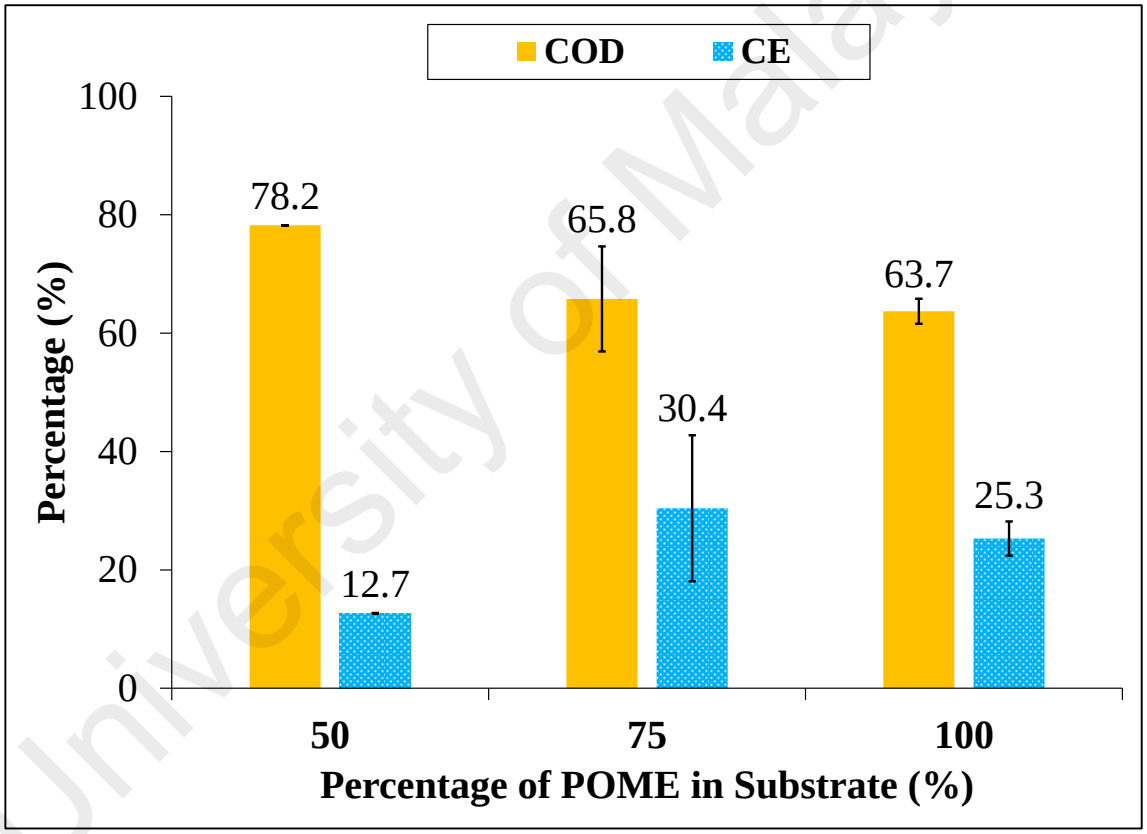

Figure 4.50: COD Removal and CE Percentage of CC-2P for Different Ratios of POME

4.9.2 Performance of GF-P using POME as Substrate

The voltage generation for the studied substrate ratio for GF-P anode is portrayed in Figure 4.51. Low voltage of 573.7 ± 14 mV was obtained for 50% POME condition while a highest voltage of 707.5 ± 8 mV was achieved for 75% POME. The potential dropped slightly to 685.5 ± 3.5 mV when 100% POME was utilized as anolyte. These values are comparable to the operation of the same anode under low molecular substrate, i.e. acetate (711.0 ± 4 mV). The repeatability of two consecutive cycles for all three substrates disclosed the stability of the biofilm in consuming the complex substrate.

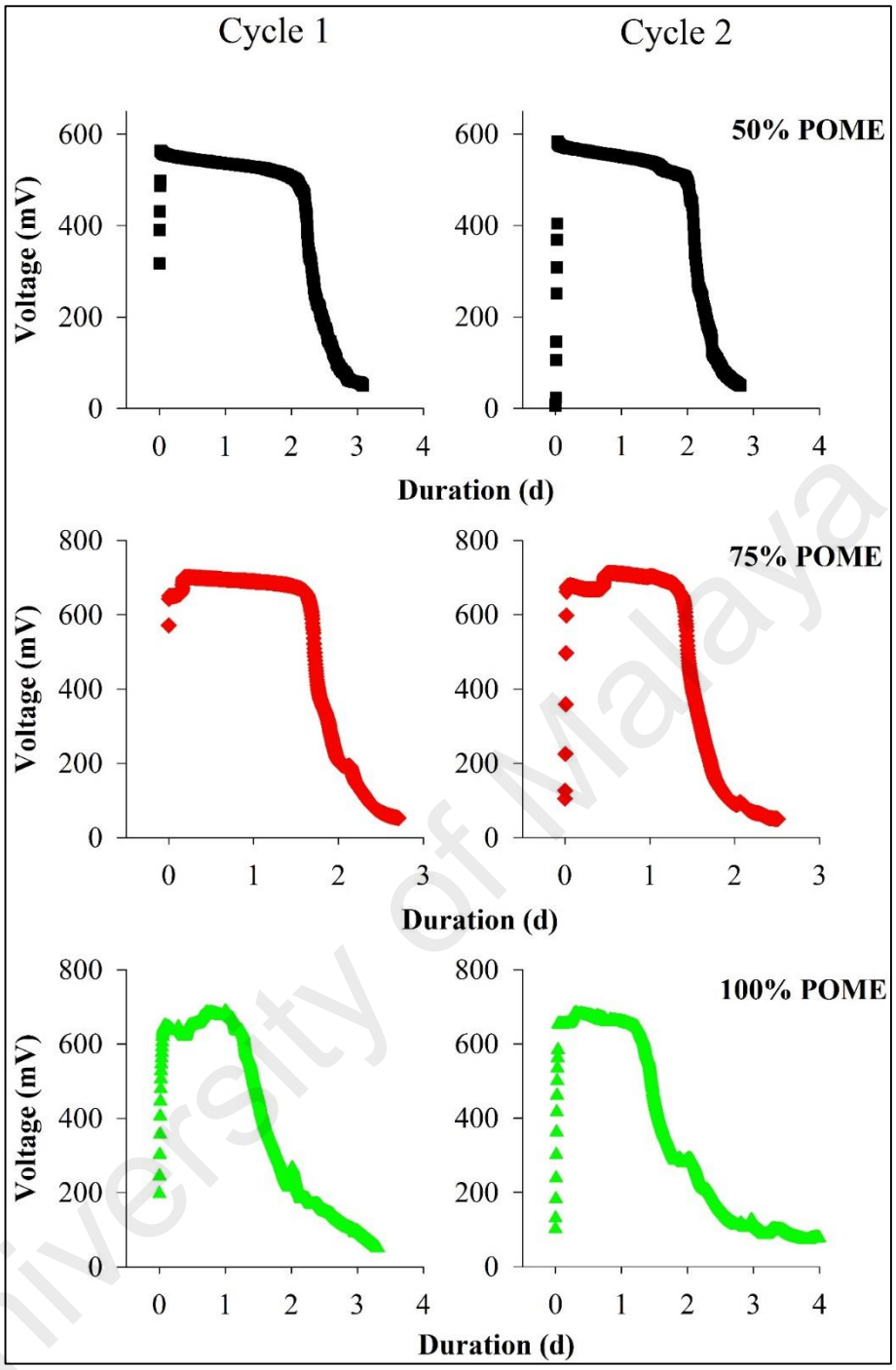

Figure 4.51: Voltage Generation for GF-P using Different Ratios of POME

Figure 4.52 illustrates the polarization and power density curve for the studied GF-P anode under varied POME: acetate concentration. The I_{sc} obtained for the three substrate ratio were in the range of 3.0 – 3.9 A/m^2 and was consistent with pure acetate condition. Similar trend was observed for the power density; with value ranging from 1.1 – 1.2 W/m^2, whereas 1.6 W/m^2 was achieved under acetate condition. The similarity in

the performance between varied substrate conditions proved the robustness of the biofilm in handling wide range of substrate. The performance of the system was optimum under 75% POME condition and dropped marginally for 100 % POME.

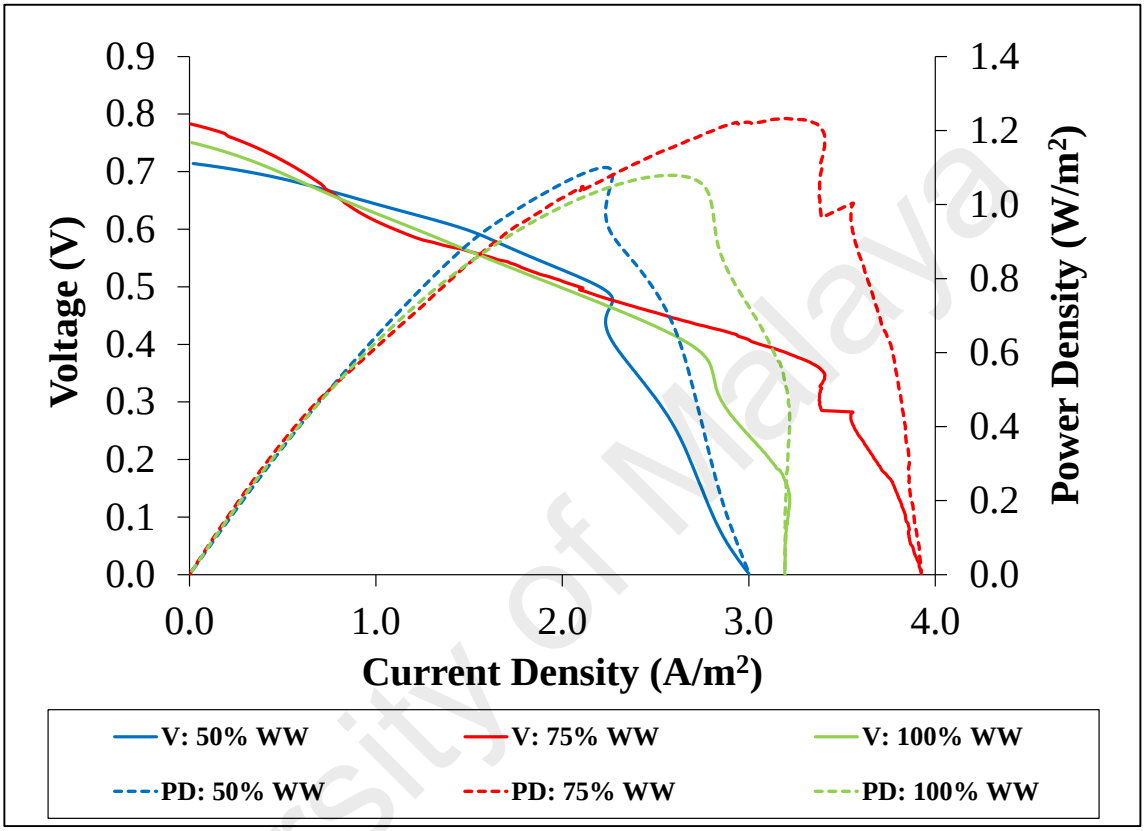

Figure 4.52: Polarization (V) and Power Density (PD) Curves of GF-P for Different Ratios of POME

The COD removal and CE performance for GF-P anode operated with varying ratio of POME is displayed in Figure 4.53. The COD removal decreases as the POME content increases as complex molecules are harder to decompose. The 75% and 100% POME exhibited similar CE performance. These numbers were consistent with the voltage generation trend as discussed above.

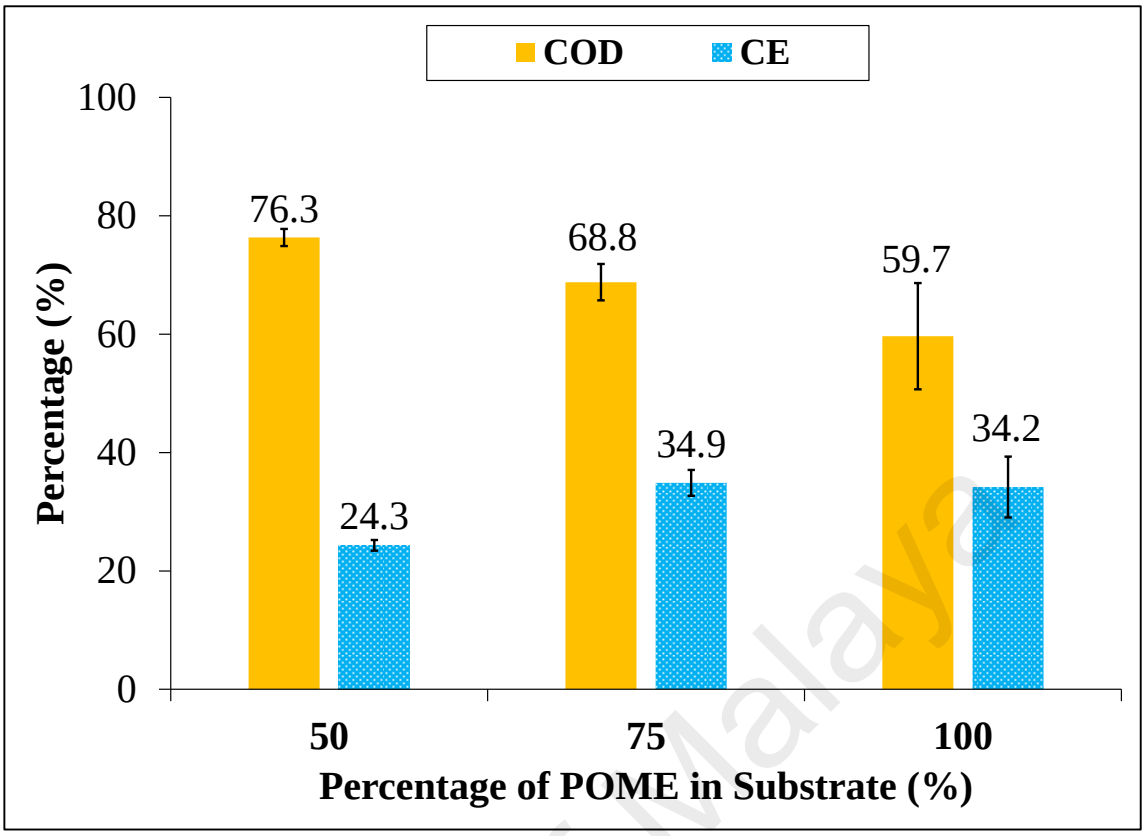

Figure 4.53: COD Removal and CE Percentage of GF-P for Different Ratios of POME

4.9.3 Summary

The above analysis showed that the anodes developed in the study were able to utilized both simple and complex molecules. The voltage generation and power density under POME substrate were comparable with the values obtained during pure acetate condition. Although the COD removal and CE performance were inferior compared to the magnitude achieved by acetate, prolonged acclimatization period and other measures ought to improve the efficiency of the system.

CHAPTER 5

CONCLUSION AND RECOMMENDATIONS

5.1 Conclusion

The main objective of this research is to develop enhanced anodes for MFC application. The stated research hypothesis was successfully accomplished by functionalizing PEDOT onto carbon-based anodes with different structural configurations. The modified anodes exhibited improved electrochemical characteristics along with enriched electrical generation. Substantial conclusions drawn from the present investigation are enumerated below:

- GF has the most efficient configuration compared to the GP and CC anodes due to its open structure and macro-porous feature.
- PEDOT synthesized through chemical oxidation was successfully incorporated into the anodes and able to maintain its stability throughout the duration of the experiments.
- The functionalization of PEDOT onto all the experimented configurations improved the overall properties of the anodes and led to better MFC performances.
- The optimum PEDOT loading are varied for different structural configurations and in most cases, the highest loading of PEDOT (7.5 mg/cm^2) proved to be detrimental to the anode performances.
- The microbial diversity experienced substantial transition from the sludge inoculum to the anodic biofilm. Exoelectrogens were below detected levels in the inoculum but became predominant in all the tested anodic biofilm.

- *Geobacter,* an exoelectrogen commonly found in acetate-fed MFC were the dominant genera of all the anodic biofilm. Hence, it can be implicated that DET is the main electron transfer mechanism in the studied systems.
- Most of the modified anodes demonstrated higher percentage of exoelectrogens compared to corresponding control anodes, establishing inherent contribution of PEDOT on the selection of electrochemically active biofilm.
- The successful utilization of POME as substrate ascertained the feasibility of these modified anodes and their corresponding anodic biofilm in utilizing complex organics.

5.2 Recommendations

The following suggestion can be taken into considerations for future research direction:

- Chemical polymerized PEDOT was successfully applied in this study. Various composites of PEDOT for further anode enhancement could be deliberated in prospective research.
- The present study was carried out under a fixed reactor configuration and optimum reactor design and operating conditions were not evaluated. Hence, the optimization of these factors could be considered in future studies.
- Batch operation was detailed in the present study. A continuous operation with appropriate reactor configuration could be studied in the future.
- The biological classifications could be extended to the anodic biofilms utilizing real complex wastewater to study their effect on biofilm diversity.

REFERENCES

Abdiryim, T., Ubul, A., Jamal, R., Xu, F., & Rahman, A. (2012). Electrochemical properties of the poly(3,4-ethylenedioxythiophene)/single-walled carbon nanotubes composite synthesized by solid-state heating method. *Synthetic Metals*, *162*(17), 1604-1608.

American Public Health Association. (2005). *Standard methods for the examination of water and wastewater*. Washington, DC, USA: American Public Health Association (APHA).

An, J., Kim, B., Chang, I. S., & Lee, H. S. (2015). Shift of voltage reversal in stacked microbial fuel cells. *Journal of Power Sources*, *278*, 534-539.

Babauta, J., Renslow, R., Lewandowski, Z., & Beyenal, H. (2012). Electrochemically active biofilms: facts and fiction. A review. *Biofouling*, *28*(8), 789-812.

Badwal, S. P., Giddey, S. S., Munnings, C., Bhatt, A. I., & Hollenkamp, A. F. (2014). Emerging electrochemical energy conversion and storage technologies. *Frontiers in Chemistry*, *2*.

Bard, A. J., & Faulkner, L. R. (2001). *Electrochemical methods: Fundamentals and applications* (2nd ed.). New York, USA: Wiley.

Beyenal, H., & Babauta, J. T. (2012). Microscale gradients and their role in electron-transfer mechanisms in biofilms. *Biochemical Society Transactions*, *40*(6), 1315-1318.

Billingham, N. C., & Calvert, P. D. (1989). Electrically conducting polymers—a polymer science viewpoint. In *Conducting Polymers/Molecular Recognition* (pp. 1-104). Berlin, Heidelberg: Springer-Verlag.

Bond, D. R., & Lovley, D. R. (2003). Electricity Production by *Geobacter sulfurreducens* Attached to Electrodes. *Applied and Environmental Microbiology*, *69*(3), 1548-1555.

Borole, A. P., Aaron, D., Hamilton, C. Y., & Tsouris, C. (2010). Understanding long-term changes in microbial fuel cell performance using electrochemical impedance spectroscopy.*Environmental Science & Technology*, *44*(7), 2740-2745.

Cai, H., Wang, J., Bu, Y., & Zhong, Q. (2013). Treatment of carbon cloth anodes for improving power generation in a dual-chamber microbial fuel cell. *Journal of Chemical Technology and Biotechnology, 88*(4), 623-628.

Chang, I. S., Jang, J. K., Gil, G. C., Kim, M., Kim, H. J., Cho, B. W., & Kim, B. H. (2004). Continuous determination of biochemical oxygen demand using microbial fuel cell type biosensor. *Biosensors and Bioelectronics, 19*(6), 607-613.

Chaudhuri, S. K., & Lovley, D. R. (2003). Electricity generation by direct oxidation of glucose in mediatorless microbial fuel cells. *Nature Biotechnology, 21*(10), 1229-1232.

Chen, S., Liu, Q., He, G., Zhou, Y., Hanif, M., Peng, X., . . . Hou, H. (2012). Reticulated carbon foam derived from a sponge-like natural product as a high-performance anode in microbial fuel cells. *Journal of Materials Chemistry, 22*(35), 18609-18613.

Cheng, S., & Logan, B. E. (2007). Ammonia treatment of carbon cloth anodes to enhance power generation of microbial fuel cells.*Electrochemistry Communications*, *9*(3), 492-496.

Choi, C., & Cui, Y. (2012). Recovery of silver from wastewater coupled with power generation using a microbial fuel cell. *Bioresource Technology, 107*, 522-525.

Choi, C., & Hu, N. (2013). The modeling of gold recovery from tetrachloroaurate wastewater using a microbial fuel cell. *Bioresource Technology, 133*, 589-598.

Chou, H. T., Lee, H. J., Lee, C. Y., Tai, N. H., & Chang, H. Y. (2014). Highly durable anodes of microbial fuel cells using a reduced graphene oxide/carbon nanotube-coated scaffold. *Bioresource Technology*, *169*, 532-536.

Corcoran, E. (Ed.). (2010). *Sick water?: The central role of wastewater management in sustainable development: A rapid response assessment*. Birkeland, Norway: United Nations Environment Programme.

Cui, H. F., Du, L., Guo, P. B., Zhu, B., & Luong, J. H. (2015). Controlled modification of carbon nanotubes and polyaniline on macroporous graphite felt for high-performance microbial fuel cell anode. *Journal of Power Sources*, *283*, 46-53.

Debabov, V. G. (2008). Electricity from microorganisms. *Microbiology, 77*(2), 123-131.

Demirbas, A. (2008). Biofuels sources, biofuel policy, biofuel economy and global biofuel projections. *Energy Conversion and Management*, *49*(8), 2106-2116.

Du, Z., Li, Q., Tong, M., Li, S., & Li, H. (2008). Electricity generation using membrane-less microbial fuel cell during wastewater treatment. *Chinese Journal of Chemical Engineering*, *16*(5), 772-777.

Elschner, A., Kirchmeyer, S., Lovenich, W., Merker, U., & Reuter, K. (2010). *PEDOT: Principles and Applications of an Intrinsically Conductive Polymer*. CRC Press.

Environmental Protection Agency. (2008). *EPA's 2008 Report on the Environment*. Washington, DC: National Center for Environmental Assessment.

Feng, C., Ma, L., Li, F., Mai, H., Lang, X., & Fan, S. (2010). A polypyrrole/anthraquinone-2, 6-disulphonic disodium salt (PPy/AQDS)-modified anode to improve performance of microbial fuel cells. *Biosensors and Bioelectronics*, *25*(6), 1516-1520.

Feng, C., Wan, Q., Lv, Z., Yue, X., Chen, Y., & Wei, C. (2011). One-step fabrication of membraneless microbial fuel cell cathode by electropolymerization of polypyrrole onto stainless steel mesh. *Biosensors and Bioelectronics*, *26*(9), 3953-3957.

Feng, Y., Lee, H., Wang, X., Liu, Y., & He, W. (2010). Continuous electricity generation by a graphite granule baffled air–cathode microbial fuel cell. *Bioresource Technology*, *101*(2), 632-638.

Feng, Y., Yang, Q., Wang, X., & Logan, B. E. (2010). Treatment of carbon fiber brush anodes for improving power generation in air–cathode microbial fuel cells. *Journal of Power Sources*, *195*(7), 1841-1844.

Fradler, K. R., Michie, I., Dinsdale, R. M., Guwy, A. J., & Premier, G. C. (2014). Augmenting microbial fuel cell power by coupling with supported liquid membrane permeation for zinc recovery. *Water Research*, *55*, 115-125.

Fraiwan, A., Mukherjee, S., Sundermier, S., Lee, H. S., & Choi, S. (2013). A paper-based microbial fuel cell: Instant battery for disposable diagnostic devices. *Biosensors and Bioelectronics*, *49*, 410-414.

Franks, A. E., & Nevin, K. P. (2010). Microbial fuel cells, a current review. *Energies*, *3*(5), 899-919.

Ghasemi, M., Daud, W. R. W., Mokhtarian, N., Mayahi, A., Ismail, M., Anisi, F., ... & Alam, J. (2013). The effect of nitric acid, ethylenediamine, and diethanolamine modified polyaniline nanoparticles anode electrode in a microbial fuel cell. *International Journal of Hydrogen Energy*, *38*(22), 9525-9532.

Gil, G. C., Chang, I. S., Kim, B. H., Kim, M., Jang, J. K., Park, H. S., & Kim, H. J. (2003). Operational parameters affecting the performannce of a mediator-less microbial fuel cell. *Biosensors and Bioelectronics*, *18*(4), 327-334.

Gnana Kumar, G., Kirubaharan, C. J., Udhayakumar, S., Ramachandran, K., Karthikeyan, C., Renganathan, R., & Nahm, K. S. (2014). Synthesis, structural, and morphological characterizations of reduced graphene oxide-supported polypyrrole anode catalysts for improved microbial fuel cell performances. *ACS Sustainable Chemistry & Engineering*, *2*(10), 2283-2290.

Godwin, J. M., & Evitts, R. (2011). Polypyrrole/Poly(Methylene Blue) composite electrode films on stainless steel. *ECS Transactions*, *33*(27), 181-188.

Goud, R. K., & Mohan, S. V. (2011). Pre-fermentation of waste as a strategy to enhance the performance of single chambered microbial fuel cell (MFC). *International Journal of Hydrogen Energy*, *36*(21), 13753-13762.

Habermann, W., & Pommer, E. H. (1991). Biological fuel cells with sulphide storage capacity. *Applied Microbiology and Biotechnology*, *35*(1), 128-133.

Hays, S., Zhang, F., & Logan, B. E. (2011). Performance of two different types of anodes in membrane electrode assembly microbial fuel cells for power generation from domestic wastewater. *Journal of Power Sources*, *196*(20), 8293-8300.

He, Z., & Mansfeld, F. (2009). Exploring the use of electrochemical impedance spectroscopy (EIS) in microbial fuel cell studies. *Energy & Environmental Science*, *2*(2), 215-219.

He, Z., Kan, J., Mansfeld, F., Angenent, L. T., & Nealson, K. H. (2009). Self-sustained phototrophic microbial fuel cells based on the synergistic cooperation between photosynthetic microorganisms and heterotrophic bacteria. *Environmental Science & Technology*, *43*(5), 1648-1654.

He, Z., Liu, J., Qiao, Y., Li, C. M., & Tan, T. T. Y. (2012). Architecture engineering of hierarchically porous chitosan/vacuum-stripped graphene scaffold as bioanode for high performance microbial fuel cell. *Nano Letters*, *12*(9), 4738-4741.

He, Z., Wagner, N., Minteer, S. D., & Angenent, L. T. (2006). An upflow microbial fuel cell with an interior cathode: Assessment of the internal resistance by impedance spectroscopy. *Environmental Science & Technology*, *40*(17), 5212-5217.

Hernandez, M. E., & Newman, D. K. (2001). Extracellular electron transfer. *Cellular and Molecular Life Sciences*, *58*(11), 1562-1571.

Hou, B., Hu, Y., & Sun, J. (2012). Performance and microbial diversity of microbial fuel cells coupled with different cathode types during simultaneous azo dye decolorization and electricity generation. *Bioresource Technology*, *111*, 105-110.

Hou, J. X., Liu, Z. L., & Li, Y. X. (2015). Polyaniline modified stainless steel fiber felt for high-performance microbial fuel cell anodes. *Journal of Clean Energy Technologies*, *3*(3), 165-169.

Hou, J., Liu, Z., & Zhang, P. (2013). A new method for fabrication of graphene/polyaniline nanocomplex modified microbial fuel cell anodes. *Journal of Power Sources*, *224*, 139-144.

Hou, J., Liu, Z., Yang, S., & Zhou, Y. (2014). Three-dimensional macroporous anodes based on stainless steel fiber felt for high-performance microbial fuel cells. *Journal of Power Sources*, *258*, 204-209.

Hutchinson, A. J., Tokash, J. C., & Logan, B. E. (2011). Analysis of carbon fiber brush loading in anodes on startup and performance of microbial fuel cells. *Journal of Power Sources*, *196*(22), 9213-9219.

Ichihashi, O., & Hirooka, K. (2012). Removal and recovery of phosphorus as struvite from swine wastewater using microbial fuel cell. *Bioresource Technology*, *114*, 303-307.

Ieropoulos, I., Winfield, J., & Greenman, J. (2010). Effects of flow-rate, inoculum and time on the internal resistance of microbial fuel cells. *Bioresource Technology*, *101*(10), 3520-3525.

International Energy Agency. (2012a). Water for Energy: Is energy becoming a thirstier resource? In *World Energy Outlook 2012*. Paris, France: International Energy Agency

International Energy Agency. (2012b). *World Energy Outlook 2012*. Paris, France: International Energy Agency.

Jayapriya, J., & Ramamurthy, V. (2014). The role of electrode material in capturing power generated in *Pseudomonas* catalysed fuel cells. *The Canadian Journal of Chemical Engineering*, *92*(4), 610-614.

Jiang, C., Chen, G., & Wang, X. (2012). High-conversion synthesis of poly(3, 4-ethylenedioxythiophene) by chemical oxidative polymerization. *Synthetic Metals*, *162*(21), 1968-1971.

Jiang, D., & Li, B. (2009). Granular activated carbon single-chamber microbial fuel cells (GAC-SCMFCs): A design suitable for large-scale wastewater treatment processes. *Biochemical Engineering Journal*, *47*(1-3), 31-37.

Jiang, X., Hu, J., Fitzgerald, L. A., Biffinger, J. C., Xie, P., Ringeisen, B. R., & Lieber, C. M. (2010). Probing electron transfer mechanisms in *Shewanella oneidensis* MR-1 using a nanoelectrode platform and single-cell imaging. *Proceedings of the National Academy of Sciences*, *107*(39), 16806-16810.

Jiang, X., Hu, J., Petersen, E. R., Fitzgerald, L. A., Jackan, C. S., Lieber, A. M., . . . Biffinger, J. C. (2013). Probing single- to multi-cell level charge transport in *Geobacter sulfurreducens* DL-1. *Nature Communications, 4*.

Jiang, Y., Liang, P., Zhang, C., Bian, Y., Yang, X., Huang, X., & Girguis, P. R. (2015). Enhancing the response of microbial fuel cell based toxicity sensors to Cu (II) with the applying of flow-through electrodes and controlled anode potentials. *Bioresource Technology*, *190*, 367-372.

Jonker, J. G. G., & Faaij, A. P. C. (2013). Techno-economic assessment of micro-algae as feedstock for renewable bio-energy production. *Applied Energy*, *102*, 461-475.

Kaur, A., Ibrahim, S., Pickett, C. J., Michie, I. S., Dinsdale, R. M., Guwy, A. J., & Premier, G. C. (2014). Anode modification to improve the performance of a microbial fuel cell volatile fatty acid biosensor. *Sensors and Actuators B: Chemical*, *201*, 266-273.

Kiely, P. D., Call, D. F., Yates, M. D., Regan, J. M., & Logan, B. E. (2010). Anodic biofilms in microbial fuel cells harbor low numbers of higher-power-producing bacteria than abundant genera. *Applied Microbiology and Biotechnology*, *88*(1), 371-380.

Kim, B. H., Chang, I. S., Gil, G. C., Park, H. S., & Kim, H. J. (2003). Novel BOD (biological oxygen demand) sensor using mediator-less microbial fuel cell. *Biotechnology Letters*, *25*(7), 541-545.

Kimura, Z. I., & Okabe, S. (2013). Acetate oxidation by syntrophic association between *Geobacter sulfurreducens* and a hydrogen-utilizing exoelectrogen. *The ISME Journal*, *7*(8), 1472-1482.

Kleerebezem, R., & van Loosdrecht, M. C. (2007). Mixed culture biotechnology for bioenergy production. *Current Opinion in Biotechnology*, *18*(3), 207-212.

Kuntke, P., Śmiech, K. M., Bruning, H., Zeeman, G., Saakes, M., Sleutels, T. H. J. A., ... & Buisman, C. J. N. (2012). Ammonium recovery and energy production from urine by a microbial fuel cell. *Water Research*, *46*(8), 2627-2636.

Lai, B., Tang, X., Li, H., Du, Z., Liu, X., & Zhang, Q. (2011). Power production enhancement with a polyaniline modified anode in microbial fuel cells. *Biosensors and Bioelectronics*, *28*(1), 373-377.

Lei, C., Wilson, P., & Lekakou, C. (2011). Effect of poly(3,4-ethylenedioxythiophene) (PEDOT) in carbon-based composite electrodes for electrochemical supercapacitors. *Journal of Power Sources*, *196*(18), 7823-7827.

Li, C., Zhang, L. B., Ding, L. L., Ren, H. Q., & Cui, H. (2011). Effect of conductive polymers coated anode on the performance of microbial fuel cells (MFCs) and its biodiversity analysis. *Biosensors and Bioelectronics, 26*(10), 4169-4176.

Li, W. W., Yu, H. Q., & He, Z. (2014). Towards sustainable wastewater treatment by using microbial fuel cells-centered technologies. *Energy & Environmental Science, 7*(3), 911-924.

Lies, D. P., Hernandez, M. E., Kappler, A., Mielke, R. E., Gralnick, J. A., & Newman, D. K. (2005). *Shewanella oneidensis* MR-1 uses overlapping pathways for iron reduction at a distance and by direct contact under conditions relevant for biofilms. *Applied and Environmental Microbiology*, *71*(8), 4414-4426.

Lim, B. S., Lu, H., Choi, C., & Liu, Z. X. (2015). Recovery of silver metal and electric power generation using a microbial fuel cell. *Desalination and Water Treatment*, *54*(13), 3675-3681.

Liu, B., Lei, Y., & Li, B. (2014). A batch-mode cube microbial fuel cell based "shock" biosensor for wastewater quality monitoring. *Biosensors and Bioelectronics*, *62*, 308-314.

Liu, X., Du, X., Wang, X., Li, N., Xu, P., & Ding, Y. (2013). Improved microbial fuel cell performance by encapsulating microbial cells with a nickel-coated sponge. *Biosensors and Bioelectronics, 41*, 848-851.

Liu, X., Wu, W., & Gu, Z. (2015). Poly(3,4-ethylenedioxythiophene) promotes direct electron transfer at the interface between *Shewanella loihica* and the anode in a microbial fuel cell. *Journal of Power Sources, 277*, 110-115.

Liu, Z., Liu, J., Li, B., Zhang, Y., & Xing, X. H. (2014). Focusing on the process diagnosis of anaerobic fermentation by a novel sensor system combining microbial fuel cell, gas flow meter and pH meter. *International Journal of Hydrogen Energy*, *39*(25), 13658-13664.

Logan, B. E. (2008). *Microbial fuel cells*. New Jersey, USA: John Wiley & Sons.

Logan, B. E. (2010). Scaling up microbial fuel cells and other bioelectrochemical systems. *Applied Microbiology and Biotechnology*, *85*(6), 1665-1671.

Logan, B. E., & Rabaey, K. (2012). Conversion of wastes into bioelectricity and chemicals by using microbial electrochemical technologies. *Science*, *337*(6095), 686-690.

Logan, B. E., & Regan, J. M. (2006a). Electricity-producing bacterial communities in microbial fuel cells. *Trends in Microbiology*, *14*(12), 512-518.

Logan, B. E., & Regan, J. M. (2006b). Microbial fuel cells–Challenges and applications. *Environmental Science & Technology*, *40*(17), 5172-5180.

Logan, B. E., Cheng, S., Watson, V., & Estadt, G. (2007). Graphite fiber brush anodes for increased power production in air-cathode microbial fuel cells. *Environmental Science & Technology*, *41*(9), 3341-3346.

Logan, B. E., Hamelers, B., Rozendal, R., Schröder, U., Keller, J., Freguia, S., ... & Rabaey, K. (2006). Microbial fuel cells: Methodology and technology. *Environmental Science & Technology*, *40*(17), 5181-5192.

Logan, B.E. (2009). Exoelectrogenic bacteria that power microbial fuel cells. *Nature Reviews Microbiology*, *7*(5), 375-381.

Lovley, D. R. (2006). Microbial fuel cells: novel microbial physiologies and engineering approaches. *Current Opinion in Biotechnology*, *17*(3), 327-332.

Lovley, D. R. (2008). The microbe electric: Conversion of organic matter to electricity. *Current Opinion in Biotechnology*, *19*(6), 564-571.

Lu, Z., Chang, D., Ma, J., Huang, G., Cai, L., & Zhang, L. (2015). Behavior of metal ions in bioelectrochemical systems: A review. *Journal of Power Sources, 275*, 243-260.

Lv, Z., Chen, Y., Wei, H., Li, F., Hu, Y., Wei, C., & Feng, C. (2013). One-step electrosynthesis of polypyrrole/graphene oxide composites for microbial fuel cell application. *Electrochimica Acta, 111*, 366-373.

Lv, Z., Xie, D., Yue, X., Feng, C., & Wei, C. (2012). Ruthenium oxide-coated carbon felt electrode: A highly active anode for microbial fuel cell applications. *Journal of Power Sources, 210*, 26-31.

Manohar, A. K., Bretschger, O., Nealson, K. H., & Mansfeld, F. (2008). The polarization behavior of the anode in a microbial fuel cell. *Electrochimica Acta*, *53*(9), 3508-3513.

Min, B., Cheng, S., & Logan, B. E. (2005). Electricity generation using membrane and salt bridge microbial fuel cells. *Water Research*, *39*(9), 1675-1686.

Min, B., Román, Ó. B., & Angelidaki, I. (2008). Importance of temperature and anodic medium composition on microbial fuel cell (MFC) performance. *Biotechnology Letters*, *30*(7), 1213-1218.

Motos, P. R., ter Heijne, A., van der Weijden, R., Saakes, M., Buisman, C. J., & Sleutels, T. H. (2015). High rate copper and energy recovery in microbial fuel cells. *Frontiers in Microbiology*, *6*.

Münstedt, H. (1988). Ageing of electrically conducting organic materials. *Polymer*, *29*(2), 296-302.

Naarmann, H, & Theophilou, N. (1987). New process for the production of metal-like, stable polyacetylene. *Synthetic Metals*, *22*(1), 1-8.

Nie, T., Zhang, K., Xu, J., Lu, L., & Bai, L. (2014). A facile one-pot strategy for the electrochemical synthesis of poly(3,4-ethylenedioxythiophene)/Zirconia nanocomposite as an effective sensing platform for vitamins B2, B6 and C. *Journal of Electroanalytical Chemistry*, *717*, 1-9.

Oh, S. E., & Logan, B. E. (2007). Voltage reversal during microbial fuel cell stack operation. *Journal of Power Sources, 167*(1), 11-17.

Osman, M. H., Shah, A. A., & Walsh, F. C. (2011). Recent progress and continuing challenges in bio-fuel cells. Part I: Enzymatic cells. *Biosensors and Bioelectronics, 26*(7), 3087-3102.

Ozkaya, B., Akoglu, B., Karadag, D., Aci, G., Taskan, E., & Hasar, H. (2012). Bioelectricity production using a new electrode in a microbial fuel cell. *Bioprocess and Biosystem Engineering, 35*(7), 1219-1227.

Pant, D., Singh, A., Van Bogaert, G., Olsen, S. I., Nigam, P. S., Diels, L., & Vanbroekhoven, K. (2012). Bioelectrochemical systems (BES) for sustainable energy production and product recovery from organic wastes and industrial wastewaters. *RSC Advances, 2*(4), 1248-1263.

Park, H. S., Ko, S. J., Park, J. S., Kim, J. Y., & Song, H. K. (2013). Redox-active charge carriers of conducting polymers as a tuner of conductivity and its potential window. *Scientific Reports, 3*.

Park, I. H., Christy, M., Kim, P., & Nahm, K. S. (2014). Enhanced electrical contact of microbes using Fe_3O_4/CNT nanocomposite anode in mediator-less microbial fuel cell. *Biosensors and Bioelectronics, 58*, 75-80.

Pham, T. H., Rabaey, K., Aelterman, P., Clauwaert, P., De Schamphelaire, L., Boon, N., & Verstraete, W. (2006). Microbial fuel cells in relation to conventional anaerobic digestion technology. *Engineering in Life Sciences, 6*(3), 285-292..

Picioreanu, C., van Loosdrecht, M. C., Curtis, T. P., & Scott, K. (2010). Model based evaluation of the effect of pH and electrode geometry on microbial fuel cell performance. *Bioelectrochemistry, 78*(1), 8-24.

Pocaznoi, D., Calmet, A., Etcheverry, L., Erable, B., & Bergel, A. (2012). Stainless steel is a promising electrode material for anodes of microbial fuel cells. *Energy & Environmental Science, 5*(11), 9645-9652.

Potter, M. C. (1911). Electrical Effects Accompanying the Decomposition of Organic Compounds. *Proceedings of the Royal Society of London. Series B, Containing Papers of a Biological Character, 84*(571), 260-276.

Qiao, Y., Bao, S. J., Li, C. M., Cui, X. Q., Lu, Z. S., & Guo, J. (2007). Nanostructured polyaniline/titanium dioxide composite anode for microbial fuel cells. *ACS Nano, 2*(1), 113-119.

Reguera, G., Nevin, K. P., Nicoll, J. S., Covalla, S. F., Woodard, T. L., & Lovley, D. R. (2006). Biofilm and nanowire production leads to increased current in *Geobacter sulfurreducens* fuel cells. *Applied and Environmental Microbiology*, *72*(11), 7345-7348.

Richter, H., McCarthy, K., Nevin, K. P., Johnson, J. P., Rotello, V. M., & Lovley, D. R. (2008). Electricity generation by *Geobacter sulfurreducens* attached to gold electrodes. *Langmuir*, *24*(8), 4376-4379.

Rismani-Yazdi, H., Carver, S. M., Christy, A. D., Yu, Z., Bibby, K., Peccia, J., & Tuovinen, O. H. (2013). Suppression of methanogenesis in cellulose-fed microbial fuel cells in relation to performance, metabolite formation, and microbial population. *Bioresource Technology*, *129*, 281-288.

Schröder, U. (2007). Anodic electron transfer mechanisms in microbial fuel cells and their energy efficiency. *Physical Chemistry Chemical Physics*, *9*(21), 2619-2629.

Selvaganesh, S. V., Mathiyarasu, J., Phani, K. L. N., & Yegnaraman, V. (2007). Chemical synthesis of PEDOT–Au nanocomposite. *Nanoscale Research Letters*, *2*(11), 546-549.

Shafiee, S., & Topal, E. (2009). When will fossil fuel reserves be diminished?. *Energy Policy*, *37*(1), 181-189.

Shehab, N., Li, D., Amy, G. L., Logan, B. E., & Saikaly, P. E. (2013). Characterization of bacterial and archaeal communities in air-cathode microbial fuel cells, open circuit and sealed-off reactors. *Applied Microbiology and Biotechnology*, *97*(22), 9885-9895.

Shin, H. J., Jeon, S. S., & Im, S. S. (2011). CNT/PEDOT core/shell nanostructures as a counter electrode for dye-sensitized solar cells. *Synthetic Metals*, *161*(13), 1284-1288.

Svardal, K., & Kroiss, H. (2011). Energy requirements for waste water treatment. *Water Science & Technology*, *64*(6), 1355-1361.

Tang, X., Li, H., Du, Z., Wang, W., & Ng, H. Y. (2015). Conductive polypyrrole hydrogels and carbon nanotubes composite as an anode for microbial fuel cells. *RSC Advances*, *5*(63), 50968-50974.

Tender, L. M., Gray, S. A., Groveman, E., Lowy, D. A., Kauffman, P., Melhado, J., ... & Dobarro, J. (2008). The first demonstration of a microbial fuel cell as a viable power supply: powering a meteorological buoy. *Journal of Power Sources*, *179*(2), 571-575.

ter Heijne, A., Hamelers, H. V., Saakes, M., & Buisman, C. J. (2008). Performance of non-porous graphite and titanium-based anodes in microbial fuel cells. *Electrochimica Acta*, *53*(18), 5697-5703.

Thorne, R., Hu, H., Schneider, K., Bombelli, P., Fisher, A., Peter, L. M., ... & Cameron, P. J. (2011). Porous ceramic anode materials for photo-microbial fuel cells. *Journal of Materials Chemistry*, *21*(44), 18055-18060.

Wang, H., Wang, G., Ling, Y., Qian, F., Song, Y., Lu, X., ... & Li, Y. (2013). High power density microbial fuel cell with flexible 3D graphene–nickel foam as anode. *Nanoscale*, *5*(21), 10283-10290.

Wang, Y., Li, B., Cui, D., Xiang, X., & Li, W. (2014). Nano-molybdenum carbide/carbon nanotubes composite as bifunctional anode catalyst for high-performance Escherichia coli-based microbial fuel cell. *Biosensors and Bioelectronics*, *51*, 349-355.

Wang, Y., Zhao, C. E., Sun, D., Zhang, J. R., & Zhu, J. J. (2013). A graphene/poly(3,4-ethylenedioxythiophene) hybrid as an anode for high-performance microbial fuel cells. *ChemPlusChem*, *78*(8), 823-829.

Wang, Z., Lee, T., Lim, B., Choi, C., & Park, J. (2014). Microbial community structures differentiated in a single-chamber air-cathode microbial fuel cell fueled with rice straw hydrolysate. *Biotechnology for Biofuels*, *7*(9).

Webb, H. K., Notley, S. M., & Evans, D. R. (2015). Observation of electron transfer between bacteria and high conductivity graphene–PEDOT composites. *RSC Advances*, *5*(57), 45642-45645.

Wei, J., Liang, P., & Huang, X. (2011). Recent progress in electrodes for microbial fuel cells. *Bioresource Technology*, *102*(20), 9335-9344.

Wen, Z., Ci, S., Mao, S., Cui, S., Lu, G., Yu, K., ... & Chen, J. (2013). TiO_2 nanoparticles-decorated carbon nanotubes for significantly improved bioelectricity generation in microbial fuel cells. *Journal of Power Sources*, *234*, 100-106.

Xiao, L., Damien, J., Luo, J., Jang, H. D., Huang, J., & He, Z. (2012). Crumpled graphene particles for microbial fuel cell electrodes. *Journal of Power Sources*, *208*, 187-192.

Xie, X., Ye, M., Hu, L., Liu, N., McDonough, J. R., Chen, W., ... & Cui, Y. (2012). Carbon nanotube-coated macroporous sponge for microbial fuel cell electrodes. *Energy & Environmental Science*, *5*(1), 5265-5270.

Xie, X., Yu, G., Liu, N., Bao, Z., Criddle, C. S., & Cui, Y. (2012). Graphene–sponges as high-performance low-cost anodes for microbial fuel cells. *Energy & Environmental Science*, *5*(5), 6862-6866.

Yamamuro, A., Kouzuma, A., Abe, T., & Watanabe, K. (2014). Metagenomic analyses reveal the involvement of syntrophic consortia in methanol/electricity conversion in microbial fuel cells. *PLOS ONE*, *9*(5).

Yang, S., Du, F., & Liu, H. (2012). Characterization of mixed-culture biofilms established in microbial fuel cells. *Biomass and Bioenergy*, *46*, 531-537.

Yuan, Y., Ahmed, J., & Kim, S. (2011). Polyaniline/carbon black composite-supported iron phthalocyanine as an oxygen reduction catalyst for microbial fuel cells. *Journal of Power Sources*, *196*(3), 1103-1106.

Zang, G. L., Sheng, G. P., Li, W. W., Tong, Z. H., Zeng, R. J., Shi, C., & Yu, H. Q. (2012). Nutrient removal and energy production in a urine treatment process using magnesium ammonium phosphate precipitation and a microbial fuel cell technique.*Physical Chemistry Chemical Physics*, *14*(6), 1978-1984.

Zhang, B., Feng, C., Ni, J., Zhang, J., & Huang, W. (2012). Simultaneous reduction of vanadium (V) and chromium (VI) with enhanced energy recovery based on microbial fuel cell technology. *Journal of Power Sources*, *204*, 34-39.

Zhang, C., Liang, P., Jiang, Y., & Huang, X. (2015). Enhanced power generation of microbial fuel cell using manganese dioxide-coated anode in flow-through mode. *Journal of Power Sources*, *273*, 580-583.

Zhang, H., Chen, X., Braithwaite, D., & He, Z. (2014). Phylogenetic and metagenomic analyses of substrate-dependent bacterial temporal dynamics in microbial fuel cells. *PLOS ONE*, *9*(9).

Zhang, J., Shan, D., & Mu, S. (2007). Chemical synthesis and electric properties of the conducting copolymer of aniline and o-aminophenol. *Journal of Polymer Science Part A: Polymer Chemistry*, *45*(23), 5573-5582.

Zhang, L. J., Tao, H. C., Wei, X. Y., Lei, T., Li, J. B., Wang, A. J., & Wu, W. M. (2012). Bioelectrochemical recovery of ammonia–copper (II) complexes from wastewater using a dual chamber microbial fuel cell. *Chemosphere*, *89*(10), 1177-1182.

Zhang, P. Y., & Liu, Z. L. (2010). Experimental study of the microbial fuel cell internal resistance. *Journal of Power Sources*, *195*(24), 8013-8018.

Zhao, F., Slade, R. C., & Varcoe, J. R. (2009). Techniques for the study and development of microbial fuel cells: An electrochemical perspective. *Chemical Society Reviews*, *38*(7), 1926-1939.

Zhao, Q., Jamal, R., Zhang, L., Wang, M., & Abdiryim, T. (2014). The structure and properties of PEDOT synthesized by template-free solution method. *Nanoscale Research Letters*, *9*(1).

Zhao, Y., Nakanishi, S., Watanabe, K., & Hashimoto, K. (2011). Hydroxylated and aminated polyaniline nanowire networks for improving anode performance in microbial fuel cells. *Journal of Bioscience and Bioengineering*, *112*(1), 63-66.

Zheng, Q., Xiong, L., Mo, B., Lu, W., Kim, S., & Wang, Z. (2015). Temperature and humidity sensor powered by an individual microbial fuel cell in a power management system. *Sensors*, *15*(9), 23126-23144..

Zhou, M., Chi, M., Luo, J., He, H., & Jin, T. (2011). An overview of electrode materials in microbial fuel cells. *Journal of Power Sources*, *196*(10), 4427-4435.

Zhou, M., Chi, M., Wang, H., & Jin, T. (2012). Anode modification by electrochemical oxidation: A new practical method to improve the performance of microbial fuel cells. *Biochemical Engineering Journal*, *60*, 151-155.

Zou, Y., Xiang, C., Yang, L., Sun, L. X., Xu, F., & Cao, Z. (2008). A mediatorless microbial fuel cell using polypyrrole coated carbon nanotubes composite as anode material. *International Journal of Hydrogen Energy*, *33*(18), 4856-4862.

LIST OF PUBLICATIONS AND PAPERS PRESENTED

Paper Published

1. Kang, Y. L., Ibrahim, S., & Saravanan, P. (2015). Synergetic effect of conductive polymer poly(3,4-ethylenedioxythiophene) with different structural configuration of anode for microbial fuel cell application. Bioresource Technology, 189, 364-369.
2. Kang, Y. L., Ibrahim, S., & Saravanan, P. (2016). Facile reconstruction of microbial fuel cell (MFC) anode with enhanced exoelectrogens selection for intensified electricity generation. *International Journal of Hydrogen Energy*. doi: 10.1016/j.ijhydene.2016.09.059

Conference presentations

1. Kang, Y.L., Ibrahim, S., & Saravanan, P. "Performance of Microbial Fuel Cell Inoculated with Mixed Culture from Anaerobic Lagoon." Asia-Oceania Top University League on Engineering, Student Conference 2012 (AOTULE 2012). 24-25 November (2012) Kuala Lumpur, Malaysia.
2. Kang, Y.L., Ibrahim, S., & Saravanan, P. "Conductive Polymer Electrode for Microbial Fuel Cell Application." 1st International Conference on Energy, Environment and Human Engineering 2013 (ICEEHE 2013). 22 -23 December (2013) Yangon, Myanmar.
3. Kang, Y.L., Rosdi, A.N, Ibrahim, S., & Saravanan, P. "Modified Graphite felt with poly(3,4-ethylenedioxythiophene) as anode for microbial fuel cell application." 2nd Asia Pacific International Society of Microbial Electrochemistry and Technology Meeting (AP-ISMET 2014). 21 -23 July (2014) NUS, Singapore.
4. Kang, Y.L., Ibrahim, S., & Saravanan, P. "Enhancement of Microbial Fuel Cell Anode through Conductive Polymer." 15th European Fuel Cell Technology & Applications Piero Lunghi Conference (EFC 2015). 16-18 December (2015) Naples, Italy.